Norwegian University
of Life Sciences

Master's Thesis 2017   30 ECTS
Faculty of Science and Technology

Investigation, Dimensions and Development of Test Setup for Propulsion Function of a Personal Transport Drone.

Utredning, dimensjonering og utvikling av testoppsett

for thrusterfunksjon til persondrone.

Anders Christian Thømt

Mechanical Engineering, Process Technology and Product
Development

INVESTIGATION, DIMENSIONS AND DEVELOPMENT OF TEST SETUP FOR PROPULSION FUNCTION OF A PERSONAL TRANSPORT DRONE.

By
Anders Thømt

Norwegian University
of Life Sciences

Master thesis – Mechanical Engineering, Process Technology and Product Development
NMBU – Faculty of Sciences and Technology.

2017

PREFACE

This thesis is the concluding part of a Master's degree in Mechanical Engineering, Process Technology and Product Development at the Norwegian University of Life Sciences. This thesis was conducted through the spring semester and consists of 30 credits.

A motivation for this project is the underlying fascination of how large masses can be fly or be suspended in air. Also, with the promising future advances in battery technology, new possibilities for personal transport can be explored. Door-to-door aerial transport has long been a dream, but has so far been restricted to helicopters. To investigate a new approach in configuration and safety to a vertical landing and take-off aircraft from a physics perspective have been interesting and challenging. This investigation is presented in Part One of this thesis and lays the foundation for the work in Part two.

First off, I would like to thank Associate Professor Jan Kåre Bøe for excellent guidance in development process, method and report structure. Thanks to Professor Tor Anders Nygaard for valuable insight in aerodynamics and rotary wings. Also, thanks to Senior Engineer Tom Ringstad for help with experimental equipment and lastly, a thanks to Engineer Gunnar Torp for contributions in manufacture process and costs.

Aas – 12th of May 2017

_____

Anders Thømt

ABSTRACT

In the desire to solve some of the challenges in personal transport and congestions in the cities, an investigation in to the specifications of a thruster based solution for hovering capabilities of a personal transport drone concept, has been conducted in this thesis. Also, a scaled test rig for evaluation and experimentation of propulsive function for a thruster was developed. The work in this thesis is presented in two parts, with the first part involving investigation for the drone concept, and the second part containing development and specifications of the experimental test rig.

To evaluate the required specifications for a thruster design, a literature review of aerodynamics was conducted, starting with basic concepts and terms. Further, a review of propulsive theory within propellers and rotors were done. Existing and future concepts were also evaluated for inspiration and as a reference. The findings in theory, specifically blade element theory were implemented in a simplified theoretical tool. This tool was applied to the specification process to determine requirements in power, weight, and efficiency one can expect to lift and hover a payload that includes one person with in-built redundancy for safety. Next, a scaled experimental setup is developed to lay the foundation for future development of a full-scale thruster that can meet the requirements found in the first part of the thesis. The investigation in part one of this thesis laid the foundation for the development of the experimental test rig in Part Two. The development of the test rig, could not be done without the investigation and development of theoretical tools in Part One.

The specification of the thruster unit in Part One was done under a regime of objectives that managed the specification process so that important properties such as safety and efficiency were maintained throughout the concept generation. The specification in Part One led to a selected layout of the thrusters through the use of development methodology with its origins from Pugh's method. The preliminary specifications include a goal for efficiency, performance, total weight of the aircraft, and power requirements. Since the nature of the theory used in this thesis is ideal, the specifications in Part One are preliminary only. Also, using only the thrusters for generation of lift, requires a very high power consumption.

The same development methodology was used in Part Two where key properties of the experimental test rig were defined and several concepts were generated and screened in a two-cycle process that yielded a best concept. This concept was constructed in CAD with full specifications and simulated for flow analysis.

The main findings in Part One were the following: Assuming a gross weight of 450 kg, a thruster unit with two coaxial contra-rotating propellers will require a power of 50 kW and a total swept area of 2.26 m². This gives a specific weight of 2.25 kg/kW. The minimum power required for hovering is 18 kW for each thruster. For Part Two the results are: An experimental test rig for measuring thrust and torque produced by a propeller is designed with full specifications and technical drawings for a total cost of 595 000 NOK. A simple experimental plan overviewing method and experimental equipment is also found in this report. The rig is 1500 mm long, 1000 mm wide and 890 mm high without the propeller. Total weight is 29 kg. The test rig is optimized for the specified engine of 1 kW and the designed propeller of 600 mm, but is also capable of handling up to 3 kW of power, and up to 800 mm diameter propellers.

The main challenge for future work, is to develop a dedicated program or code including vortex theory to accurately predict performance and generate design parameters for the propeller blades. This program should also be able to predict characteristics in forward flight. Also, an

investigation in to how a wing area can be implemented in the drone/aircraft design to improve efficiency is recommended.

SAMMENDRAG

I ønsket om å løse noen av utfordringene i personlig transport og overbelastning av trafikk-nettet i byene, har en utredning i krav-spesifikasjoner for en thruster-basert løsning for sveveegenskaper for et drone-konsept for person transport, blitt gjennomført i denne oppgaven. Det ble også utviklet en skalert testrigg for evaluering og eksperimentering av skyvekraftfunksjon for en thruster. Arbeidet i denne avhandlingen er presentert i to deler, med den første delen som involverer utredning av drone-konseptet, og den andre delen inneholder utvikling og spesifikasjoner for den eksperimentelle testriggen.

For å evaluere de nødvendige spesifikasjonene for et thruster-design ble det gjennomført en litteraturstudie av aerodynamikk, med utgangspunkt i grunnleggende begreper og konsepter. Videre ble det gjennomført en gjennomgang av propulsiv-teori innen propeller og rotorer. Eksisterende og fremtidige konsepter ble også evaluert for inspirasjon og som referanse. Funnene i teoristudiet ble implementert i et forenklet teoretisk verktøy. Dette verktøyet ble brukt gjennom spesifikasjonsprosessen for å bestemme krav til skyvekraft, vekt og effektivitet man kan forvente for å løfte og sveve en nyttelast som inkluderer en person med innebygd overflødighet for sikkerhet. Deretter utvikles et skalert eksperimentelt oppsett for å legge grunnlaget for fremtidig utvikling av en fullskala thruster som kan tilfredsstille kravene i første del av oppgaven. Utredningen i Del 1 av denne avhandlingen la grunnlaget for utviklingen av den eksperimentelle testriggen i Del 2. Utviklingen av test riggen kunne ikke funnet sted uten utredning og utvikling av teoretiske verktøy i Del 1.

Spesifikasjonen av thrusterenheten i Del 1 ble gjort under et målregime for styring av prosjektet slik at viktige egenskaper som sikkerhet og effektivitet ble opprettholdt gjennom konseptgenerasjonen. Spesifikasjonen i Del 1 førte til en valgt utforming av thruster gjennom bruk av utviklingsmetodikk med utgangspunkt i Pughs metode. De foreløpige spesifikasjonene inkluderer et mål for effektivitet, ytelse, totalvekt på dronen samt effektkrav. Siden karakteren av teorien som brukes i denne oppgaven er ideell, er spesifikasjonene i Del 1 kun foreløpige. Ved bruk av bare thrustere for generering av løft, kreves det også et meget høyt energiforbruk.

Den samme utviklingsmetoden ble brukt i del to hvor nøkkelegenskaper til den eksperimentelle testriggen ble definert og flere konsepter ble generert og screenet i en to-syklusprosess som ga et beste konsept. Dette konseptet ble konstruert i CAD med fulle spesifikasjoner og simulert for strømningsanalyse.

De viktigste funnene i Del 1 var følgende: Forutsatt en bruttovekt på 450 kg vil en thruster med to koaksiale kontraroterende propeller kreve en effekt på 50 kW og et totalt sveipet areal på 2,26 m^2. Dette gir en spesifikk vekt på 2,25 kg / kW. Minste effekt som kreves for svevning er 18 kW for hver propell. For Del 2 er resultatene: En eksperimentell testrigg for måling av skyvekraft og dreiemoment produsert av en propell er utformet med fulle spesifikasjoner og tekniske tegninger for en total kostnad på 595 000 NOK. En enkel plan for eksperimentell metode og eksperimentelt utstyr finnes også i denne rapporten. Riggen er 1500 mm lang, 1000 mm bred og 890 mm høy uten propell. Total vekt er 29 kg. Test riggen er optimalisert for den angitte motoren på 1 kW og den konstruerte propellen på 600 mm, men er også i stand til å håndtere opptil 3 kW effekt og propeller på inntil 800 mm.

Hovedutfordringen for videre arbeid er å utvikle et dedikert program eller kode, inkludert turbulensteori, for å nøyaktig forutsi ytelse og generere presise designparametere for propellbladene. Dette programmet skal også være i stand til å forutsi forholdene under

horisontal flyvning. Det anbefales også å undersøke hvordan et vingeområde kan implementeres i drone / fly-designet for å forbedre effektiviteten.

CONTENTS   PAGE

PART ONE

PART TWO

PART ONE: INVESTIGATION AND EARLY SPECIFICATIONS OF PROPULSION FOR A PERSONAL DRONE

1 INTRODUCTION

The starting chapter introduces the reader to the background of this thesis and a historical perspective on vertical take-off and landing aircrafts.

With increasing movement of people towards cities, traffic congestion is a rising problem. The transport systems today are restricted by movement along a single plane, limiting transport flow. By elevating traffic in multiple planes of traffic in the sky, congestion and transport time can be reduced. With a promising future advancement in battery capacity and progress in lightweight materials, a developing interest in drone-based aerial concepts for personal transport is emerging.

The light weight vehicle concept called Dolphin has been under development since 2010. With a multifuel hybrid system featuring a gass-turbine combined with a steam turbine to generate electricity to power electric motors and/or charging batteries - [3], [4] and [5]. This concept has the potential to be adapted in to a drone based aerial vehicle, assuming lightweight structure and an advancement in battery technology.

1.1 VTOL HISTORY AND TRENDS

1.1.1 BELL X-22

In the 1960's the United States Department of Defense supported several programs for investigating the possible use of vertical take-off and landing aircrafts. One of the more successful programs was the Bell X-22. With four 7 feet diameter ducts, fitted with Hamilton Standard three blade propellers powered by four General Electric-YT58-GE-8D turboshaft engines (Figure 1.1.1 A). The engines where mounted on the rear wing and powers all four ducted fans through a drive train. All engines are connected to the four fans through a gearbox, in case of engine failure all four fans can be powered by the remaining three engines. This safety feature is critical since the ducted fan configuration eliminates the possibility for autorotation which is used by open air rotors such as helicopters to land safely during an engine failure if the aircraft has sufficient altitude.
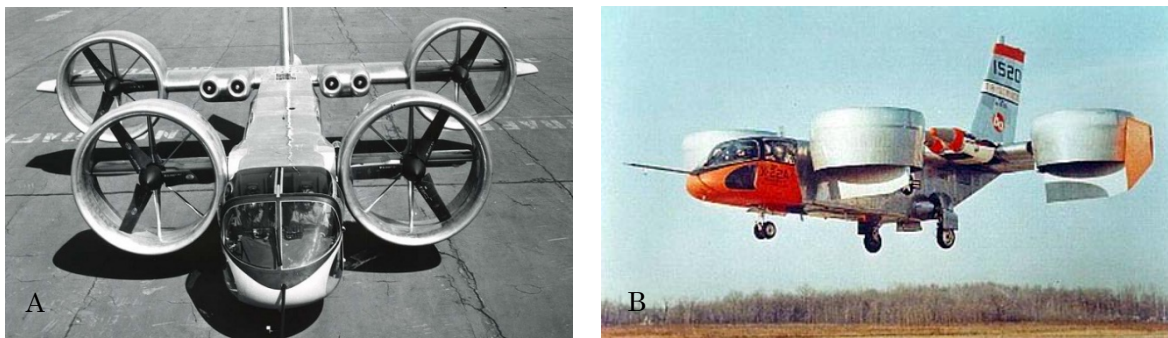
Figure 1.1.1. Bell X-22. [2]. A: The ducts positioned for forward flight. B: In hovering.

Specifications	Type/Value
Engine type	Gass-turbine
Power	3780 kW
Cruise speed	520 km/h
Endurance	1 hour at cruising speed + 10 min hover
Gross weight	8030 kg
Specific weight	2.1 kg/kW

Two aircrafts where made. After 40 successful flights, the first aircraft was damaged during a crash on August 8, 1966 caused by simultaneous faults on both hydraulic systems. The second aircraft made its first flight in January the following year. The program was eventually cancelled after the maximum required speed of 525 km/h was never reached. Another problem at the time was the added weight of the ducted fans. The ducts where made from an aluminum skeleton covered with fiberglass as seen in Figure 1.1.2, weight of the ducts effected the load carrying capabilities.
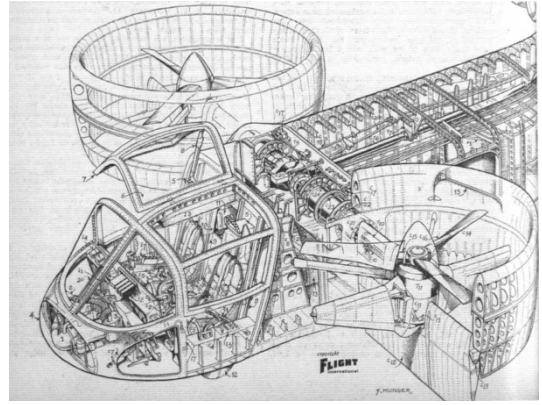
Figure 1.1.2. Technical drawing of front part. [2].

1.1.2 BOEING SKY COMMUTER

In the late 1980's a group of Boeing engineers built the Sky Commuter flying car. Designed for day-to-day personal use it is powered by a gas turbine engine that drives three ducted fans through a helicopter-based driveshaft. The ducted fans produced the lift needed for vertical take-off and landing capabilities and exhaust from the gas turbine is expelled in the rear to produce forward flight.

The Sky Commuters creators claimed that it made several successful test flights, but there are no photos or film footage known to support this claim.

Figure 1.1.3. To the left: Overview of the Sky Commuter. To the right: The fan blades are visible, revealing cord length and angle of attack [6].

Specifications	Type/Value
Engine type	Gass-turbine
Cruise speed	135 km/h
Range	360 km
Gross weight	
Development costs	$6 million (late 80's)
Specific weight	

Little is known about the technical details of this project, but the pictures reveal the overall architecture of the three ducted fans. The body is supposedly made from fiberglass. The diameter of the duct and the upstream placement of the stators are of interest. Furthermore, the number of fan blades and their cord length are of interest. From the right picture in Figure 1.1.3 it may look like hub is fitted with a variable pitch mechanism for the seven fan blades.

1.1.3   MOLLER SKYCAR

Ongoing for 20 years and in its fifth generation, the Moller SkyCar 400 is designed to carry four people from short-to medium long distances. Lift and propulsion is delivered by four thrust vectoring nacelles that houses a dual rotary engine with a fixed single seven-blade fan. The two rotary engines are there for redundancy in case of engine failure. Previous designs of the nacelle featured two counter rotating short cord fans, but it looks like Moller has opted for a single fan more recently. A prototype has been around for years, but only hover tests has been performed to an altitude of approximately 30 meters.

Figure 1.1.4. To the left: Skycar 400 in hovering mode. To the right: Power plant and rotor assembly for Skycar 400. [7]

Specifications	Type/Value
Engine type	Rotary combustion
Power (continuous)	541 kW
Cruise speed	457 km/h
Range	1206 km
Gross weight	1088 kg
Endurance	5.9 h
Specific weight	2.0 kg/kW

The nacelles are in their takeoff/hover position in Figure 1.1.4. Since the nacelles cannot be rotated to a fully vertical position the thrust is vectored down by vanes at the end of the duct (not visible). There is also a single vane in the longitudinal direction for each nacelle for sideways stability.

2   PROJECT OBJECTIVES AND PROGRESS PLAN

In this chapter, a plan overviewing the work progress with milestones are defined. Together with the objectives, limitations and constraints are also defined.

2.1   PROJECT OBJECTIVES

For planning and executing this project an objective-fulfillment strategy is used (section 3.2). The governing main objective for the project is stated below in a hierarchy of objectives containing a strategy for how the main objective is to be achieved. After the main objective, a set of objectives for the concept's desired effects for its user and surroundings are presented. Next, a set of physical objectives for achieving these effects. Further, these objects of achievement are broken down to specific milestones needed to fulfill the objectives above. A progress plan showing timed activities and milestones is presented on the next page.

Main Objective

To investigate and develop initial specifications for a thruster solution which facilitate hovering capabilities and safety aspects for a personal transport drone. Furthermore, to develop a scaled test rig for evaluation and experimentation of the propulsive function.

Objectives of effect

- o   Personal safety.
- o   Vertical take-off and landing capabilities.
- o   Light weight.
- o   Energy efficient.
- o   Low noise.

Objectives of Achievement

- o   Redundant lift capacity.
- o   Parachute compatible.
- o   Physical protection against moving parts.
- o   Can be integrated in Dolphin concept.
- o   Electric power source.
- o   Thruster layout.

Milestones

- ✓   To review relevant literature and existing solutions for VTOL-aircrafts and drones.
- ✓   To study aerodynamic theory and estimate necessary thrust and power required.
- ✓   To study blade element theory to lay the foundation for detailed specifications.
- ✓   To specify the metric specifications for the thrusters.
- ✓   To define a simple experimental plan for prototype testing.
- ✓   To design a prototype.
- ✓   CAD-modeling, material choice and CFD-simulations.
- ✓   To finalize the report.

2.2 PROGRESS PLAN

Table 2.2.1. Progress plan with timed activities and milestones for spring semester 2017.

Activity	January	February	March	April	May
Literature review		✓			
Theoretical work			✓		
Product specification			✓		
Concept generation			✓		
Experimental plan				✓	
Prototype planning				✓	
CAD-modeling					✓
Report work.					✓
Report deadline	15. May, 15:00				
Presentation	9 June, 12:15				

Preliminary review of literature and existing concepts were done in late spring and early fall 2016 and will be reported in January 2017.

2.3 THESIS CONSTRAINTS AND LIMITATIONS

Part One:

o   Effects of vorticity are not included in analytical studies.

o   Only vertical take-off and landing capabilities are evaluated, effects of forward flight, inflight stability and control are not evaluated.

Part Two:

o   Design and specifications of a duct is not considered.

o   Strength analysis and dimensioning of propeller blades are not considered.

o   Frequency analysis of rotating parts are not evaluated.

o   Detailed specifications for attachment of duct on to the experimental setup will not be designed.

o   Placement of hall-sensor and magnet are not detailed.

o   Stability of the experimental test rig is not evaluated.

o   Only cost calculation of one prototype is included.

o   Method for measuring power component of noise are not evaluated.

3 METHODOLOGY

This chapter presents the methods and tools used for product development in this thesis.

3.1 TERMINOLOGY AND NOMENCLATURE

Glossary of terms, abbreviations, nomenclature and symbols with units in this report follows.

- o When referring to rotating wings; the terms propellers, fans and rotors are used across each other.
- o Gross weight – total operational weight of aircraft including passengers and energy.

3.1.1 ABBREVIATIONS

Table 3.1.1. List of abbreviations used in this thesis.

Index		Description
LE	o	Leading edge
TE	o	Trailing edge
VTOL	o	Vertical take-off and landing
ac	o	Aerodynamic center
BET	o	Blade element theory
HMS	o	Healt and Safety
CDS	o	Component Design Specification
PDS	o	Product Design Specification
MT	o	Momentum theory
EM	o	Electric motor
IPD	o	Integrated Product Development
MIT	o	Massachusetts Institute of Technology
FS	o	Solidworks Flow Simulation
CDF	o	Computational Fluid Dynamics
RealTek	o	Faculty of Science and Technology
Texcel	o	Spreadsheet used for propeller calculations.

3.1.2 SYMBOL AND UNITS

Table 3.1.2. List of symbols used in this thesis with description and units using the SI-system. Continues on the two next pages.

Index		Description	Unit SI
A_p	o	Propeller disk area	m^2
a	o	Weld throat thickness	m
B	o	Electric current	A
C_D	o	Coefficient of drag	-
C_L	o	Coefficient of lift	-
c	o	Chord length	m
D	o	Drag force	N
F	o	Force	N
F_x	o	Force in x-direction	N
F_z	o	Force in z-direction	N
G	o	Gravitational force	N
h	o	Measured value	-

Table 3.1.3. Continued

Index		Description	Unit SI
i	o	Gear ratio	-
I_p	o	Polar second moment of area	mm^4
I_{zz}	o	Second moment of area about z-axis	mm^4
j	o	Standard deviation	-
k	o	Performance factor	-
L	o	Lift force	N
M	o	Figure of merit	-
Mc	o	Mach number	-
$\dot{m}$	o	Mass flow	kg/s
N	o	Number of measurements	-
P	o	Power	W
P_i	o	Ideal power	W
p_d	o	Pressure downstream	Pa
p_u	o	Pressure upstream	Pa
p_∞	o	Freestream pressure	Pa
Q	o	Torque	Nm
Q_x	o	Torque about x-axis	Nm
Q_z	o	Torque about x-axis	Nm
q	o	Evenly distributed load	kg/m
$\boldsymbol{R}$	o	Reynolds number	-
R	o	Blade tip radius	m
r	o	Radius	m
r_h	o	Hub radius	m
SF	o	Safety factor	-
s	o	Solidity	-
T	o	Thrust	N
U	o	Resultant velocity	m/s
u	o	Electrical voltage	V
V	o	Average velocity	m/s
V_i	o	Induced velocity	m/s
$\bar{V}_i$	o	Mean induced velocity	m/s
V_∞	o	Freestream velocity	m/s
V_s	o	Slipstream velocity	m/s
V_d	o	Velocity just downstream of propeller disk plane	m/s
V_c	o	Speed of sound	m/s
W_G	o	Gross weight	N
W_b	o	Section modulus	mm^3
x	o	Distance in x-direction	mm
y	o	Distance in x-direction	mm
ν	o	Kinematic viscosity	m^2/s
σ_b	o	Bending stress	MPa
$\sigma_\perp$	o	Normal stress	MPa
σ'	o	VonMises stress	MPa
$\tau_\perp$	o	Normal shear stress	MPa
$\tau_\parallel$	o	Parallel shear stress	MPa
$\delta_{\bar{h}}$	o	Standard error of mean	-

Index	Description		Unit SI
ω	o	*Angular velocity*	*rad/s*
φ	o	*Downwash angle*	*Degrees*
$\varphi_{0.75}$	o	*Downwash angle at 75 % of blade radius*	*Degrees*
α	o	*Aerodynamic angle of attack*	*Degrees*
θ	o	*Aerodynamic pitch angle (relative to zero-lift-line)*	*Degrees*
θ_c	o	*Pitch angle (relative to chord line)*	*Degrees*
η	o	*Efficiency*	-
η_p	o	*Propeller efficiency*	-

3.1.3   NOMENCLATURE
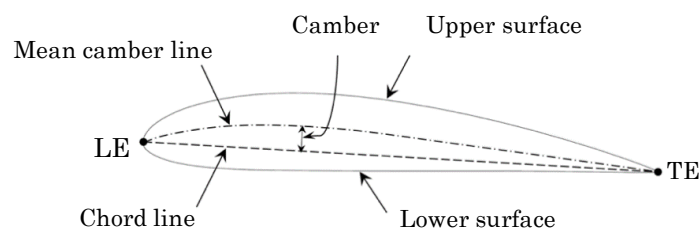
Figure 3.1.1. A typical airfoil cross-section with nomenclature.

3.1.4   FUNDAMENTAL FORMULAS

Table 3.1.5. Fundamental formulas used in this thesis are listed.

Description	Formula	Index
Torque	$Q = F\mathrm{x}$	(3.1.1)
Power	$P = FV$	(3.1.2)
	$P = Q\omega$	(3.1.3)
	$P = uB$	(3.1.4)
VonMises stress fillet weld [8].	$\sigma' = \sqrt{\sigma_\perp{}^2 + 3(\tau_\perp{}^2 + \tau_\parallel{}^2)}$	(3.1.5)

3.2   METHOD AND TOOLS

This section presents the method and tools used in development work in this thesis.

3.2.1   IPD- INTEGRATED PRODUCT DEVELOPMENT
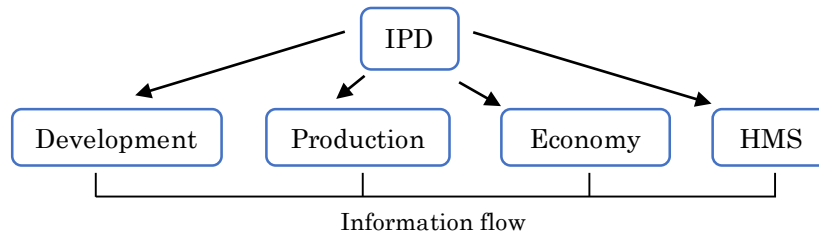
Figure 3.2.1. Overview of main elements in the IPD methodology.

This philosophy puts product development in a broader perspective than the traditional "economy" or "engineer" driven product development. The intent of this method is to increase efficiency and learning by implementing knowledge from other areas such as psychology, sustainability and environmental impact. Implementing these areas such as sustainability and environmental impact makes economically sense in the field of Industrial Ecology. This is because large values lie within the waste- and byproducts from the production that can be sold to other manufacturers or reused in the production itself. Through IPD, these activities will be implemented and overlap from an early point in the development process. Main points presented in Table 3.2.1 acts as a checklist during the development, and prevents important points from being neglected.

Table 3.2.1. Checklist for Integrated Product Development.

Main elements of IPD

- o   Determine customer needs and marked.
- o   Planning and managing the development process.
- o   Product development groups and teamwork.
- o   Integrating process design.
- o   Managing project costs from the beginning.
- o   Involving suppliers early in the development process.
- o   Developing a robust design.
- o   Integrating relevant computer tools such as, CAE, CAD and CAM.
- o   Computer simulations of properties and production method.
- o   Continuous improvement on the development process.
- o   Efficient approach to the development.

3.2.2   PROJECT MANAGEMENT

To get a strategic hold of the project early on, an objective fulfillment strategy is used. Containing a hierarchy of objectives from three perspectives to increase the chances of success for the project as a whole [9]. The hierarchy of objectives are displayed on the next page.
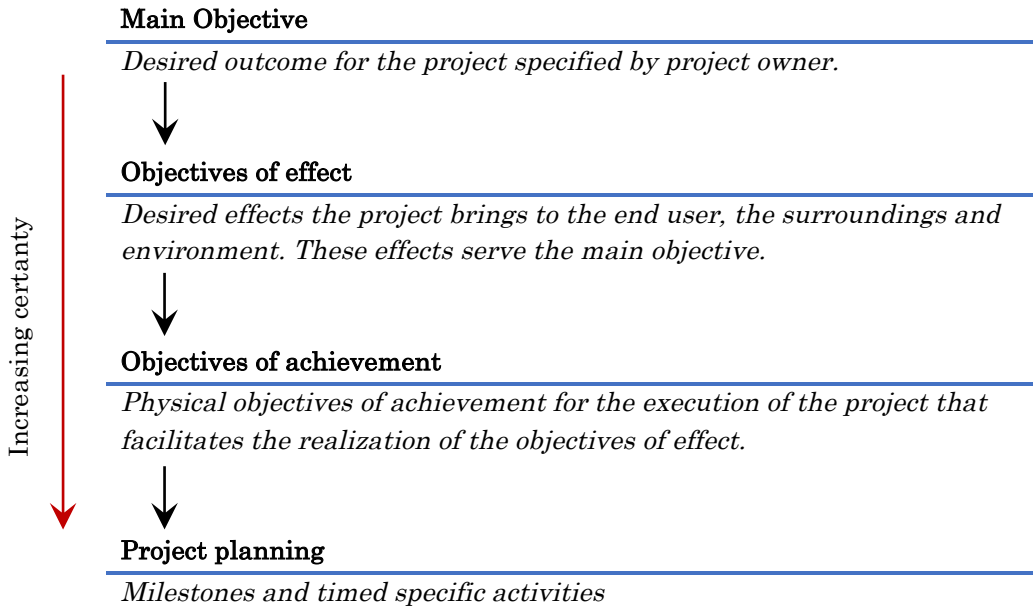
Main Objective

Desired outcome for the project specified by project owner.

↓

Objectives of effect

Desired effects the project brings to the end user, the surroundings and environment. These effects serve the main objective.

↓

Objectives of achievement

Physical objectives of achievement for the execution of the project that facilitates the realization of the objectives of effect.

↓

Project planning

Milestones and timed specific activities

Figure 3.2.2. General structure of the hierarchy of objectives.

As one moves down the hierarchy, the objectives become more specific, hence the chances for successfully accomplishing the objectives at the bottom increases. In this way, the main objective that is bound with uncertainty can be fulfilled by a set of specific activities with high individual chances of accomplishment. This, naturally relies of the consistency of the hierarchy.

3.2.3   TOTAL DESIGN PROCESS

Building on the design philosophy of Stuart Pugh, the total design process presented in this section is based on the design core described by Pugh [10]. The design core has been adapted and combined with development management in section 3.2.2. Figure 3.2.3 below shows how Pugh's design core has been adapted to reflect the project in this thesis.

Design Core by Pugh	**Design Core for this thesis**
Market (user need)	*Objectives of effect*
↓	↓
Product Design Specification	*Objectives of achievement*
↓	↓
Conceptual design	*Product Design Specification*
↓	↓
Detailed Design	*Conceptual design*
↓	↓
Manufacture	*Detailed Design*
↓	↓
Sales	*Manufacture*

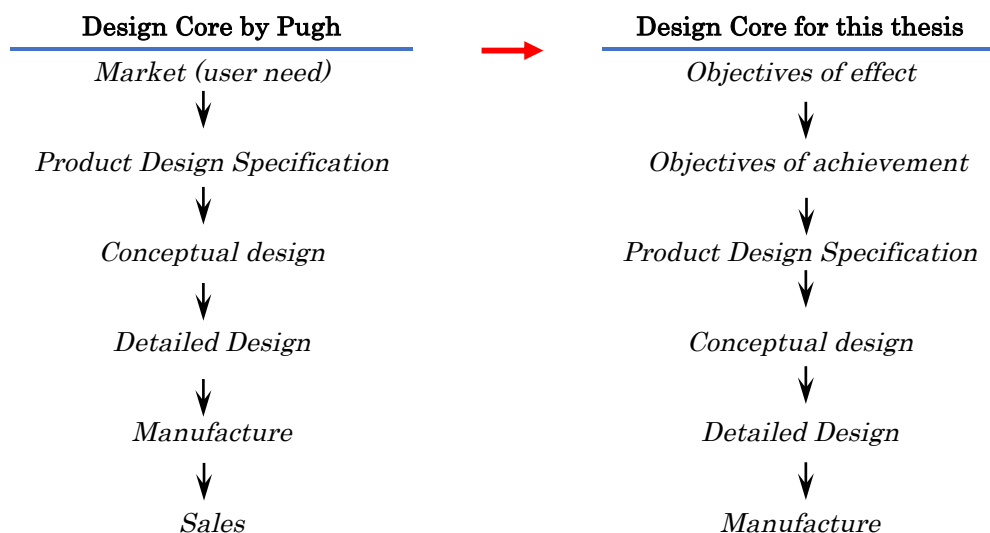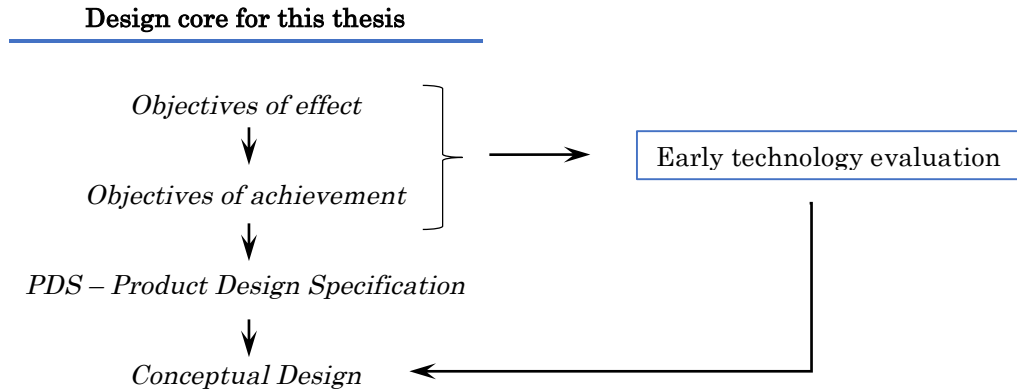*Figure 3.2.3. Pugh's design core in its vertically form is shown to the left. To the right the design core for this thesis is shown.*

The first step in Pugh's design core, market (user need) is divided in to objectives of effect and objectives of achievement. This is to implement the objective fulfillment strategy in section 3.2.2. Essentially, the objectives of effect reflect the user need. Put in another way, the

objectives of effect state the effects the product must provide to the user to fulfill user needs. The objectives of achievement state the tangible results that the product must provide, to produce the desired effects. Following from these objectives, the PDS can now be formed and must not violate the objectives of effect or objectives of achievement. In this way, any conceptual designs generated within the boundaries of the PDS will not violate the objectives of effect or objectives of achievement. Considerations of sales are not included because this project focuses on a subsystem of a larger product, hence sales considerations are outside the scope of this thesis. The design core used in this thesis is explained in greater detailed below.

Design core for this thesis

Objectives of effect

↓

Objectives of achievement   →   Early technology evaluation

↓

PDS – Product Design Specification

↓

Conceptual Design   ←

The conceptual design phase cycles between two major components:

1. Generation of solutions to meet the objectives.

2. The evaluation of solutions to select the one that is most suited to meet the objectives within the limitations of the PDS.

These two components will cycle through iterations that will finally arrive at the concept that is considered to meet the constrains of the PDS most efficiently.
The iterative process consists of applying an evaluation matrix on the generated concepts with criteria deduced from the PDS. The concepts least suited will then be omitted. New concept(s) may emerge and added to the evaluation. A new evaluation including the new concept(s) through the evaluation matrix is repeated. This process is repeated until one final concept remains.

↓

Detailed Design

In designing individual components that make up the product, a component design specification – CDS, should be formed. Similar to the PDS, the CDS is less detailed and is typically performance based. Key elements in the CDS are:
- o Local performance – input/output, loads, stresses, durability.
- o Local environment – temperature range, vibrations, corrosion, shock.
- o Local constraints – physical dimensions constrained by surroundings and interfacing components,

↓

Manufacture

Early Technology Evaluation

Before the concept generation stage, a pre-screening of technologies is made. Technologies that inherently are unable to fulfill the objectives of achievement and objectives of effect will not enter the concept generation. Thus, avoiding unnecessary complexity in the selection process. Figure 3.2.4 graphically shows early screening of technologies.
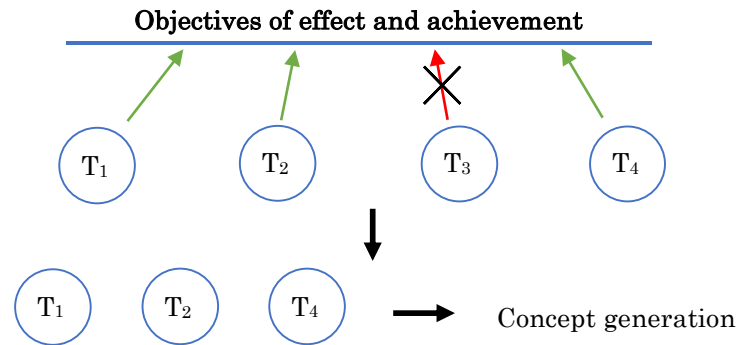

Figure 3.2.4. Technologies (T), that does not fulfill objectives of effect and achievements are not evaluated in the concept generation.

3.2.4   OSBORN'S CHECKLIST – SCAMPER
A creative method to help with creativity and exploration of all the inherent properties/possibilities within the concept. SCAMPER is an abbreviation for the following key words: Substitute, Combine, Adapt, Magnify, Minify, Eliminate, Elaborate, Rearrange, Reverse. By following these key words, the method helps you explore the concept's possibilities and combinations that otherwise would be hard to detect.

3.2.5   QUALITY ASSURANCE

Programs used.

- Word 2015 for report writing.
- EndNote X7 for references.
- PowerPoint 2015 and SolidWorks 2015/2016 for sketching figures.
- Excel 2015 for calculations and plots.
- SolidWorks 2015/2016 student edition for CAD-modeling.
- SolidWorks FlowSimulation for flow analysis.
- CES EduPack – Granta Design for material data.

Sources.

o The written sources used in this thesis are either educational books or frequently sited articles. Material from books where the author is *not* connected professionally to the field of aerodynamics or have an educational profile are not used directly in this thesis. Material of this kind are only used for preliminary conceptual studies. Hence, no such material is referenced in this thesis.

o Web sources are used mainly in the investigation of existing and future concepts, except for some airfoil data from data-bases online. These databases are founded on the airfoil predictor Xfoil, which is a code that originates from MIT, used for predicting airfoil characteristics. Xfoil has been validated through wind-tunnel testing [11].

Theory.

- o   Each part of the sections in the theory chapter is cross-checked with at least another source. Special attention was given section 4.3.2, since the predictions at first glance looked too good to be true. Two written sources confirm these results in addition to confirmation by [11]. Calculations of strength and deflection are based on formulas in [12].

Calculations.

- o   To solve integrals derived in section 4.5, the website wolframalpha.com were used to produce analytical results. These results were then solved in Excel. Each numerical result in Excel was cross-checked again with wolframalpha.com to verify the numerical answer when a calculator was not adequate.

CDF-program.

- o   Only one CFD-program was used in this thesis for flow analysis. The flow analysis can be done as an external or internal case. Both were tested and yielded the same results both numerically and with flow plots. The simulations were run with averaged results, since good convergence were found for all cases. This was to avoid transient (time dependent) analysis which increases computational time drastically.

3.2.6   DEVELOPMENT PROCESS

A schematic illustration of the development process follows:
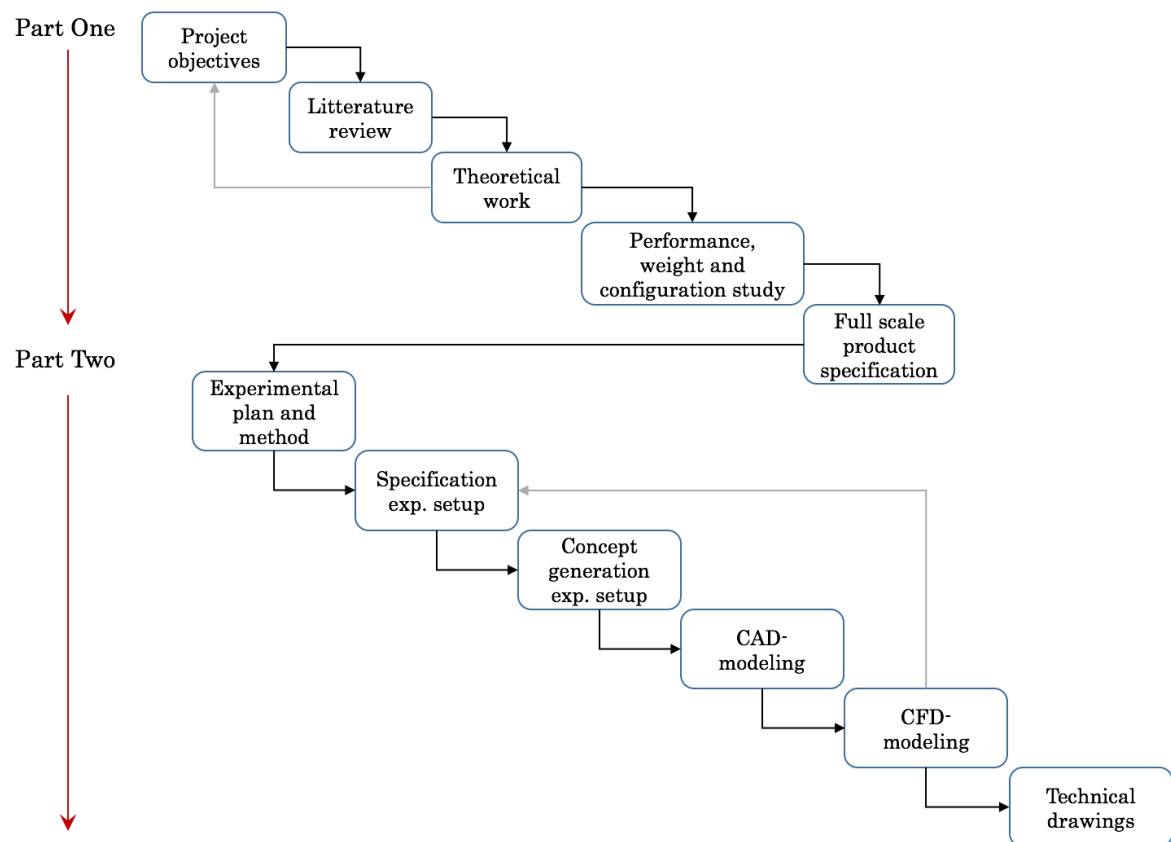
Figure 3.2.5. Chart overviewing the development process.

4 THEORY

In this chapter, fundamental aerodynamic concept and propulsive theory are presented.

4.1 REYNOLDS NUMBER AND DYNAMIC SIMILITUDE

Reynolds number is the measure of the magnitude of the pressure forces relative to the viscous forces. In other words, how dominant is pressure forces and viscous forces?

$$\boldsymbol{R} = \frac{F_d}{F_v} = \frac{L^2 V^2 \rho}{LV\mu} = \frac{LV\rho}{\mu} = \frac{LV}{\nu} \tag{4.1.1}$$

Where ν is the kinematic viscosity and L is the characteristic length significant to the flow. In lift devices such as an airfoil the chord length is normally used for L [13].

Mach number is the ratio of air velocity to the speed of sound and is used as an indication for compressibility effects.

$$M_c = \frac{U}{V_c} \tag{4.1.2}$$

Since the air travels faster over the top surface of the airfoil compressibility effects here can occur long before the airstream onto the airfoil reaches Mach 1. These compressibility effects produce shockwaves on the front of the airfoil and a catastrophic increase in drag. Known as critical Mach number, the Mach number in the airstream that is equivalent to Mach 1 locally over the top surface of the airfoil. Typically, critical Mach numbers are 0.7-0.8 for most subsonic airfoils. As a general rule, keeping the tip Mach number for propellers or rotors below 0.6 prevents significant compressibility effects [11].

To obtain dynamic similitude between a model and a prototype of different linear dimensions, the Reynolds number in both cases must be equal [14].

$$\left(\frac{LV}{\nu}\right)_m = \boldsymbol{R}_m = \boldsymbol{R}_p = \left(\frac{LV}{\nu}\right)_p \tag{4.1.3}$$

Linear dimensions and velocity must be chosen so that Eq. (4.1.3) is valid given the same fluid conditions. However, for high velocities one must also account for compressibility effects [15] given by the Mach number to obtain dynamic similitude.

$$\left(\frac{V}{V_c}\right)_m = Mc_m = Mc_p = \left(\frac{V}{V_c}\right)_p \tag{4.1.4}$$

A frequently used definition is solidity, which is the ratio of the total propeller blade area to propeller disk area.

$$s = \frac{A_b}{A_p} \tag{4.1.5}$$

4.2   LIFT

A brief physical explanation for lift produced by an airfoil [16] is presented without going into the rigorous concepts such as circulation and lifting line theory. When streamlines flow around an airfoil, the airfoil causes the streamlines to curve over the top surface, as seen in Figure 4.2.1 A. Considering a small parcel of air moving along a streamline just above the airfoil's top surface, Figure 4.2.1 C. Since the parcel follows a curved path it must be accelerated in the centripetal direction, hence a net force on the parcel must exist downward in the radial direction. Since the effects of gravity on the air parcel is negligible, the only forces present to explain this net force are pressure forces. To produce a downward net force, the pressure at the top of the parcel must be greater than at the bottom. This means that the ambient pressure far above the airfoil is greater than the pressure just above the airfoil, hence the pressure drops as one moves downward towards the top surface of the airfoil.
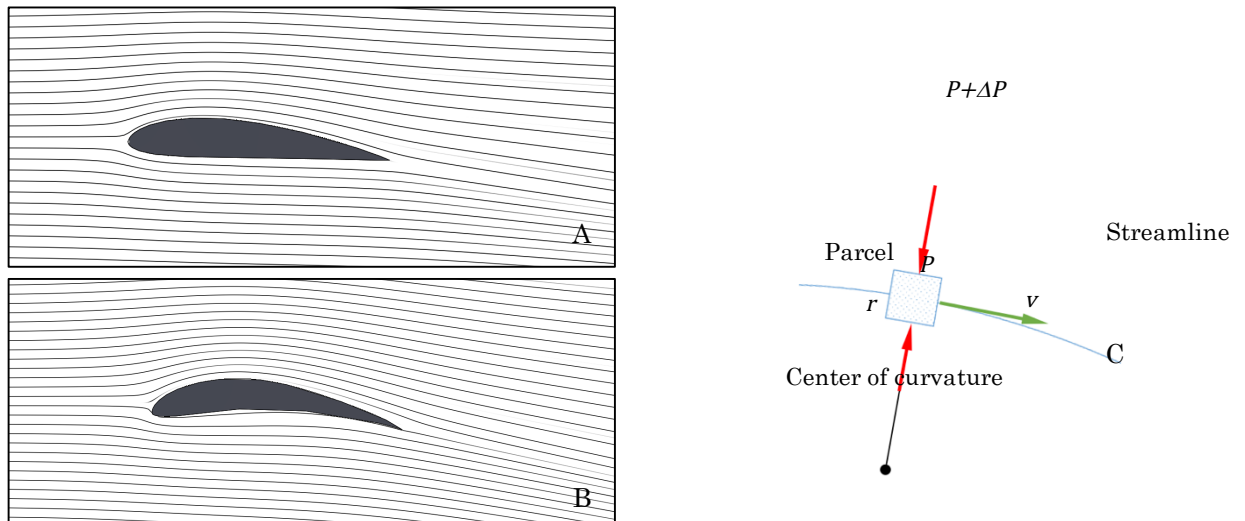

Figure 4.2.1. A: NACA 4412 airfoil produces curvature of streamlines over the top surface. B: GOE 531 airfoil with large camber produces curved streamlines over and under the cross section. C: A parcel of air moving along a curved streamline must experience an inward acceleration caused by the difference in pressure ΔP.

An airfoil with a curved bottom surface also generates streamlines with curvature in the same direction as the streamlines on the top, as seen in Figure 4.2.1 B. The air parcels in the streamlines below the airfoil are also accelerated downward, meaning that the pressure just below the airfoil must be greater than the ambient pressure far below the airfoil. Hence the pressure increases as one moves up toward the bottom surface of the airfoil. With a negative- and positive relative pressure at the top and bottom surfaces respectively, a net upward force acts on the airfoil, producing lift. From a design perspective, creating surfaces that causes the streamlines to curve, will induce lift as explained above. This insight will affect the choice of airfoil cross section and design of other aerodynamic surfaces.

Considering the wing air system globally, the air leaving the wing has a downward component. Thus, considering Newton's third law, lift can be considered as the reaction of the downward action of the air mass. This lays the basis for section 4.3.

4.3   MOMENTUM THEORY - MT

Momentum theory applies Newton's laws and the basic conservation laws of fluid dynamics to the propeller and flow as a whole, to estimate propeller performance. Conservation of mass, momentum and energy are applied to the system. When the fluid gains speed after leaving the

propeller, its momentum has been changed. It then follows from Newton's second law, $\Sigma F = d(m\mathbf{v})/dt$ that a force has been applied to the fluid. But, for every action there must be an equal and opposite reaction given by Newton's third law. The fluid then pushes back on the propeller with the same force, thus producing thrust. The momentum increase given by the propeller to produce thrust, implies that energy has been added by the propeller. This energy constitutes the induced power of the rotating wing, which is equivalent to the induced drag of a fixed wing.

The assumptions for momentum theory are the following:

1. *The flow is assumed to be inviscid and incompressible.*

2. *All rotation of the fluid within the streamtube is neglected.*

3. *The flow velocity is assumed uniform over each cross-section of the streamtube.*

4. *The pressure is assumed uniform over each cross-section of the streamtube.*

4.3.1   OPEN AIR PROPELLERS

The model for momentum theory is illustrated in Figure 4.3.1. The ideal propeller disk consists of an infinite number of blades with area, A_p which is enclosed by a streamtube. At station 1 just downstream of the propeller disk, the pressure jumps to p_d and the velocity induced by the propeller is desinated V_i. At the end of the streamtube at station 2 the pressure returns to freestream pressure and the slipstream velocity is designated V_s.
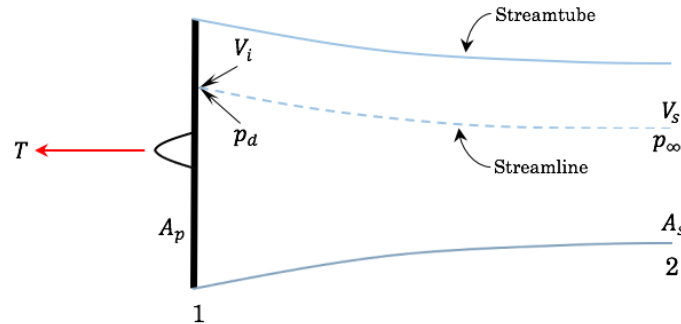
Figure 4.3.1. Momentum theory model for open air propeller.

Since the conditions are static and the freestream velocity is considered to be zero, the conservation of energy requires that all of the mechanical power on the propeller is found again in the slipstream at station 2, where freestream/ambient pressure has been reached:

$$P_i = \frac{1}{2}\dot{m}V_s^2$$

(4.3.1)

This power is the same as the induced power given off by the propeller:

$$P_i = TV_i$$

(4.3.2)

Combining Eq. (4.3.1) and (4.3.2):

$$TV_i = \frac{1}{2}\dot{m}V_s^2$$

(4.3.3)

Considering the momentum theorem for the streamtube, with freestream velocity equal to zero this becomes:

$$T = \dot{m}V_s$$

(4.3.4)

Using Eq. (4.3.4) to eliminate thrust from Eq. (4.3.3) and reducing:

$$\dot{m}V_sV_i = \frac{1}{2}\dot{m}V_s{}^2$$

$$V_i = \frac{1}{2}V_s \qquad (4.3.5)$$

This result also implies that $A_p = 2A_s$. Revisiting Eq. (4.3.4) combined with Eq. (4.3.5) to remove V_s and inserting for mass flow:

$$T = 2\rho A_p V_i^2$$

Solving for V_i

$$V_i = \sqrt{\frac{T}{2\rho A_p}} \qquad (4.3.6)$$

Inserting Eq. (4.3.6) in (4.3.2) gives the ideal power required, for an open air propeller in static conditions:

$$P_i = T\sqrt{\frac{T}{2\rho A_p}} \qquad (4.3.7)$$

Eq. (4.3.7) reveals that for a given power the gain in thrust decreases as the propeller disk area grows. Conversely, for a required thrust, reducing the propeller disk area increases the demand for power dramatically.

4.3.2   DUCTED FANS

Figure 4.3.2. Momentum theory model for a ducted fan in static conditions.

The same physical assumptions for momentum theory with open air propellers apply for ducted fans. A new parameter δ, called the diffusion parameter is introduced. This parameter is defined by the ratio of the slipstream area to the fan disk area.

Momentum theory models for ducted fans in the established literature are scarce. The following derivation is based upon the paper, *"Aerodynamics of Shrouded Propellers"* by M. Lazareff [17] and crosschecked with [18].
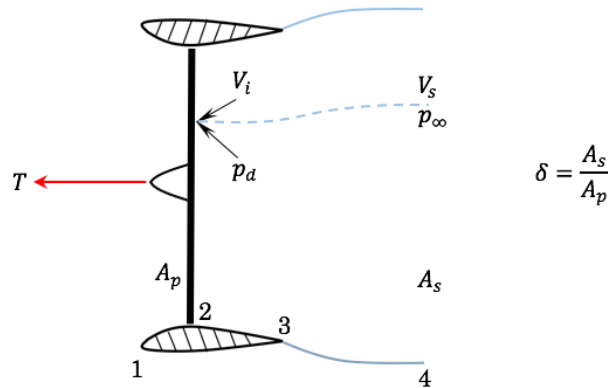
Since the conditions are static and the freestream velocity is considered to be zero, the conservation of energy requires that all of the mechanical power on the propeller is found again in the slipstream at station 4, where freestream/ambient pressure has been reached:

$$P = \frac{1}{2}\dot{m}V_s{}^2 = \frac{1}{2}\rho A_s V_s{}^3 \tag{4.3.8}$$

Solving for V_s and inserting the diffusion parameter, δ shown in Figure 4.3.2:

$$V_s = \left[\frac{2P}{\rho A_s}\right]^{\frac{1}{3}} = \left[\frac{2P}{\rho \delta A_p}\right]^{\frac{1}{3}} \tag{4.3.9}$$

Considering the momentum theorem for the streamtube, with freestream velocity equal to zero this becomes:

$$T = \dot{m}V_s = \rho A_s V_s{}^2 \tag{4.3.10}$$

Solving for V_s and inserting the diffusion parameter, δ:

$$V_s = \left[\frac{T}{\rho \delta A_p}\right]^{\frac{1}{2}} \tag{4.3.11}$$

Setting Eq. (4.3.9) equal to (4.3.11) and solving for the induced power required:

$$\left[\frac{2P}{\rho \delta A_p}\right]^{\frac{1}{3}} = \left[\frac{T}{\rho \delta A_p}\right]^{\frac{1}{2}}$$

$$P_i = \frac{T}{2}\sqrt{\frac{T}{\rho \delta A_p}} \tag{4.3.12}$$

As a check of Eq. (4.3.12), inserting $\delta = 0.5$ which is equivalent of an open air propeller under static conditions, Eq. (4.3.12) reduces to Eq. (4.3.7).

The results for the preceding derivations are summarized in Table 4.3.1. Momentum theory predicts that the ducted fan not only produces 20 % more thrust for a given disk area and power over the open air propeller, but also consumes 30 % less energy for a given thrust and disk area.

Table 4.3.1. Comparison of momentum theory results for open and ducted fans.

| | Open propeller | Ducted fans | |
Condition	$(\delta = 0.5)$	$\delta = 1$	$\delta = 2$
Given P_i and T	D_p	$0.707\,D_p$	$0.5\,D_p$
Given P_i and D_p	T	$1.26\,T$	$1.55\,T$
Given T and D_p	P_i	$0.707\,P_i$	$0.707\,P_i$

The results obtained in this section are highly theoretical and gives an early estimate for performance of propellers and ducted fans. It has been shown that the prediction of 20 % higher thrust for ducted fans over an equivalent open air propeller is a low estimate. Experiments has shown that ducted fans can produce as much as 50 % more thrust over equivalent open air propellers [19] depending on duct shape. This is because momentum theory does not account for the additional lift produced by the duct itself. In addition, the effective area of an open air propeller is smaller than the propeller's physical area due to tip vortices.

4.4   PROPULSIVE EFFICIENCY

4.4.1   SPECIFIC THRUST

Consider the basic relations for ideal power and thrust above, Eq. (4.3.1) and (4.3.4). Defining specific thrust as

$$\frac{T}{P_i} = \frac{\dot{m}V_s}{\frac{1}{2}\dot{m}V_s{}^2} = \frac{2}{V_s} \tag{4.4.1}$$

From an energy-economic standpoint this simple relation shows that to maximize thrust for a given energy input, one must move large amounts of air with a low velocity increase.

4.4.2   FIGURE OF MERIT

For a rotor or fan in hover condition, figure of merit is used to measure the aerodynamic hovering efficiency [13]. It compares the actual rotor performance with the performance of an ideal rotor.

$$M = \frac{P_i}{P} \tag{4.4.2}$$

From [20] the figure of merit for several experimental VTOL-aircraft has an effective mean value of M≈0.75. Figure of merit is useful for comparing rotors with different airfoil sections or twist.

4.5   BLADE ELEMENT THEORY - BET

The following derivation is a simplified form of BET guided by [21] and [13]. This theory will lay the foundations for designing the blades. In Figure 4.5.1 below, a cross section of the blade with relations to wind speeds is shown. The lift- and drag forces acts perpendicular and parallel to the relative wind vector U respectively. The force vectors act at the aerodynamic center on the cross-section located 0.25c from LE for cambered airfoils [21].
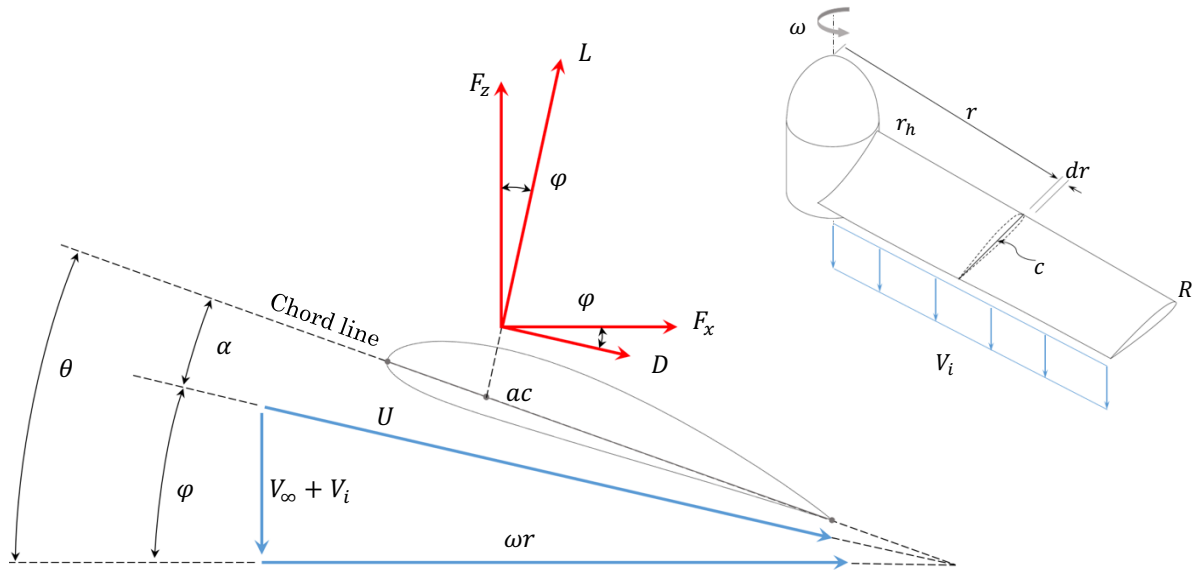

Figure 4.5.1. Blade cross-section at an arbitrary radius, r on the blade shown in the top right corner. Showing air velocities (blue vectors) and forces acting on the section (red vectors).

Sectional lift- and drag forces per unit length are defined as the following:

$$L = \frac{1}{2}\rho U^2 c C_L \tag{4.5.1}$$

$$D = \frac{1}{2}\rho U^2 c C_D \tag{4.5.2}$$

Where U is the resultant velocity seen by the airfoil section, c is the chord length and C_L, C_D are the coefficient of drag and lift respectively.

From tabulated airfoil data, the coefficients C_L and C_D are functions of $\boldsymbol{R}$. When reviewing data for a selection of common airfoils in [22] and [1], the coefficients vary little within the relevant range of $\boldsymbol{R}$ given by Eq. (4.1.1). With relevant parameters, the relevant range of $\boldsymbol{R}$ becomes:

$$\boldsymbol{R}(r) = \frac{Uc}{\nu} \quad , r_h < r < R \tag{4.5.3}$$

Hence, average values for C_L and C_D within the relevant range of $\boldsymbol{R}$ are used to simplify calculations with only a small sacrifice in accuracy.

Expressing U in terms of its component speeds:

$$U^2 = \omega^2 r^2 + (V_\infty + V_i)^2 \tag{4.5.4}$$

Where ω is the angular velocity, r is the radius and V_∞, V_i are freestream and induced velocity respectively.

The forces perpendicular and parallel to the propeller plane can be written as:

$$F_z = L \cos\varphi - D \sin\varphi = \frac{1}{2}\rho U^2 c [C_L \cos\varphi - C_D \sin\varphi] \tag{4.5.5}$$

$$F_x = L \sin\varphi + D \cos\varphi = \frac{1}{2}\rho U^2 c [C_L \sin\varphi + C_D \cos\varphi] \tag{4.5.6}$$

Thrust

If the blade consists of an infinite number of cross-sections, thrust per section can be expressed in terms of N, number of blades:

$$dT = N F_z \, dr \tag{4.5.7}$$

Inserting Eq. (4.5.4) and (4.5.5):

$$dT = \frac{N\rho c}{2} [\omega^2 r^2 + (V_\infty + V_i)^2][C_L \cos\varphi - C_D \sin\varphi] \, dr \tag{4.5.8}$$

The total thrust for all the blades is then found by integrating from the hub radius to the blade tip radius. Assuming uniform inflow, constant chord with averaged coefficients and constant aerodynamic angle of attack, the twist is given by the ideal twist distribution:

$$\varphi(r) = \tan^{-1}\left(\frac{V_\infty + V_i}{\omega r}\right) \quad , r_h < r < R \tag{4.5.9}$$

Where V_i is given by MT and Eq. (4.3.6) and (4.3.11) for open-and ducted respectively. Inserting (4.5.11) in (4.5.8) and evaluating total thrust gives the following integral:

$$T = \frac{N\rho c}{2} \int_{r_h}^{R} [C_L \cos \varphi(r) - C_D \sin \varphi(r)][\omega^2 r^2 + (V_\infty + V_i)^2] \ dr \qquad (4.5.10)$$

This integral can be simplified using the downwash angle at 0.75R to approximate $\varphi(r)$. The trigonometric functions can then be moved outside of the integral:

$$T = \frac{N\rho c}{2} [C_L \cos \varphi_{0.75} - C_D \sin \varphi_{0.75}] \int_{r_h}^{R} \omega^2 r^2 + (V_\infty + V_i)^2 \ dr \qquad (4.5.11)$$

$$T = \frac{N\rho c}{2} [C_L \cos \varphi_{0.75} - C_D \sin \varphi_{0.75}] \left[\frac{\omega^2 r^3}{3} + (V_\infty + V_i)^2 r \right]_{r_h}^{R} \qquad (4.5.12)$$

Torque

Torque per section is defined as follows:

$$dQ = NF_x r \ dr \qquad (4.5.13)$$

Inserting Eq. (4.5.4) and (4.5.6) and with the same assumptions as above, the integral for torque becomes:

$$Q = \frac{N\rho c}{2} \int_{r_h}^{R} [C_L \sin \varphi(r) + C_D \cos \varphi(r)][\omega^2 r^2 + (V_\infty + V_i)^2] r \ dr \qquad (4.5.14)$$

Using the same simplification with constant downwash angle at 0.75R, the torque can be expressed as:

$$Q = \frac{N\rho c}{2} [C_L \sin \varphi_{0.75} + C_D \cos \varphi_{0.75}] \left[\frac{\omega^2 r^4}{4} + \frac{(V_\infty + V_i)^2 r^2}{2} \right]_{r_h}^{R} \qquad (4.5.15)$$

Power

The power needed to turn the propeller is:

$$P = Q \ \omega \qquad (4.5.16)$$

4.6   DUCTED FANS/PROPELLERS

From section 4.3.2 momentum theory showed that ducted fans have appealing benefits. However, some undesirable effects are associated with ducted fans in transversal flight [23], illustrated in Figure 4.6.1 below.
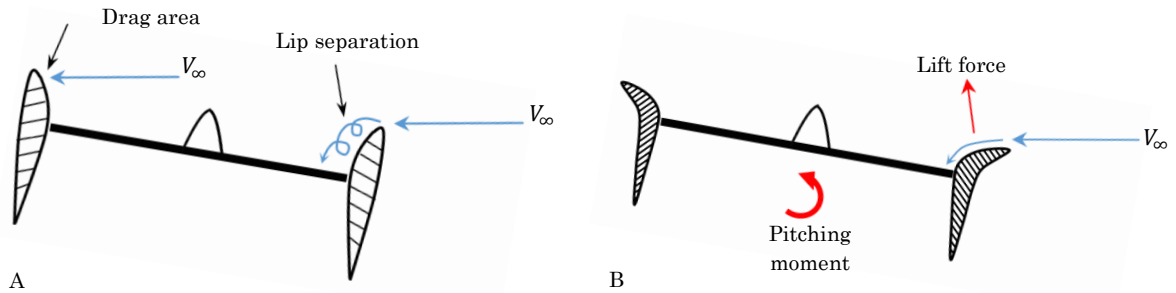

Figure 4.6.1. A: The incoming freestream hits the leading edge of the duct, causing separation and turbulent air-flow hits the fan. The trailing part of the duct has a surface perpendicular to the freestream crating drag. B: Added lips keeps flow on to fan laminar, but the curved surface creates a lift force causing a pitching moment on the whole duct.

4.7   STATORS

A propeller leaves rotation or swirl in the slipstream imposed by the rotating blades. This means that some of the kinetic energy of the air-mass in axial direction has been converted in to rotational energy. The tangential component of the rotating air constitutes a loss in thrust compared to if the air had purely axial movement. By placing stationary blades vertically, the rotation of the slipstream can be straightened and regaining some of the loss in thrust.
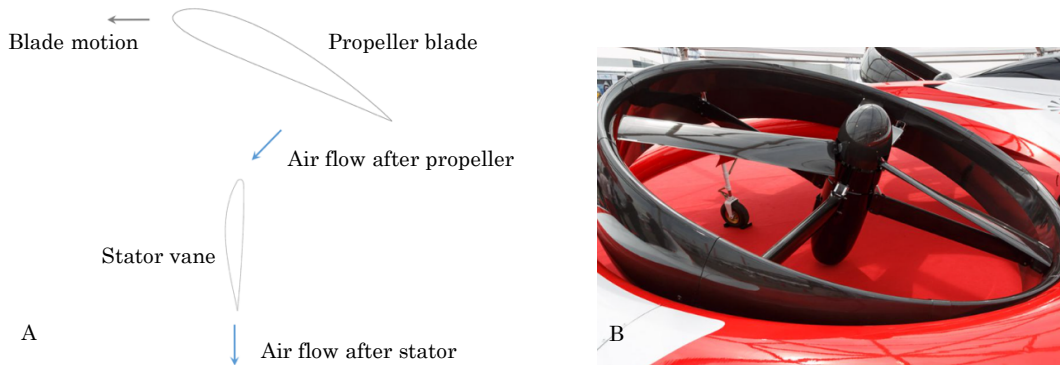
Figure 4.7.1. A: Illustration of stator principle showing cross-section of propeller blade and stator vane. The rotation in the slipstream created by the propeller can be straightened by a stator. B: Example of a ducted propeller with four stator vanes supporting the propeller/engine assembly. [24]

In the case of ducted propellers, struts are needed to support the duct. It is then natural that these struts are designed with an airfoil section to straighten the flow. Figure 4.7.1 shows the principle of stators, the stator vane can be implemented as struts for the duct.

The stator blades, also known as straightener vanes can be design so that they not only straighten the flow, but also counter the reaction torque imposed on the aircraft by the propeller and engine. The stator vanes have to be designed to match the torque generated by the propeller for each radial station, se [25] for "Flow straightener design by element torque matching"

4.8   NOISE

One of the most dominant noise components in rotating wings are noise from the blade tip vortices. The vortex shed from the blade tips have high local air speeds that generate a high-pitched sound. This sound can be heard as the buzzing sound from propeller planes. A way to reduce noise is to reduce the size or eliminate the tip vortices. This can be done by reducing tip speed and/or having a slim cross-section profile and tapered or swept blade profile at the tips. In this way, the transition between the upper and lower surfaces of the blades are smoothened and vortex size are reduced. Lowering not only noise, but at the same time increasing aerodynamic efficiency by minimizing energy loss by increased drag to the vortices. Another way of dealing with the tip vortices are to mount winglets on the blade tips to create a barrier that reduces the vortices formation. This is used extensively on commercial jets to decrease drag, however not in rotating wings. Finally, a duct can be fitted around the propeller, and with sufficiently small gap between the blade tips and the duct's inner wall, the vortices can be eliminated as the duct acts as a physical barrier between the lower and upper side of the blades, preventing the high pressure under the blade to travel around the tip and in to the low-pressure region of the blades top surface.

Noise have been found to be a function of tip speed to the power of five. So, any changes in tip speed has a profound impact on noise levels [11].

4.9   THEORETICAL TOOLS

The derived equations for MT and BET in sections 4.3 and 4.5 were implemented in an excel-sheet, from now on referred to as Texcel. This excel-sheet will be used as a development tool throughout the rest of this thesis and a printout can be seen in [J]. Solutions for the BET-integrals can be seen in [G-I].

5   EXISTING AND FUTURE CONCEPTS

With the theoretical foundation presented, a closer look at existing and future concepts follows.

The review of existing concepts will mainly focus on people carrying drones and VTOL-aircrafts. Various concepts will be explored, both pure design studies and more substantial concepts with prototypes. Most time will be spent on concepts from well established companies in aviation, but various design studies are also valuable considering the possibility that established aviation companies can be somewhat conservative or fixed in their thinking.

5.1.1   EHANG 184

The Ehang 184 is a drone based personal transport concept from the Chinese based company Ehang. It features two contra-rotating open air propellers in each corner at the end of retractable arms. The drone is designed for carrying one person over short to medium distances with a maximum height of 500 meters above sea-level. The operation of the drone is fully autonomous, the passenger just enters the destination and the flight is controlled by a control center located in each country of use. At this time, Ehang has only permission to fly in China where they have built a control center. According to Ehang, over 200 successful test flights have been made. Video footage exists of the drone in flight. [26]

Figure 4.9.1. To the left: Overview of the Ehang 184 with specifications. To the right: Image of the control center in China. [26]

Specifications	Type/Value
Engine type	Electric
Power	152 kW (8 motor)
Battery capacity	17 kWh
Cruise speed	60 km/h
Range	25 min cruise time – Approx. 25 km
Gross weight	340 kg (100 kg payload)
Specific weight	2.2 kg/kW
Rotor diameter	1.6 meter

The whole structure is made from carbon fiber composite with a few parts in aluminum. Also, stability in crosswind makes a good case for open air propellers. Considering that this type of vehicle is designed to be used in densely populated areas. Apart from the humming noise from the end vortices of the propeller blades, one major concern arises with the propeller layout; Safety, both propellers are in leg height (Figure 4.9.3). It is hard to imagine this drone landing and

Figure 4.9.2. The propellers sit low above ground

taking off in areas where there are people nearby. The low placement of the rotors also makes the drone inherently less stable than if the rotors where placed higher.

5.1.2 TERRAFUGIA TF-X

The TF-X concept comes from the Boston based company Terrafugia. Small enough to fit in a garage it's basically a car with VTOL capabilities. It has four wheels and operates like and ordinary car on the road. For flight, the wings with an electric rotor and six blade rotor folds out and takes off much like the Bell Boeing V-22 Osprey or the AgustaWestland AW609. Both a car and a VTOL aircraft the TF-X might be the most complete concept of a flying car to date. No prototype has been built yet, but Terrafugia hopes to have a working prototype by 2021.

Figure 4.9.4. From the left: 1. TF-X in driving mode with wings and nacelles tucked in to the body. 2. VTOL mode. 3. Flying mode with rotor blades folded in and a ducted fan in the rear generating thrust for forward flight. [27]

Specifications	Type/Value
Engine type	Hybrid electric
Power (electric motor pods)	1000 kW
Cruise speed	320 km/h
Range	800 km
Gross weight	
Specific weight	

When transitional flight is achieved the large ducted fan in the rear - powered by a 300-horsepower combustion engine - provides forward thrust, the rotor blades folds back to reduce drag and the wings providing all the lift. Each rotor is powered by a 500 kW electric motor and the combustion engine charges the batteries during flight in addition to powering the ducted fan.

5.1.3 AUGUSTAWESTLAND PROJECT ZERO

The rotor division of the Italian Company Finmeccanica, AgustaWestland has built a VTOL prototype called Project Zero. A testbed for future technology Project Zero has a radical design with two ducted tilt-rotors built in to the wings. The two in wing rotors are the only propulsion devices on the aircraft providing both VTOL-capabilities and thrust in forward flight when all the lift is produced by the wing area.
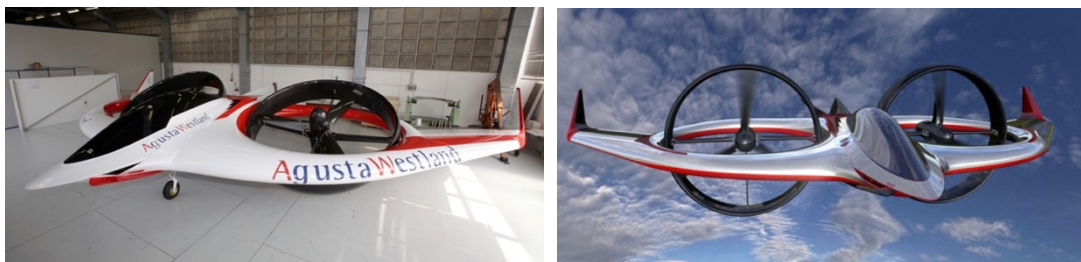

Fiure 4.9.5 AgustaWestland's Project Zero. [28]

Specifications	Type/Value
Engine type	Electric
Power	
Gross weight	

Specifications of this project are scarce. The fuselage is made from carbon fiber and the electric motors fitted in the rotor hubs are powered by a battery pack. The large rotor design with only three blades suggest that AW main focus for this VTOL-design is efficiency. As shown in section 4.3, efficient rotors are large rotors and few blades reduces the induced power needed. Interestingly it also features individual control over each rotor blade's pitch: "*We can vary the blade angle constantly as it goes around the azimuth to reduce vibration, cancel eternal noise, improve aerodynamic efficiency and alleviate gust response to produce a smoother and quieter flight*" – James Wang, VP Marketing [29].

5.1.4   XTI TRIFAN 600

This VTOL private plane combines ducted fans and a fuselage to replace both a helicopter and a private jet. Taking off horizontally with its three seven-foot diameter, five blade ducted fans, powered by two Honeywell HTS900 turboshaft engines shortens travel time on medium to long distances. Once transitional flight has been made the rear fan inside the fuselage is covered and the two in-wing fans provides forward propulsion.
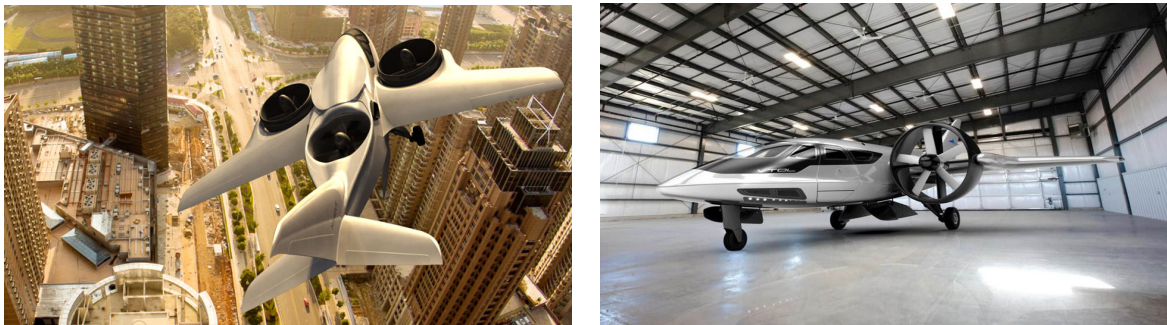

Figure 4.9.6. Trifan 600 in hovering and flight mode. [30]

Specifications	Type/Value
Engine type	Gassturbine
Power	1900 kW
Cruise speed	630 km/h
Range	2780 km
Gross weight	3850 kg
Specific weight	2.0 kg/kW

Still in design stage no prototype yet exists and funding for a prototype is ongoing. Designed by people who has had a long career in aviation industry this concept deserves some attention. Like the Boeing Sky Commuter, XTI has also opted for a three-fan configuration and not four like the Ehang 184 or Moller SkyCar. Like the AW Project Zero the fan blades are also of constant-cord design which is typical for ducted fans. The cord of the ducts is medium long, designed for greater efficiency in higher forward speeds.

5.1.5   SKELDAR UAV HELICOPTER

A joint venture between UMS AERO Group AG and Saab AB, the Skeldar unmanned helicopter is designed for surveillance operations for military and civil applications. With a 4.6-meter diameter two blade rotor and light weight structure, energy consumption can be kept low with the use of a high revving gas turbine.

Figure 4.9.7. Skeldar V-200 in flight. [31]

Specifications	Type/Value
Engine type	Gassturbine
Power	40 kW
Max air speed	140 km/h
Range	5 + hours
Max take-off weight	235 kg
Specific weight	5.8 kg/kW
Rotor diameter	4.6 m

5.1.6   VOLOCOPTER

The German based company E-VOLO aim to bring helicopter based transport more accessible by making a fully electric helicopter/drone design that is low cost and require very little training to operate.

Figure 4.9.8. Volocopter VC200. [32]

Specifications	Type/Value
Engine type	Electric
Power	-
Range	20 min

With 18 small rotors, the Volocopter has opted for redundancy in form of numbers. According to E-VOLO, the Volocopter can still fly if several of the engines fail. A parachute is also fitted for worst case scenarios. Keeping rotor-size low, enables the use of small electric motors with none or low gear-ratio. In this way costs can be kept low compared to using large engines and gearbox. Specifications of the

Figure 4.9.9. Volocopter in flight.

Volocopter are scarce in terms of weight and power. However, like most electrical drones a flight time of 20 min is stated.

5.1.7 DRONE AMBULANCE CONCEPT

A purely conceptual design from the Texas based design house Agrodesign, displays an ambulance drone with room for one patient and one medic. This concept shows one of the many application of people-carrying drones. This concept could fill the gap between an ambulance car- and helicopter. With a small footprint, it could land almost anywhere with a quick response time.

Figure 4.9.10. Ambulance drone in parked position with rotors folded up. [33]

The concept is purely regarded for inspiration. Not paying too much attention to the details, the overall layout is interesting. Placing the rotors high up for in flight stability and integrating the propeller shroud in the structure are interesting features. However, folding rotor arms and landing gear, prompts a heavy construction. There is also no space for engine placement in the rotors.

Figure 4.9.11. The ambulance drone in flight with patient and medic inside.

5.2   SAFETY PHILOSOPHY

Since a new transport mode is in its infant stages; small scale VTOL personal transport by air. An opportunity for implementing safety as an integrated part of the design from the very beginning is present. In other transport modes, such as automobiles and airplanes, attention was only made to the physical and technological challenges to overcome when they were conceived. Safety was only thought of as accidents and other safety issues emerged over time. Hence safety features were only integrated ad-hoc over time as focus on safety grew. With no present regime or paradigm for small scale VTOL personal transport, safety should be intergraded in the design from the very beginning. The vision for safety should be superior than the closest present technology, helicopters. Catastrophic accidents caused by malfunctions in the helicopters drivetrain, or even rotor separation leaving the fuselage helpless, should not be an accepted scenario for this new mode of transport.

It is evident that Ehang and E-VOLO has the same philosophy in their designs by redundancy of rotors, but keeping the aircraft from falling out of the sky is only one aspect of safety. While the people inside the aircraft are kept safe, open rotors in densely populated areas can not be considered safe for the surroundings. First off, a person could too easily come in contact with the rotors by accident or wrongdoing. Secondly, the rotors could encounter surrounding objects or the ground if the aircrafts tips over. This can lead to fragmentation of the blades and sending projectiles out in the surroundings.

6   PRODUCT DESIGN SPECIFICATION

In this chapter, the theory in chapter 4 together with the stated objectives are applied to develop specifications for a thruster unit.

6.1   PROJECT OBJECTIVE

From section 2.1 the objectives are:

Main Objective

To study and design a turbine based thruster that enables VTOL capabilities, accounts for safety aspects and can be integrated in a future system solution for the light weight transport concept Dolphin.

Objectives of effect

- o   Personal safety.
- o   VTOL-capabilities.
- o   Light weight.
- o   Energy efficient.
- o   Low noise.

Objectives of Achievement

- o   Redundant lift capacity.
- o   Parachute compatible.
- o   Physical protection against moving parts.
- o   Can be integrated in Dolphin concept.
- o   Electric power source.
- o   Thruster design.

6.2   EARLY TECHNOLOGY EVALUATION

This section evaluates what types of thrust producing technologies that are available, within the project objectives in the section above, in order to facilitate VTOL-capabilities. Technologies that inherently violates the project objectives are discarded and not evaluated in the concept generation.

The selection of technologies is done by comparing the technologies against a reference technology, with criteria based on important product objectives. In this case propellers are used as a reference because of the widespread use of propellers and rotors in hovering aircrafts today. The criteria in the evaluation are absolute; this means that a potential technology must fulfill all criteria. Technologies that are significantly worse in a given criteria than the reference are given a red cross. Conversely, technologies as good as or better a given a green checkmark.

Table 6.2.1. Absolute evaluation matrix for thrust producing hovering technologies.

Technology	Efficiency	Noise	Electric powered
Rotors	✓	✓	✓
Propellers	R e f e r e n c e T e c h n o l o g y		
Ducted fans	✓	✓	✓
By pass turbo jets	✓	✗	✗
Turbo jets	✗	✗	✗
Rockets	✗	✗	✗

In addition to propellers, rotors and ducted fans are the only technologies viable to meet the product objectives according to Table 6.2.1. Figure 6.2.1 shows different technologies with associated slipstream velocities. Since noise is a function of air velocity, the technologies with significantly higher slipstream velocities than the reference, does not qualify. In addition to noise, a high slipstream velocity also contributes to ground erosion and up-swirl of particles from the ground.
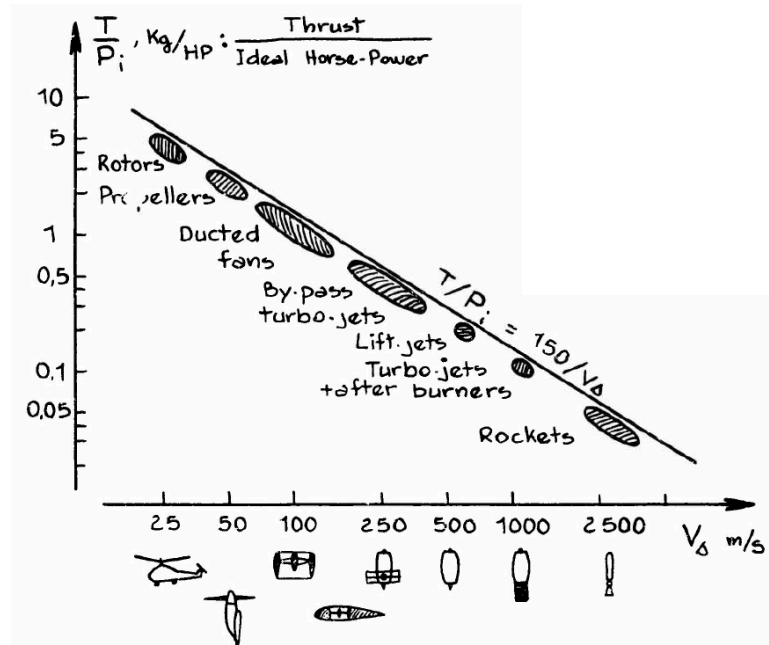

Figure 6.2.1. Slipstream velocity plotted against specific thrust for various VTOL-technologies. Adapted from [20]

From Eq. (4.4.1), high values of V_s also equates to a low specific thrust as seen in Figure 6.2.1. This indicates a low efficiency. In general, this section concludes that combustion bases technologies are left behind and air-pushing rotating wing technologies are candidates for concept generation.

6.3 TECHNOLOGICAL CHALLENGES AND LIMITATIONS

6.3.1 EFFICIENCY

Left with three technologies from the previous section, this section gives a general comparison of the rotor, ducted fan and propeller against each other. In general, large rotors are favorable in terms of efficiency. A large amount of thrust can be produced with a low angular velocity, high mass flow and low slipstream velocity, maximizing specific thrust. This explains the success of large rotors in helicopters. The specific thrust decreases with decreasing disk diameter as shown in Figure 6.3.1.
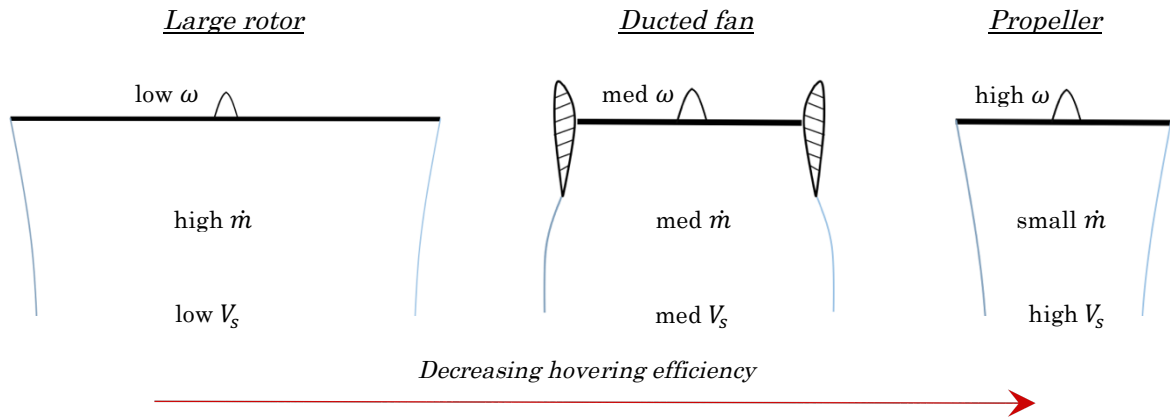
Figure 6.3.1. Hovering efficiency decreases as the diameter of the rotor or propeller gets smaller.
However, adding a duct to a propeller inhibits the slipstream contraction and increasing the mass flow.

Adding a shroud or duct surrounding the propeller improves efficiency and can generate the same specific thrust on a smaller disk diameter given by the results in Table 4.3.1.

6.3.2 LIMITATIONS OF ENGINE TYPE

Large rotors give low power requirements - since specific weight can be kept high- , but need high torque. Thus, electric engines are not suitable due to their low rpm characteristics. Therefore, gas turbines with low power at high rpm can be reduces via ratio to give high torque to the rotor. This has long been the winning recipe for helicopters.
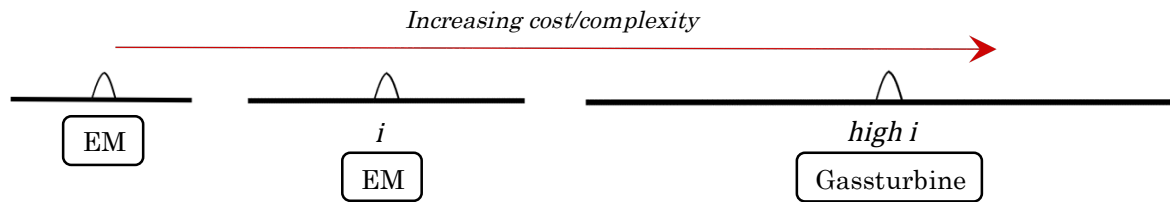

Figure 6.3.2. Illustration of the relationship between engine type, the need for gear ratio and rotor size.

When electric engines are used, limitations naturally falls on the rotor diameter to keep torque low. With high performing electric engines, the rpm can be reduced to give needed rotor torque. Otherwise, reducing size of the rotors and increasing number of rotors to maintain swept area and avoiding gearboxes.

6.3.3 NOISE

Noise is a function of air speed. Tip vortices have large local air speeds – high pitch noise. Se section 4.8.

6.3.4 DUCT/SHROUD

Separation of airflow into to the propeller/fan and drag areas. Se section 4.6.

6.4   PRELIMINARY EVALUATION OF KEY CONCEPT FIGURES

In order to establish baseline parameters for the thruster unit, required performance, efficiency and weight of the aircraft has to be evaluated. The resulting figures will give a baseline and constraints on the thruster unit.

6.4.1   PERFORMANCE

For convenience, the total thrust needed is expressed in terms of the gross weight, W_G of the aircraft times a performance factor, k.

$$T_T = kW_G \tag{6.4.1}$$

In order to estimate the total thrust, the components of the total thrust are defined and summarized to give total thrust in terms of gross weight and a performance factor. For vertical acceleration, the maximum value is set to 2.0 m/s².

Components of total thrust

Hover	Vertical acceleration 2.0 m/s²	Parasitic drag	Redundancy
W_G	$ma_v = W_G \dfrac{a_v}{g} = 0.2W_G$	$0.1W_G$	$0.1W_G$

$$T_T = W_G + 0.2W_G + 0.1W_G + 0.1W_G$$

$$T_T = 1.4W_G \tag{6.4.2}$$

The total needed thrust is thus 1.4 times the gross weight. This result is similar to existing commercial helicopters, se [L].

6.4.2   WEIGHT AND EFFICIENCY

In order to estimate a minimum swept area and gross weight-range in terms of efficiency, the definition for specific thrust is used as a starting point.

$$\frac{T}{P_i} = \frac{2}{V_s}$$

Inserting the V_s result from section 4.3.1 (Eq.(4.3.6)) and the definition of figure of merit (Eq.(4.4.2)) gives:

$$\frac{T}{P} = \frac{M}{\sqrt{\dfrac{T}{2\rho A_p}}} \tag{6.4.3}$$

Inserting the expression for total thrust, Eq.(6.4.2):

$$k\left(\frac{W_G}{P}\right) = \frac{M}{\sqrt{\dfrac{kW_G}{2\rho A_p}}}$$

Solving for W_G expressed in terms of specific weight $\left(\frac{W_G}{P}\right)$, the performance factor k and figure of merit, gives the following linear expression with swept area A_p as variable:

$$W_G = \frac{2M^2\rho}{\left(\frac{W_G}{P}\right)^2 k^3} \cdot A_p \qquad (6.4.4)$$

The equation shows that gross weight is sensitive to efficiency $\left(\frac{W_G}{P}\right)$, and highly sensitive to performance (k) as one would expect. Considering the ranges of specific weight for different aircrafts with - hovering capabilities - to help narrow out a relevant range of specific weight to implement in Eq. (6.4.4).
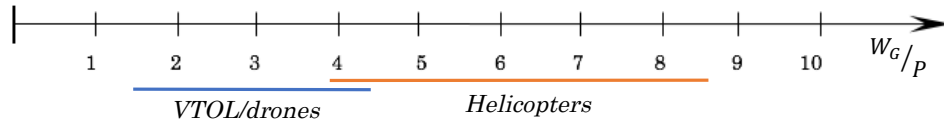
Figure 6.4.1. Range of specific weight for helicopters and VTOL/drones.

With the typical experimental figure of merit result of 0.75, $k = 1.4$ and standard atmosphere at sea level at 20 C° [F], Eq. (6.4.4) is plotted in Figure 6.4.2. The range of $(2 - 4.5)$ kg/kW for specific weight is selected since most existing solutions from section 5, has a specific weight of approx. 2.0 kg/kW. This project should aim to be more efficient than these existing concepts. Therefore, a design with specific weight less than 2 kg/kW are not considered. The diagram below explores possible combinations of gross weight and swept area with specific weight from 2 to 4.5 kg/kW.
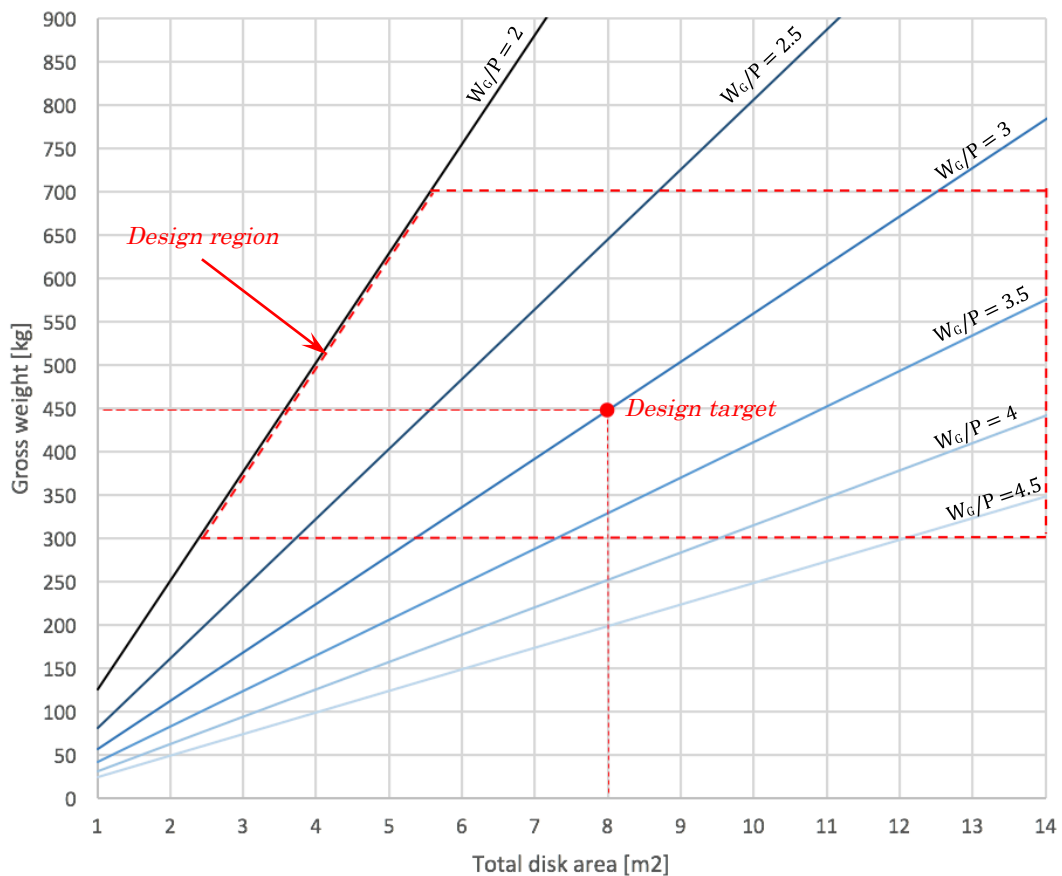

Figure 6.4.2. Gross weight plotted against total swept area with specific weight in the range of 2 - 4.5 with increments of 0.5. Notice how for a given weight, the gain in efficiency decreases with increasing swept area.

From Figure 6.4.2 above, a design target has been selected. This design target gives the following baseline specifications, summarized in Table 6.4.1 below.

Table 6.4.1. Estimates of key figures for the concept to target.

Design target	Value	Unit
Gross weight	≤ 450	kg
Specific weight	3.0	kg/kW
Total Power	≥ 150	kW
Total swept area	≥ 8	m^2
Total thrust	≥ 6180	N
Performance factor	1.4	-

Assuming advances in battery technology in the near future, the aircraft is assumed to carry 50 kWh within the gross weight limit of 450 kg. Estimates of flight time becomes:

$$Max\ flight\ time = \frac{50kWh \cdot 60}{150kW/1.4} = 30\ min$$

The power, total swept area and total thrust figures in Table 6.4.1 are minimum parameters that the thruster unit(s) must fulfill. These are values necessary to generate adequate operating performance of the aircraft. However, redundant performance in case of malfunction is not included here. Therefore, the values for power, total swept area and total thrust are considered minimum viable values.

6.5   SWEPT AREA LAYOUT EVALUATION

Based on the specifications in Table 6.4.1, four different architectures for layout of swept area has been evaluated using Texcel with a thrust requirement of 1.4W$_G$. The main drawbacks and advantages reflecting the product objectives for the four alternatives are summarized below. Figure 6.5.1 - Figure 6.5.4 below, show possible layouts of swept area, placed over an arbitrary fuselage, all with 8 m^2 total swept area. The diameters of the swept areas (blue regions) are scaled relative to each other. It is assumed that the placement of the propellers are made symmetrical about the aircrafts center of mass.

Single rotor   P = parachute

- Incompatible with parachute.
- No effective lift if rotor fails.
- Challenging to protect rotating blades from environment.
- High torque requirements.
- High Mach numbers at blade tip.
- Needs a mechanism for countering reaction torque.
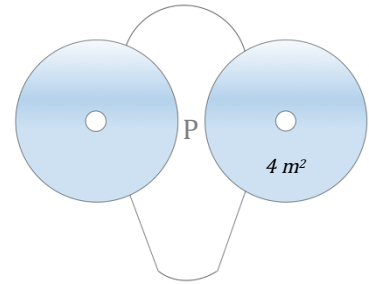- Trust vectoring by rotor tilt – high complexity.

$A_p = 8\ m^2$

P
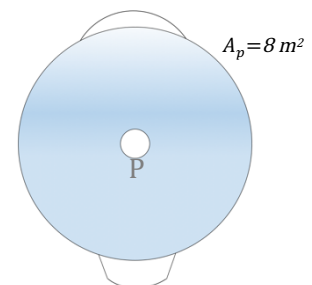
Figure 6.5.1. Single rotor layout with 8 m^2 swept area.

Two rotor   P = parachute

- o   Challenging to implement parachute.
- o   No effective lift if one rotor fails.
- o   Challenging to protect rotating blades from environment.
- o   High engine torque requirements.
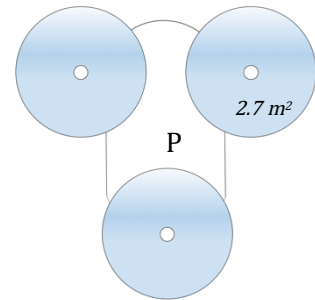- o   Trust vectoring by rotor tilt – high complexity.

Figure 6.5.2. Two rotor layout with 8 m2 swept area.

Three propeller   P = parachute

- o   Parachute compatible.
- o   No effective lift if one propeller fails.
- o   Compatible with protection of rotating blades.
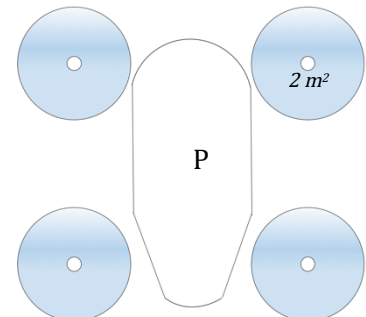- o   Thrust vectoring possible by rpm regulation – low complexity.

Figure 6.5.3. Three propeller layout with 8 m2 swept area.

Four propeller   P = parachute

- o   Parachute compatible.
- o   Possible effective lift if one rotor fails – but unstable.
- o   Compatible with protection of rotating blades.
- o   Thrust vectoring possible by rpm regulation – low complexity.

Figure 6.5.4. Four propeller layout with 8 m2 swept area.

Six propeller   P = parachute

- o   Parachute compatible.
- o   Possible effective lift if one rotor fails.
- o   Compatible with protection of rotating blades.
- o   Thrust vectoring possible by rpm regulation – low complexity.
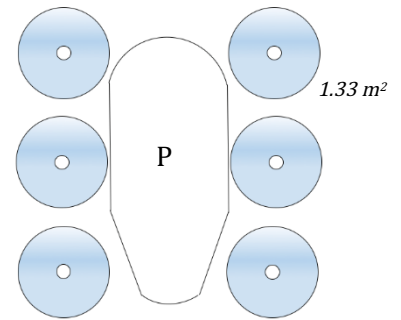- o   High number of connection points between fuselage and thrusters.

1.33 m²

P

Figure 6.5.5. Six propeller layout with 8 m2 swept area.

Eight propeller – coaxial contra rotating   P = parachute

- o   Parachute compatible.
- o   Possible effective lift if one rotor fails.
- o   Compatible with protection of rotating blades.
- o   Thrust vectoring possible by rpm regulation – low complexity.
- o   High redundancy with eight separate motors
- o   Loss in efficiency in downstream propeller.
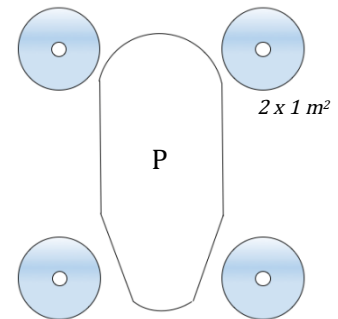
2 x 1 m²

P

Figure 6.5.6. Eight contra rotating propellers layout with 8 m2 swept area. One contra rotating pair in each corner.

The layout for the two rotor- and three propeller configurations have one other possibility for rotor/propeller placement, but this does not affect this evaluation. The focus here is to see what layouts are compatible with the demands for safety.

In selecting a layout of swept area, the requirements of safety are absolute. Meaning if the layout is not compatible with parachute *and* has redundant lift capacity, it will not pass the evaluation. The table below summarizes the results from evaluation of swept area layout.

Table 6.5.1. Absolute evaluation matrix for swept area layout configurations.

Layout	Parachute	Redundant lift
Single rotor	✘	✘
Two rotor	✘	✘
Three propeller	✓	✘
Four propeller	✓	✓
Six propeller	✓	✓
Eight propeller	✓	✓

The four-to-eight propeller layouts pass the evaluation above. A closer look must be made to separate the three layouts from each other. In Table 6.5.2 below, the three layouts are

Anders Thømt   37

evaluated against safety and complexity. The table is separated in two horizontally, with separate evaluation for safety and complexity. This is to avoid evaluating complexity on the same level as safety.

Table 6.5.2. Evaluation of the three resulting layouts from the absolute evaluation above.
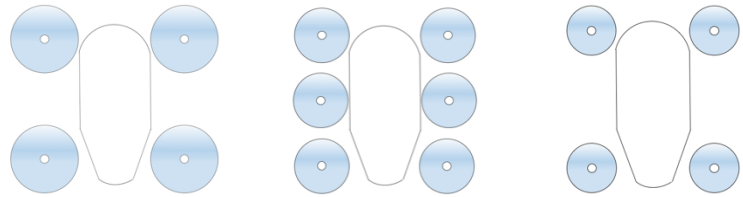
Criteria	Four propeller	Six propeller	Eight propeller
Redundancy	-	0	+
Stability if one engine fail	-	0	+
Sum safety criteria	**-2**	**0**	**2**
Structural complexity	+	-	0
Electrical complexity	+	0	-
Sum complexity	**2**	**-1**	**-1**

The evaluation above is made on the assumption that there is one electrical engine per propeller. Each engine has its own separate electrical system so that any malfunction on an engine or engine control does not affect the operation of other engines.

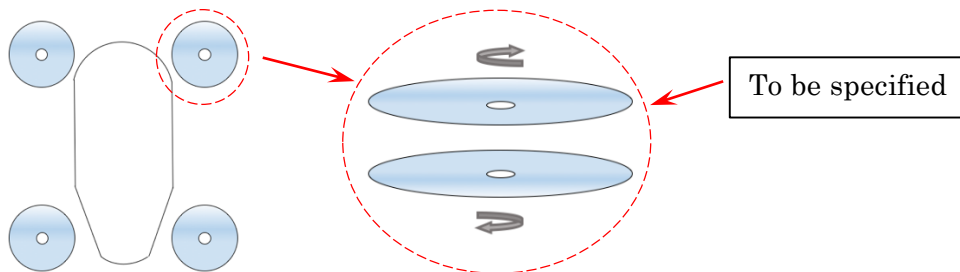The eight-propeller layout is evaluated as the best overall configuration.

Figure 6.5.7.Visual representation of selected layout of swept area which is the foundation for detailed specification.

The swept area layout shown in Figure 6.5.7 gives the basis for the thruster design. Performance figures for each thruster are shown in Table 6.5.3 below.

Table 6.5.3. Baseline figures for each thruster unit.

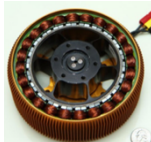| Performance	Value	Unit
Thrust	≥1545	N
Power	≥37.5	kW
Swept area	≥2	m^2
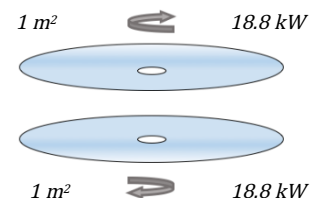
Figure 6.5.8. Baseline setup for thruster unit.

As stated at the end of section 6.4 these are minimum values that create a baseline for detailed specifications of the thruster unit.

6.6   EARLY ENGINE EVALUATION

Five suitable direct-current engines were found and their key specifications are displayed in the table below. Se [N] and [O] for full specifications.

Table 6.6.1. Table overviewing five engine alternatives with relevant specifications.

Manufact.	Lynch Motor [34]				Joby Motor [35]	
Model	LEM200 D135RAGS	LEM200 D135RAG	LEM200 D135	LEM200 D127	JM2	
Performance	Value	Value	Value	Value	Value	Unit
Cont. power	18.00	16.84	14.39	12.56	14	kW
Cont. torque	42	39.9	36.4	33.3	53	Nm
Cont. rpm	4400	4032	3780	3600	2500	rpm
Peak power	36	34.3	29	25.4	20.9	kW
Peak torque	84	82.8	74	68	80	Nm
Peak rpm	4400	4032	3780	3600	3500	rpm
Diameter	200	200	200	200	200	mm
Mass	11	11	11	11	4	kg

The Joby Motor Company builds electric engines specifically for lightweight aircraft applications. Both the Lynch Motor LEM D135 RAGS and Joby Motor JM2 are the most powerful in their respective model range.

Compering the specs of these engines with the specifications in Table 6.5.3 and Figure 6.5.8, the Lynch motors should have plenty of power available with peak power of 36 kW. The Joby Motor however, may have too little available power with only 20.9 kW. Still within the requirement of 18.8 kW, but a continuous power of 14 kW may prove too little. Les't consider a case where one engine fails during flight.
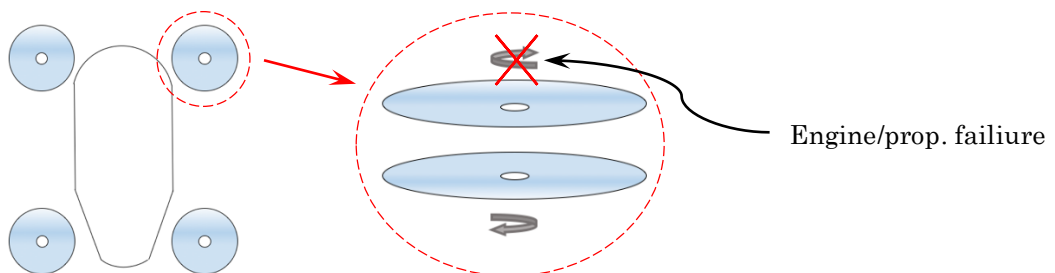
Figure 6.6.1. Scenario where one engine/prop. fails.

The seven remaining propellers must produce enough thrust to hover and maneuver the aircraft to make a safe landing. Assuming the thrusters are placed symmetric about the center of mass and the aircraft is programmed to land immediately after a malfunction is detected, the engines short term peak power can be applied. Taking into account reduction in density with increasing temperature, a maximum operating temperature is set to 40 C°.

Using equation Eq. (6.4.3) to solve for thrust and Eq. (6.4.1) for performance factor:

$$T = \sqrt[3]{2} \cdot \sqrt[3]{A_p} \cdot M^{\frac{2}{3}} \cdot \sqrt[3]{\rho} \cdot P^{\frac{2}{3}} \tag{6.6.1}$$

$$k = \frac{T_T}{W_G} \tag{6.6.2}$$

With 7 m² swept area remaining and a maximum operating temperature of 40 °C [F], the five engine candidates are evaluated with the two equations above and the results are summarized in Table 6.6.2 below.

Table 6.6.2. Total thrust and performance factor for the five engine alternatives with one engine/prop failure.

Manufact.	Lynch Motor				Joby Motor	
Model	LEM200 D135RAGS	LEM200 D135RAG	LEM200 D135	LEM200 D127	JM2	
Performance	Value	Value	Value	Value	Value	Unit
T_T	9031	8745	7819	7158	6285	N
k	**2.0**	**1.98**	**1.77**	**1.62**	**1.42**	-

A performance factor of 1.42 for the Joby motor should be more than adequate to give the aircraft enough control to make a safe landing. However, the remaining propeller in the top right corner must produce enough thrust to keep the aircraft stable. Assuming symmetry, the remaining propeller must produce a minimum thrust, equivalent to a quarter of the gross weight:

$$T_{1/4} = 1100 \ N$$

Again, using Eq. (6.4.1), solving for power and inserting 1 m² for swept area:

$$P = \frac{T}{M}\sqrt{\frac{T}{2\rho A_p}} = \frac{1100}{0.75}\sqrt{\frac{1100}{2 \cdot 1.128 \cdot 1}} = \mathbf{34.7 \ kW}$$

For the given swept area, only the most powerful Lynch motor will support the aircraft sufficiently in case of an engine failure with 1 m² swept area for each propeller.

Alternatively, swept area can be increased to accommodate the weaker engines. The five engines are plotted in Figure 6.6.2 with Eq. (6.6.1) on next page. Peak power is inserted and swept area acts as a variable to give the minimum swept area for each engine to produce 1100 newton of thrust.
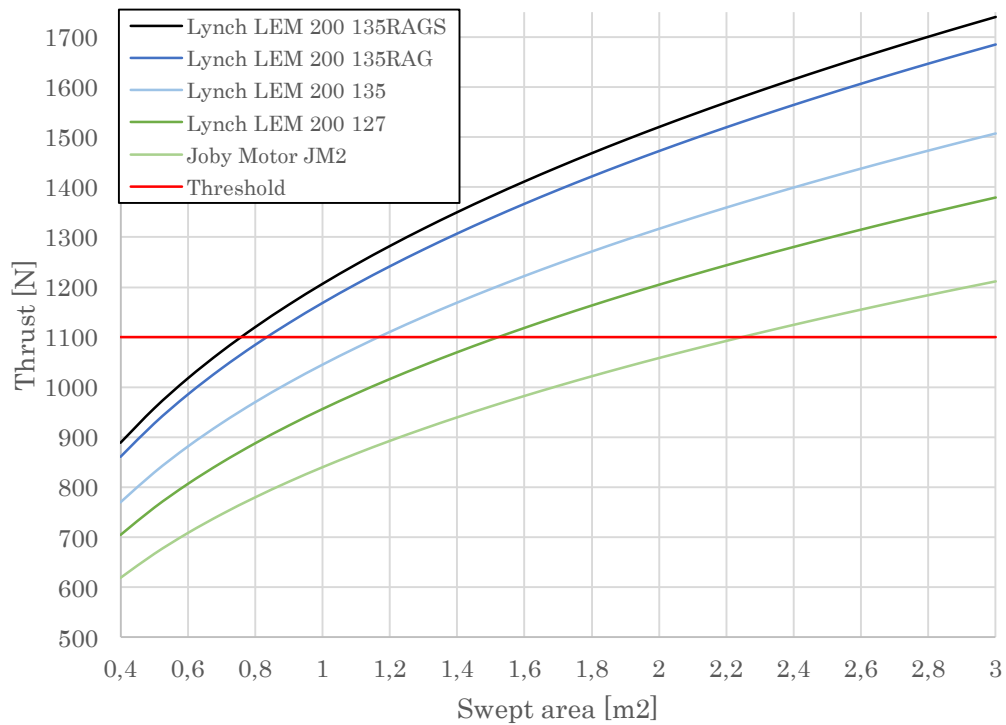
Figure 6.6.2. Eq. (6.6.1) plotted for the five engine alternatives with swept area as variable.

The swept area could be increased to accommodate the Joby engine, it would have to be increased to 2.25 m² to produce 1100 N as shown in Figure 6.6.2. This is something to consider when taking into account the weight of the Joby engine, which is less than half of the Lynch alternatives.

6.7   BOUNDARY SPECIFICATIONS

Based on the evaluations in sections 6.4- 6.6 the following boundary specifications for *each* propeller are as follows:

Table 6.7.1. Boundary specifications with min and max values.

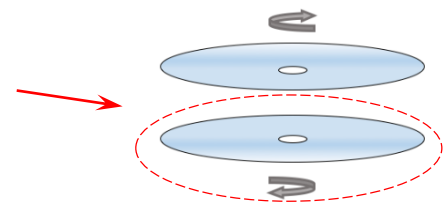| Performance	Min value	Max value	Unit
Swept area	1.0	2.5	m²
Diameter	1.1	1.8	m
Thrust	1100	-	N
Peak power	18.8	36	kW
Op. temp	5	40	C°

Figure 6.7.1. Boundary specifications apply for one propeller/engine unit.

The lowest operating temperature should be minimum 5 °C to avoid ice forming on the blades – disrupting airflow and reducing lift capacity. Ice on the rest of the fuselage will also add weight.

7 PRELIMINARY CONCEPT GENERATION

The results from the previews chapter are used to make some early considerations for concept generation.

7.1 PROPELLER DESIGN

The aim for this section is to estimate a propeller design within the boundary specifications and to fit on the engines alternatives *without* the need for a gear ratio. Meaning, the propeller can be mounted directly on the engine shaft. This is to take in to account the effects on the swept area the propeller can impose. The objective is then to develop a design target within the boundary specifications.

7.1.1 INITIAL AIRFOIL CROSS SECTION CONSIDERATIONS

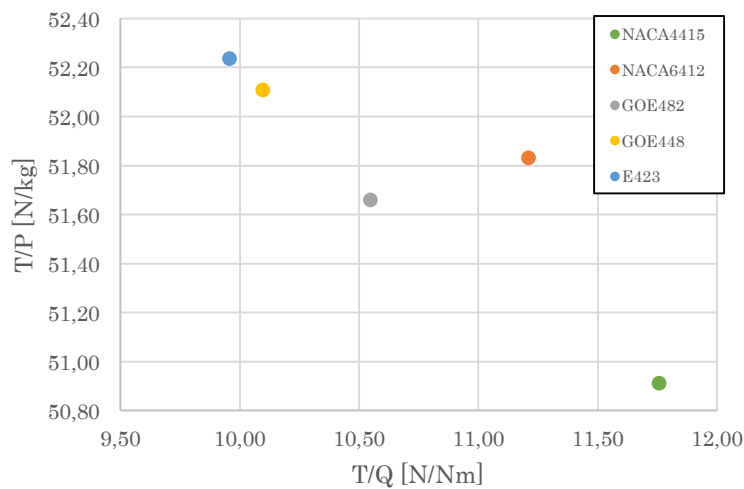Five different airfoil sections are selected as candidates.

Figure 7.1.2. Specific thrust of each section plotted against ratio of thrust per torque. There are differences in efficiency, but at the expense of higher torque requirements.
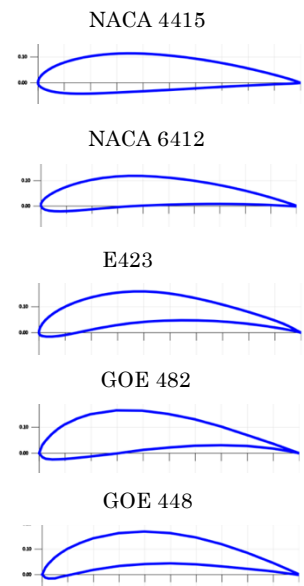

Figure 7.1.1. Drawings of each airfoil evaluated.

From Figure 7.1.2 the E423 airfoil has the largest specific thrust and should be considered. However, the NACA 4415 is very well documented and have a robust boundary layer.

7.1.2 NUMBER OF BLADES

Since thrust and power are proportional with number of blades, specific thrust stays constant with increasing number of blades. Hence, hovering efficiency does not change with number of blades. Therefore, the number of blades should be limited to two, to reduce complexity and costs. The loss in solidity compared to more blades, is compensated by increasing the rpm, however tip speed must be kept at a reasonable level. The rpm and torque characteristics of the engine alternatives naturally limits the blade number, the number of blades are limited to two or possibly three per engine.

In cases where only performance is important and the swept is limited, it can make sense to increase the number of blades. Solidity is then increased in order to generate more thrust on a given swept area. Power demands naturally follows.

7.1.3 INITIAL PROPELLER DIMENSIONS

By using Texcel, the following initial specifications for the propeller were found:

Tabell 7.1.1. Initial specifications for each of the propellers in a thruster.

Dimensions	Value	Unit
Diameter	1.2	m
Chord	8	cm
Cross-section	NACA4415	-
Thrust	1100	N
Peak power	25	kW

7.2 RESULTS AND SUMMARY OF PART ONE

In this section, the main findings of the investigation and evaluation of swept area layout are presented. Furthermore, a brief discussion of considerations for the next step in the development process are found.

7.2.1 MAIN FINDINGS

In Figure 7.2.1 below, the result of the swept area configuration and considerations of stability and access are illustrated.
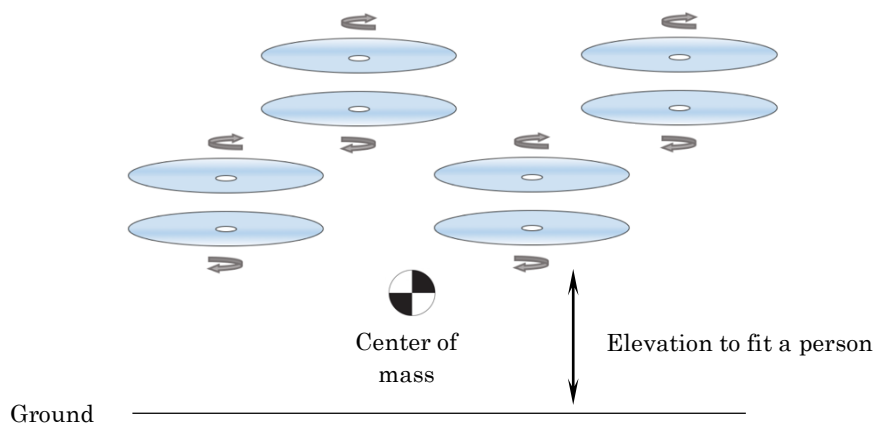

Figure 7.2.1. Schematic of four coaxial thruster units elevated above the ground to fit a person underneath. The cockpit is proposed mounted below the thrusters so that the center of mass is below the thrusters for stability.

The numerical findings are presented in Table 7.2.1 below, giving an overview of the specifications for the whole drone/aircraft, each thruster unit and each propeller/fan.

Table 7.2.1. Summary of the preliminary specifications for the drone and thrusters.

| Performance | Preliminary target | | | Unit |
	In Total	Each Thruster	Each Propeller	
Gross weight drone	450	-	-	kg
Swept area	9	2.26	1.13	m²
Diameter	-	1.2	1.2	m
Max Thrust	8800	2200	1100	N
Peak power	200	50	25	kW
Min hover power	72	18	9	kW
Specific weight	2.25	-	-	kg/kW

Four coaxial thruster units with two contra-rotating two or three blade propellers each is proposed for a 450 kg single seater personal drone including payload, with a propeller diameter of 1.2 meters which is likely to grow slightly as work progresses. A coaxial thruster lowers tip speed compared to a single propeller, due to the sharing of load between the two propellers at normal operating conditions. This is favorable when considering the noise objectives. In consideration of the objective regarding protection of rotating parts, a duct/shroud or other type of barrier needs to be considered. There are significant benefits in efficiency and noise reduction in implementing ducts. However, there are also many challenges connected and they are most likely the reasons use of ducts are limited in present aviation. Also, the placement of the thrusters should be elevated relative to the center of mass of the air craft for stability purposes. This is also in compliance with safe entry/exit of the aircraft and avoiding conflict between user and thruster units.

Due to the limitations imposed by the simplifications in the theory used in this investigation and development – further work on the full-scale thruster warrants a deeper investigation and understanding of rotating wings.

7.2.2   NEXT STEP: CONSIDERATIONS FOR PART TWO

The work in part one then lays the foundation for developing a scaled test rig for evaluating aerodynamic performance, efficiency and effects of ducts and other expansions. The specifications for the experimental setup are constrained by costs, engine size and Reynolds numbers. As an initial experiment, dynamic similitude defined by Eq. (4.1.3) are considered too ambitious to pursue. Keeping the setup at a reasonable level in costs and size and preventing unknown problems that may occur during testing growing too large. However, it is important to stay within the known domain of airfoil characteristics which is constrained by Reynolds numbers.

Conventional metric scaling of outer dimensions such as propeller diameter or swept area are not directly useful. To try to represent aerodynamic effect of a larger propeller with an airfoil cross section which has well known characteristics, the conditions these characteristics are present needs to be recreated. The airfoil characteristics are a function of Reynolds number which is proportional to air speed seen by the airfoil and chord length. A smaller propeller with the same airfoil needs to compensate for reduction in Reynolds number by either increase speed and/or solidity. Increasing rotational speed imposes problems such as centrifugal forces and natural frequencies. An increase in solidity in the form of a longer chord seems more manageable, but has a higher demand for torque.

When conducting experiments on compressible fluids such as air, precautions must be made to not cause an increase in pressure were it is not desirable. The space in which the experiment is conducted need to be large enough for the air from the slipstream to escape freely and circulate back to the front of the propeller.

PART TWO: DEVELOPMENT OF A SCALED TEST RIG FOR PROPULSIVE FUNCTION

8   EXPERIMENTAL PLAN AND SETUP

*A brief plan with objectives is presented.*

8.1   PLAN

8.1.1   MAIN OBJECTIVE

To develop a plan for conducting a simple experiment with a scaled prototype that maps the energy flow through the system, thrust force with and without ground effect and effects by introducing a duct.

8.1.2   PARTIAL OBJECTIVE

- o To develop and select a setup for the experiment.
- o To measure thrust produced at relevant rage of rpm.
- o To measure power needed at relevant rage of rpm.
- o To measure the effects of introducing a duct.
- o To compere measurements with theoretical- and simulated results.

8.2   EXPERIMENTAL SETUP
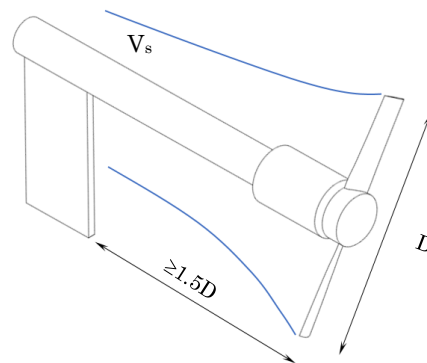
Figure 8.2.1. Base-line setup for experimental prototype. A vertical plate supports the beam/motor/propeller assembly.

Through initial simulation in FS the slipstream contraction is estimated to complete at approximately 1.5D. Therefore, the slipstream should not have any restrictions until 1.5D. To support the motor/propeller assembly a horizontal beam of circular cross-section is proposed to not interfere with the rotation in the slipstream. A circular cross-section is also suitable for absorbing any vibrations in the propeller plane - whose direction is unknown.

9 EXPERIMENTAL METHOD AND EQUIPMENT

An overview of the experimental method and equipment follows.

9.1 EXPERIMENTAL METHOD

This section defines the experimental method through decomposing the energy flow of the system and determining which energy components can be measured. Type of equipment and expected range of values are also defined. Opportunities and weaknesses for research are explored with necessary calibration. Recommendations for treatment of results and uncertainty are also presented.

9.1.1 ENERGY FLOW ANALYSIS

Figure 9.1.1 shows how the energy is distributed as it travels through the system.
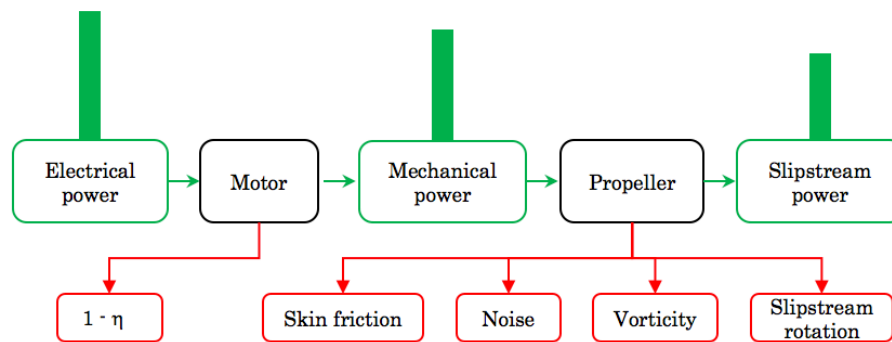

Figure 9.1.1. Energy flow chart. Constructive energy that contributes to thrust are marked in green and green bars indicates the amount of constructive energy left at each step. Energy losses are marked in red.

Table 9.1.1 showing the energy components that can be measured directly. The remaining components must be calculated by elimination, but not determined separately.

Table 9.1.1. The energy components that can be measured are given a green checkmark.

Energy components	Measure	Energy components	Measure
Electrical power	✓	Noise	✓
Mechanical power	✓	Skin friction	✗
Slipstream power	✓	Vorticity	✗
Slipstream rotation	✗	Vibrations	✗

The measurable energy components except noise are listed in Table 9.1.2 with related equations, type of measurement, equipment and expected range of values. Method for determining audible power is outside the scope of this thesis.

Table 9.1.2. Overview of the different measurements required with expected range of values and type of equipment.

Energy components	Eq.	Measure/test	Equipment	Range	Unit
Electrical power	(3.1.4)	Voltage	Volt meter	$0 - 48$	V
		Current	Amp meter	0 - 40	A
Mechanical power	(4.5.16)	Torque, Q	Load cell	0 - 10	Nm
		Rpm, n	Hall sensor	0 - 5000	rpm
Slipstream power	(4.3.2)	Thrust, T	Load cell	0 - 200	N
		Axial component of V_i	Pitot tube	0 - 15	m/s

9.1.2   SWOT-ANALYSIS OF EXPERIMENTAL SETUP

- **Strengths:**
    - Flexibility in modes of testing
    - Simple structure, can be easily modified.
    - Mechanical measurements directly on the propeller axis.

- **Weaknesses:**
    - Low clearing between propeller tip and base. Can influence incoming flow.
    - Friction from bearings.

- **Opportunities:**
    - Measure and account for the majority of the energy flow through the system.
    - Horizontal rotation axis – the propeller can be tested in both directions with a uninterrupted slipstream. Influence of motor in slipstream can be accounted for. Also, a plate can be mounted directly behind the propeller to simulate proximity to the ground and asses ground effect.

- **Threats:**
    - Not able to account for friction that can influence results.
    - The component of friction is large relative to the measured value – causing large uncertainty in the results.
    - Proximity of supply cables to the motor and signal cables from the rpm sensor – magnetic field from supply cables can influence the signal from rpm sensor.

9.1.3   CALIBRATION

When measuring torque and thrust, any friction must be accounted for. Figure 9.1.2 A and B shows the influence of friction on a thrust or torque loaded shaft.
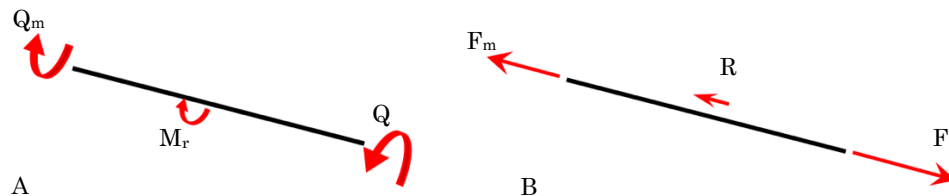

Figure 9.1.2. A: Simple illustration of the torque components along a supported shaft. Q is applied torque, M_r is frictional torque and Q_m is measured torque at the end of shaft. B: Illustration of axial force component along a supported shaft. F is applied force, R is friction and F_m is measured force at the end of shaft.

As Figure 9.1.2 shows, the measured force or torque at the end of a shaft does not equal the applied force or thrust due to friction. The following adjustment must be made:

$$\Sigma M = 0 \qquad\qquad\qquad\qquad \Sigma F = 0$$
$$Q = Q_m + M_r \qquad\qquad\qquad F = F_m + R$$

If the cases in Figure 9.1.2 are combined, M_r can be proportional with F and increase linearly with F, causing difficulties to account for friction.

9.1.4   RESULTS AND ERROR ANALYSIS

Managing Measured Values

To obtain a representative result from measurements, each measurement needs to be repeated and the mean of these values will be the best estimate [36]. The mean is defined as:

$$\bar{h} = \frac{1}{N}\sum h_i \tag{9.1.1}$$

Where N is number of measurements and h_i is measurement i. The standard deviation which represents the average uncertainty of each measurement is defined as:

$$j_h = \sqrt{\frac{1}{N-1}\sum(h_i - \bar{h})^2} \tag{9.1.2}$$

To obtain an uncertainty for the mean calculated by Eq. (9.1.1), the standard error of mean is used:

$$\delta_{\bar{h}} = \frac{j_h}{\sqrt{N}} \tag{9.1.3}$$

As the number of measurements increases the uncertainty becomes smaller by definition of Eq. (9.1.3). Due to the fraction in Eq. (9.1.2) the minimum number of measurements in each series must be three or larger – recommending at least five measurements.

The results of each measurement series should be presented in the following way:

$$Value = \bar{h} \pm \delta_{\bar{h}} \tag{9.1.4}$$

Result Treatment

In addition to figure of merit and specific thrust defined in chapter 4; if a mean value of the induced velocity is obtained a propeller efficiency can be calculated:

$$\eta_p = \frac{T\bar{V}_i}{Q\omega} \tag{9.1.5}$$

Which in turn can be plotted against rotational speed to determine the most effective operating region. Also, if the induced velocity is successfully measured at several points along the radius the speed profile can be plotted.

9.1.5 RESEARCH POTENTIAL

- o The propeller efficiency and speed profile of the induced velocity can be used to track and evaluate changes in blade design and configuration.

- o Possibility to place a fan with flow straighteners to simulate oncoming air from the freestream to simulate vertical flight. The fan can also be placed at an angle relative to the rotational axis to simulate cross-wind and forward flight.

- o A wall can be introduced in the slipstream to evaluate effects of pressure build up in the slipstream also known as ground effect.

- o A function relating noise to tip speed to confirm the claim of the noise being a function of tip speed to the power of five [11].
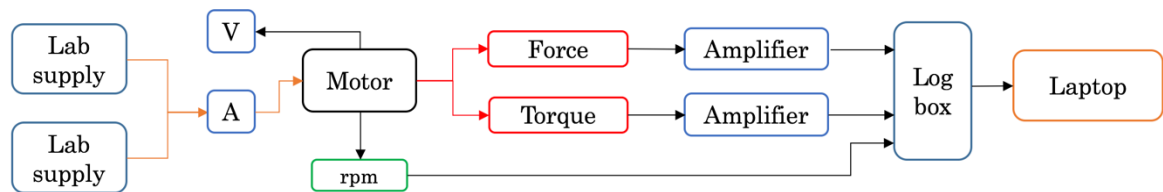
9.2 EXPERIMENTAL EQUIPMENT

A table of the experimental equipment needed follows.

Table 9.2.1. Showing the required equipment to each measurement activity and power supply. Middle column lists existing equipment in-house at RealTek.

Measure/Supply	Existing equipment	Desired equipment
Thrust	100 kg s-type load cell	2-axis load sensor
Torque	10 kg bending load cell	
Amplifier	2 x Analog – digital amplifier	-
Logging	Multi-channel log box	-
Motor speed	Hall sensor: Honeywell 2SS52M	Hall sensor + magnet
	-	
Motor current	Ampere meter	-
Motor voltage	Volt meter	-
Slipstream velocities, V_i, V_s	-	Pitot tube
Electrical power supply	Lab supply 750 W	2 x 24 volt batteries + one lab supply.
	Lab supply 300 W	

Figure 9.2.1 shows how the experimental equipment can be set up in schematic form.

Figure 9.2.1. Schematic layout of the experimental equipment using in-house equipment, where V is volt meter and A is ampere meter.

9.3 HEALTH AND SAFETY

When rotary equipment is used, some precautions must be made. The main considerations are as follows:

o   Any fastening device such as nuts and bolts that secures rotary parts, should be secured in some way prevent loosening. Either by a safety pin, thread locking products or pretension. Using a safety pin if possible is the most desirable option.

o   Given the high rotational speeds of the propeller assembly, caution must be made to both personnel and the surroundings in case of a failure in the propeller assembly. Recommend that a wall or another physical barrier is between any personnel and the test rig at all times when the rig is in use.

o   As a measure to prevent damage to both the test rig and personnel, basic instruction for use and caution should be permanently printed on the test rig.

10   DESIGN SPECIFICATION OF EXPERIMENTAL SETUP

This chapter presents key properties and specifications of the experimental setup.

10.1   PROPERTIES OF THE EXPERIMENTAL SETUP

When considering the partial objectives in section 8.1.2, the setup needs to have the following properties. Each property is given a score from ranging $1 - 5$, where 1 is not important and 5 is regarded as an absolute requirement.

Table 10.1.1. Required properties for the experimental setup.

Key Properties	Comment	Imp
Flexibility	The setup can be disassembled and modified	3
Complexity	Low number of components and simple structure	4
Production	Easy to manufacture – low cost	3
Support motor	Structure can to hold and support motor.	5
Low friction	Lowest friction possible for motor support.	4
Aerodynamic loads	Structure can cope with aerodynamic loads.	5
Measure reaction torque$\pm$	Accommodate torque sensing equipment.	4
Measure motor speed	Accommodate rpm sensor and wiring.	4
Measure thrust $\pm$	Accommodate force sensing equipment.	5
Low slipstream disturbance	Minimal slipstream disturbance of the construction.	4
Compatible with a duct	Space and mounting capabilities for a duct.	4
Cabling	Support and protect any cables from damage.	4
Experimental equipment	Protection of expensive and delicate equipment.	3
Weight	The whole rig can be easily moved by two people.	4
Safety	Securing nuts and bolts holding rotating parts.	5

10.2   METRIC BOUNDARY SPECIFICATIONS

The boundary specifications for the experimental setup are displayed in Figure 8.2.1 below. The setup is proposed specified by Table 10.2.2. Keeping the Reynolds numbers no lower than 50 000 at the hub, the airfoil characteristics along the blades will be known. Also, keeping the diameter of the propeller at a reasonable size keeping the blade forces low.

Exploring with Texcel the requirements for torque and rpm for the relevant Reynolds range with high lift/drag airfoils, implies a low kv-motor is needed. Considering price and weight, the following engine was found.

Unite motor MY1020

Figure 10.2.1. Picture of MY1020. (Own photo).

Table 10.2.1. Table of specifications for MY1020.

Performance	Value	Unit
D $(2r_h)$	108	mm
Weight	5.25	kg
Rated power	1000	W
Rated voltage	48	V
Rated torque	3.2	Nm
Rated rpm	3000	rpm
Peak power	1200	W
Peak Torque	4	Nm
Peak current	33.5	A

Using Texcel combined with the specifications on the motor presented in Table 10.2.1, the following boundary specifications for performance are seen in Table 10.2.2 below. The "Target"-column represents the expected values using the MY1020 motor and the "Max value"-column will be the foundation for specifying the experimental setup.

Table 10.2.2. Metric boundary specifications for performance of the experimental setup.

Performance	Min value	Target	Max value	Unit
D	300	600	800	mm
Thrust	-	70	200	N
Peak power	-	1.2	3	kW
Peak torque	-	3.2	10	Nm
Op. temp	5	20	40	C°
Re number range	60k-150k	60k-230k	60k-400k	-
Tip Mach nr.	-	0.28	0.4	-

Combined with the product properties in Table 10.1.1 and specifications in Table 10.2.2, the following boundary specifications for the outer dimensions of the whole setup are seen in Table 10.2.3 below.

Table 10.2.3. Metric boundary specifications for the outer dimensions of the experimental setup.

Dimension	Min value	Target	Max value	Unit
Length	1000	1500	2000	mm
Width	800	1000	1500	mm
Height	500	1000	2000	mm
Weight	20	35	80	kg

11 CONCEPT GENERATION AND SELECTION

Concept generation and selection of important properties for the experimental setup follows.

11.1 EXPERIMENTAL SETUP

Based on the work in the previous section three initial concepts for the experimental was generated and displayed below. Setup 3 is selected as reference setup because it has similar architecture to other test rigs [23].

Setup 1   F = load cell   M = motor   ◯ hinge

The engine propeller assembly is mounted on two parallel beams that are connected to the base through two hinges.
- o Low complexity.
- o Structural loads and vibrations through load cell.
- o Minimal slipstream interference.
- o Thrust need to be calculated using measured lengths – sources of error.
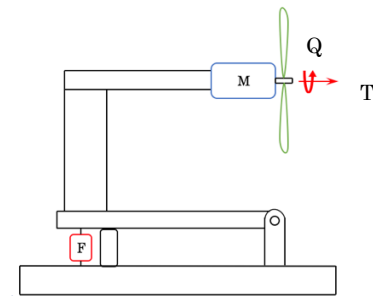
Figure 11.1.1. Sketch of Setup 1.

Setup 2   F = load cell   M = motor   ◯ hinge

The engine propeller assembly is mounted to the base through a single hinge. The load cell is connected through a rod that keeps the assembly from rotating.
- o Slipstream interference by the rod/load cell.
- o Low lateral stability by a single hinge at base.
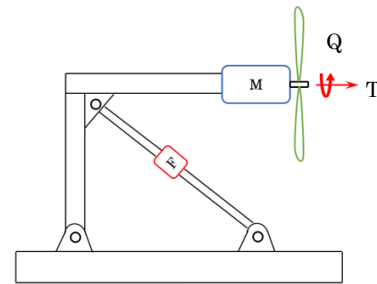- o Thrust need to be calculated using measured angle – source of error.

Figure 11.1.2. Sketch of Setup 2.

Setup 3   F = load cell   M = motor   ▨ = linear bearing

The engine propeller assembly is mounted on a plate with four linear bearings that slides on two parallel rods that are connected to the base.
- o Linear bearings make a good connection to the base.
- o Load cell are mounted in axial direction avoiding vibrations.
- o Higher complexity.
- o Minimal slipstream interference.
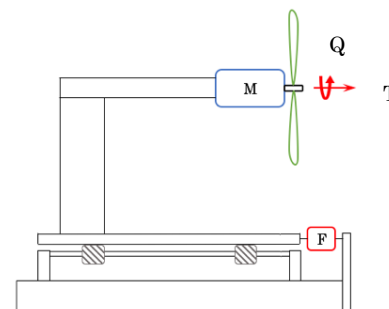- o Direct read of thrust on load cell.
- o Calculated torque

Figure 11.1.3. Sketch of Setup 3.

The three initial concepts are then screened through selection matrix, Table 11.1.1. Each concept was given a score 0, - or + relative to the reference concept.

Table 11.1.1. Selection matrix for initial concepts.

Criteria	Setup 1	Setup 2	Setup 3
Flexibility	0	-	
Complexity	+	0	
Production	0	-	
Support motor	0	0	R
Low friction	+	-	e
Aerodynamic loads and stability	-	-	f
Measure reaction torque$\pm$	-	-	e
Measure motor speed	0	0	r
Measure thrust$\pm$	-	0	e
Low slipstream disturbance	0	-	n
Compatible with a duct	0	-	c
Cabling	0	0	e
Experimental equipment	0	0	
Weight	0	0	
Safety	0	0	
Sum	-1	-7	

The result of initial concept screening is that none of the two were better than the reference concept, hence the negative sums of Setup 1 and 2.

A new concept generation was done. Along with Setup 3 a new concept, Setup 4 was developed leaving two final concepts seen below.

Setup 3   F = load cell   M = motor   ▨ = linear bearing

The engine propeller assembly is mounted on a plate with four linear bearings that slides on two parallel rods that are connected to the base.
- o Linear bearings make a good connection to the base.
- o Load cell are mounted in axial direction avoiding vibrations.
- o Higher complexity.
- o Minimal slipstream interference.
- o Direct read of thrust on load cell.
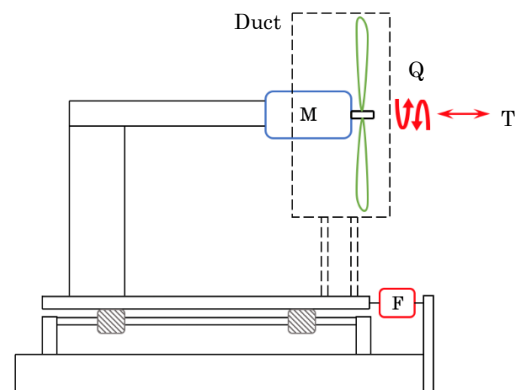- o Calculated torque

Figure 11.1.4. Sketch of Setup 3.

Setup 4

F = load cell   M = motor   ▨ = linear bearing

The engine propeller assembly is mounted to a shaft that floats on two linear bearings inside the circular beam.

- o Low complexity
- o Slipstream interference after 1.5D.
- o Direct read of thrust on load cell at end of shaft.
- o Direct read of torque on load cell through a lever arm at end of shaft.
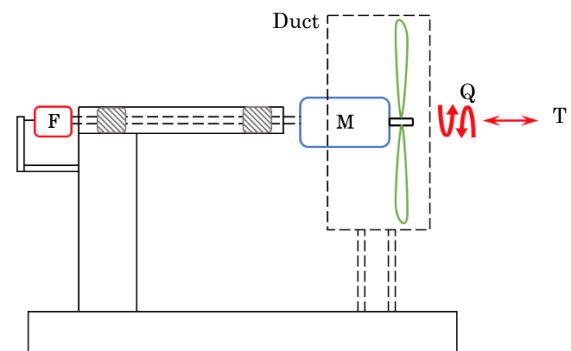- o Only measurement of duct thrust component, if duct is mounted to the engine.

Figure 11.1.5. Sketch of Setup 4.

The two final concepts were screened in a selection matrix were the criteria are weighted from Table 10.1.1.

Table 11.1.2. Selection matrix for the final concepts.

Criteria	Setup 2	Setup 4	Imp
Flexibility	0	1	3
Complexity	0	1	4
Production	0	1	3
Support motor	1	1	5
Low friction	0	1	4
Aerodynamic loads and stability	0	1	5
Measure reaction torque$\pm$	0	1	4
Measure motor speed	1	1	4
Measure thrust$\pm$	1	1	5
Low slipstream disturbance	1	1	4
Compatible with a duct	1	1	4
Cabling	1	1	4
Experimental equipment	1	1	3
Weight	1	1	4
Safety	1	1	5
Sum	38	**62**	62

Chosen concept: Setup 4

11.2 ALTERNATIVES FOR THRUST AND TORQUE MEASUREMENT

It is desirable to measure the torque through a load cell to obtain accurate power figures. Two alternatives for measuring torque were found.

- o Mounting a 2-axis load cell directly at the end of the shaft - Figure 11.2.1 A.

o Mechanically decomposing the rotation and axial motion, then measuring torque and thrust separately by two bending beam load cells - Figure 11.2.1 B.

Figure 11.2.1. A: 2-axis load sensor, capable of measuring compression/tension and torque in both directions [37]. B: Bending beam load cell, capable of measuring compression/tension [38]. C: S-type loading cell, capable of measuring compression/tension [38]

Based on the load cells types presented above, three concepts for measuring thrust and torque are presented in Figure 11.2.2 below.
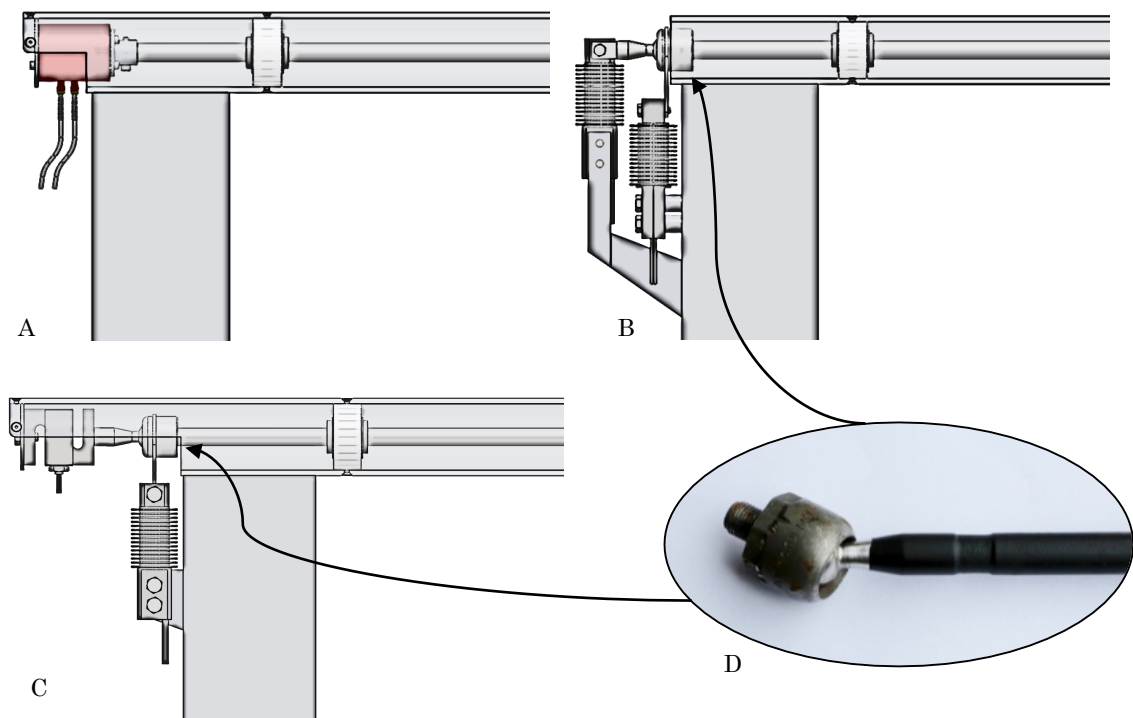
Figure 11.2.2. A: Concept for 2-axis load sensor connected directly to the end of the shaft. B: Concept for two bending beam load cells where torque and thrust are separated by an automotive ball joint. C: Concept for one s-type load cell measuring thrust and one bending beam load cell measuring torque, same use of ball joint as in B. D: Automotive ball joint from a steering rack.

The three concepts are evaluated in Table 11.2.1 below, were the 2-axis concept is considered best and used as a reference.

Table 11.2.1. Selection matrix for load cell concept. Continues on next page.

Criteria	Concept		
	A	B	C
Complexity	R	-	-
Production	e	-	-
Low slipstream disturbance	f	-	-
Low friction	e	-	-

Table 11.2.2. Continued

Criteria	A	B	C
Experimental equipment	r	0	-
Cabling	e	0	0
Cost	n	+	+
Sum	c	**-3**	**-4**

Neither B or C were a better concept than A. However, the 2-axis load cell are almost ten times more expensive [P] than a single s-type or bending beam load cell. Therefore, concept B is chosen.

Chosen concept: B

11.3 LOADS, MATERIALS AND CROSS SECTION CHOICES

11.3.1 USE LOADS

The maximum loads the rig is estimated to experience rig is summarized in Table 11.3.1 below. Also, since it is to be used in experimentation number of load cycles is expected to be insignificant in a fatigue perspective.

Table 11.3.1. Table of maximum use loads the test rig must handle.

Load	Value	Unit
T	± 200	N
G	52	N
Q	± 10	Nm
q [39]	2.86	kg/m

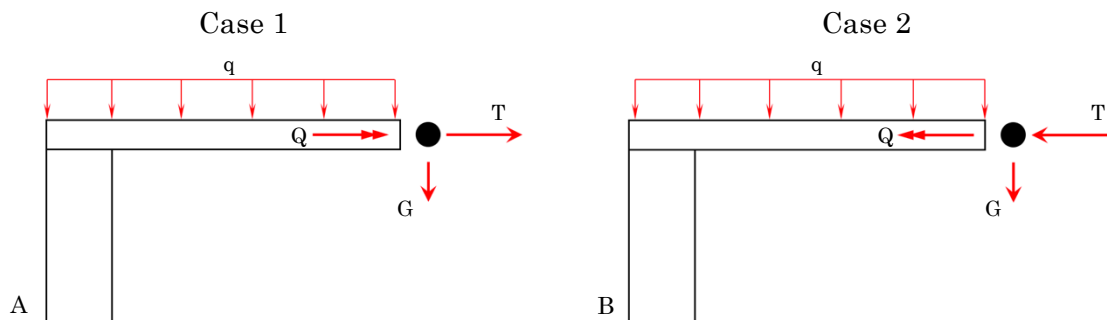The use loads on the test consists of two cases shown in Figure 11.3.1 below.

Figure 11.3.1. A: Loading Case 1 where the thrust vector is dircectet outward. B Loading Case 2, where the thrust vector is directed inward.

11.3.2 PROPOSED MATERIALS

Considering a reasonable low weight requirement with a low-cost requirement in production and some resistance against corrosion. The proposed materials for the main components are summarized in Table 11.3.2 below.

Table 11.3.2. Proposed materials for the main components.

Main Components	Material	Comment
Circular beam	Aluminum	Low weight and easy to manufacture.
Support plate	Aluminum	Low weight and easy to manufacture.
Base	Wood	Inexpensive and light-weight, easy to manufacture.
Base plate	Plywood	Good stiffness and durability, easy to mount upon.

11.3.3 STATIC FORCES, MOMENTS AND SAFETY FACTOR

Moments

Since the shaft is connected to the support plate through the torque load cell, no torque is transferred through the circular beam.
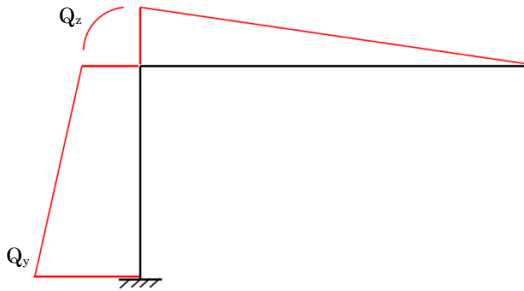
Moment diagrams

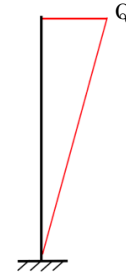Figure 11.3.2. Side view of the construction with moment diagrams.

Figure 11.3.3. Rear view of construction with moment diagrams.

Cross Section Choices

The circular beam is already chosen to have a circular cross section from considerations done in section 8.1. Also, the support plate should have a low cross section normal to the slip stream to avoid pressure build up. Figure 11.3.2 Figure 11.3.3 show the bending moments the circular beam and support plate must handle. Taking into account the considerations just described, combined with availability of materials at RealTek, the following cross section choices were made:
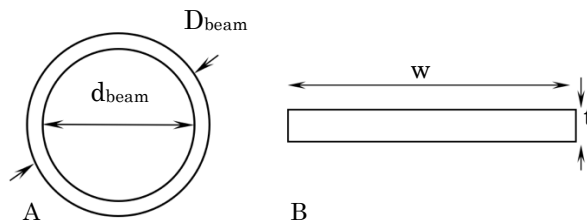

Figure 11.3.4. A: Cross section of circular beam. B: Cross section of support plate.

A list of dimensions used for the following calculations can be seen in Table 11.3.3 below.

Table 11.3.3. List of dimensions used in the following calculations.

Dimension	Value	Unit	Dimension	Value	Unit
x	885	mm	D_{beam}	70	mm
x_1	52	mm	d_{beam}	60	mm
y	735	mm	d_j	37	mm
w	120	mm	D_{shaft}	16	mm
t	10	mm			

Welds

For cosmetic reasons a full weld is chosen at the top and bottom of the support plate. The stresses are therefore moderate as the following calculations shows. Only Q_{zb} and Q_{zb} has any significant contribution to the stresses in the welds.

Calculations for stresses in welds. The large cross section of weld seams causes moderate stresses and only bending stresses are significant.
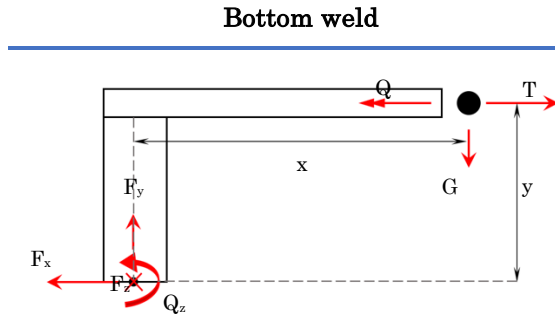
Bottom weld	Top weld

Figure 11.3.5. Reaction forces and moments in the bottom weld.

Figure 11.3.6. Reaction forces and moments in the bottom weld.

$$Q_z = Ty + Gx = 19.26 \cdot 10^4 \; Nmm$$

$$F_x = T$$
$$F_y = G$$
$$F_z = \frac{Q}{y} = \frac{10 \cdot 10^3}{735} = 13.6 \; N$$
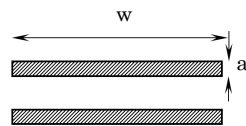

Figure 11.3.7. Schematic of weld cross-section.

$$W_b = \frac{I_{zz}}{w/2} = \frac{2 \cdot 4 \cdot 120^3}{12 \cdot 120} = 9600 \; mm^4$$
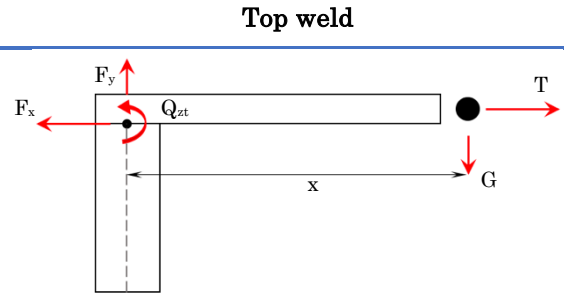
$$\sigma_b = \frac{Q_z}{2W_b} = \mathbf{10 \; MPa}$$

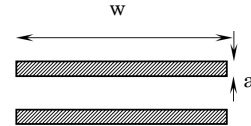$$Q_{zt} = Gx + T\frac{D_{beam}}{2} = 52.58 \cdot 10^3 Nmm$$

$$F_x = T$$
$$F_y = G$$

Figure 11.3.8. Schematic of weld cross-section.

$$W_b = \frac{I_{zz}}{w/2} = \frac{2 \cdot 4 \cdot 120^3}{12 \cdot 120} = 9600 \; mm^4$$

$$\sigma_b = \frac{Q_{zt}}{2W_b} = \mathbf{2.8 \; MPa}$$

Calculation of stresses in torque lever welds. Only shear stresses are significant.
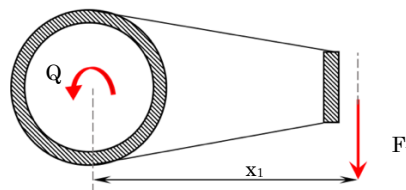
Welds on torque cell lever

Figure 11.3.9. Circular weld must handle Q and the weld for the sleeve must handle F_t.

$$I_p = \frac{\pi}{32}((d_j + 2a)^4 - d_j{}^4)$$
$$= \frac{\pi}{32}((37 + 2 \cdot 2)^4 - 37^4) = 93423 \; mm^4$$

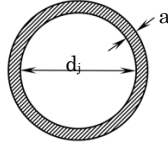$$F_t = \frac{Q}{x_1} = \frac{10 \cdot 10^3}{52} 192N$$

Figure 11.3.10. Schematic of weld cross-section.

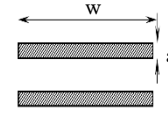
Figure 11.3.11. Schematic of weld cross-section.

$$\tau_{\parallel} = \frac{Q}{I_p}\left(\frac{d_j}{2} + a\right) = \frac{10 \cdot 10^3}{93423}\left(\frac{37}{2} + 2\right) = 2.2 \, Mpa$$

$$\tau_{\parallel} = \frac{F_t}{A_s} = \frac{192}{2 \cdot 10 \cdot 2} = 5 \, MPa$$

$$\sigma' = \sqrt{3\tau_{\parallel}{}^2} = \sqrt{3 \cdot 2.2^2} = \boldsymbol{4 \, MPa}$$

$$\sigma' = \sqrt{3\tau_{\parallel}{}^2} = \sqrt{3 \cdot 5^2} = \boldsymbol{9 \, MPa}$$

Stresses in beams

Support plate	Circular beam

$$W_b = \frac{I_{zz}}{w/2} = \frac{2 \cdot 10 \cdot 120^3}{12 \cdot 120} = 24000 \, mm^4$$

$$W_b = \frac{I_{zz}}{D_{beam}/2} = \frac{2\pi(70^4 - 60^4)}{64 \cdot 70} = 15498 \, mm^4$$

$$\sigma_b = \frac{Q_{zb}}{W_b} = \boldsymbol{8 \, MPa}$$

$$\sigma_b = \frac{G \cdot x}{W_b} = \boldsymbol{2.7 \, MPa}$$

Screws

The three M4 screws that hold the thrust cell plate have a combined cross section area that makes the shear stresses in each screw - due to the thrust force - small. Also, the M8 screws holding the torque cell experience low stresses.

Safety factor

The lowest safety factor is found in the bottom weld. Assuming use of welding material with same material properties, the safety factor becomes:

$$SF = \frac{250 \, Mpa}{10 \, Mpa} = \boldsymbol{25}$$

Deflection

The relevant cases of deflection will be the circular beam and how it's deflection affects alignment of the linear bearings. Also, the deflection of the engine relative to the circular beam will be checked.

Circular beam:

$$I_{beam} = \frac{\pi}{64}\left(D_{beam}{}^4 - d_{beam}{}^4\right) = \frac{\pi}{64}(70^4 - 60^4) = 542415 \, mm^4$$

Checking deflection due to weight of circular beam:

$$y_q = \frac{qL^4}{8EI_{beam}} = \frac{2.86 \cdot 0.001 \cdot 9.81 \cdot (820 - 60)^4}{8 \cdot 70000 \cdot 542415} = 0.03 \, mm$$

Checking deflection due to weight of motor:

$$y_G = \frac{GL^3}{3EI_{beam}} = \frac{5.25 \cdot 9.81 \cdot (820 - 3)^3}{3 \cdot 70000 \cdot 542415} = 0.20 \; mm$$

Deflection of circular beam:

$$y_{beam} = \mathbf{0.23 \; mm}$$

Shaft:

$$I_{shaft} = \frac{\pi}{64} D_{shaft}{}^4 = \frac{\pi}{64} 16^4 = 3217 \; mm$$

Checking in shaft due to weight of motor:

$$y_{shaft} = \frac{GL^3}{3EI_{shaft}} = \frac{5.25 \cdot 9.81 \cdot 135^3}{3 \cdot 200000 \cdot 3217} = 0.66 \; mm$$

Deflection of motor relative to the circular beam:

$$y_{shaft} = \mathbf{0.7 \; mm}$$

## *Fatigue*

When considering the safety factor above, the fatigue threshold is far from reached. This combined with the expected use being limited to intermittent experimentation throughout its life, hence a small number of loading cycles, fatigue is not considered an issue.

12 SETUP ARCHITECTURE

In this chapter, the assembled architecture of the experimental setup is presented with details, functionality, options and design of components. Also, a preliminary design of propeller blades is found.
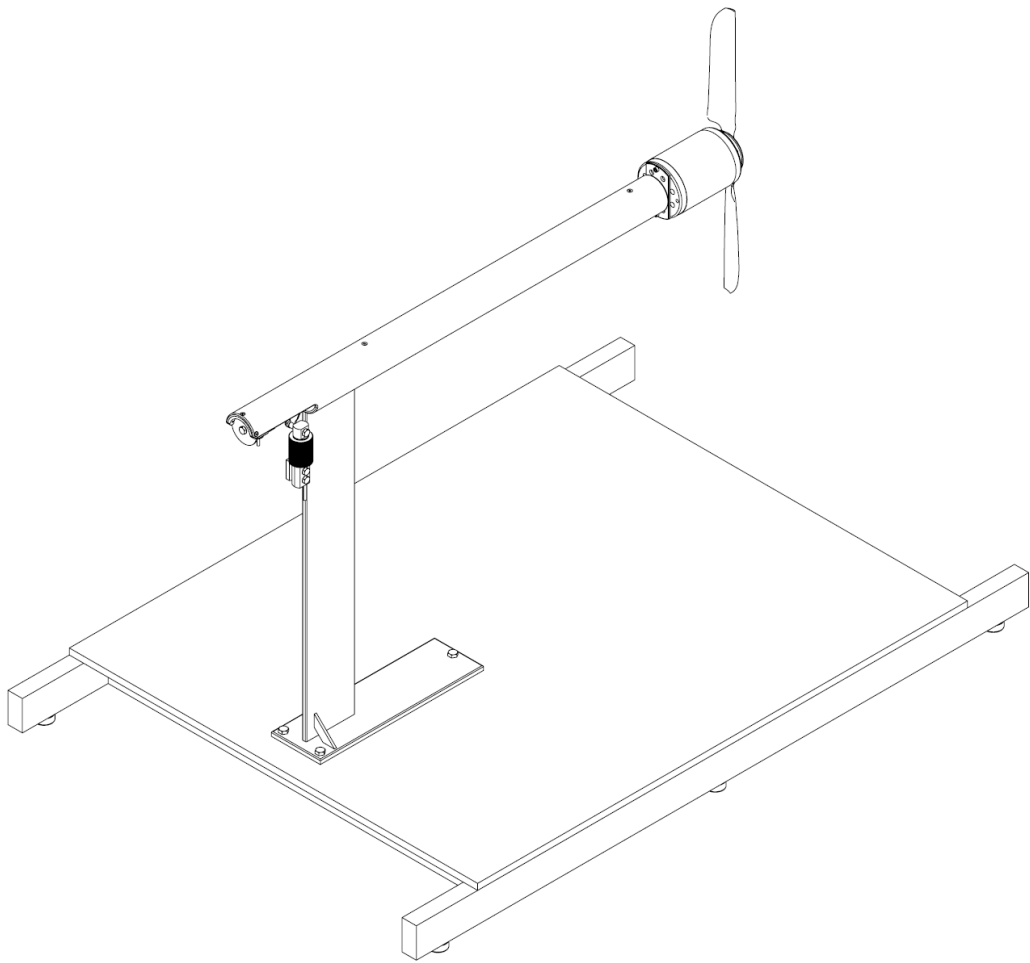
12.1 ASSEMBLY
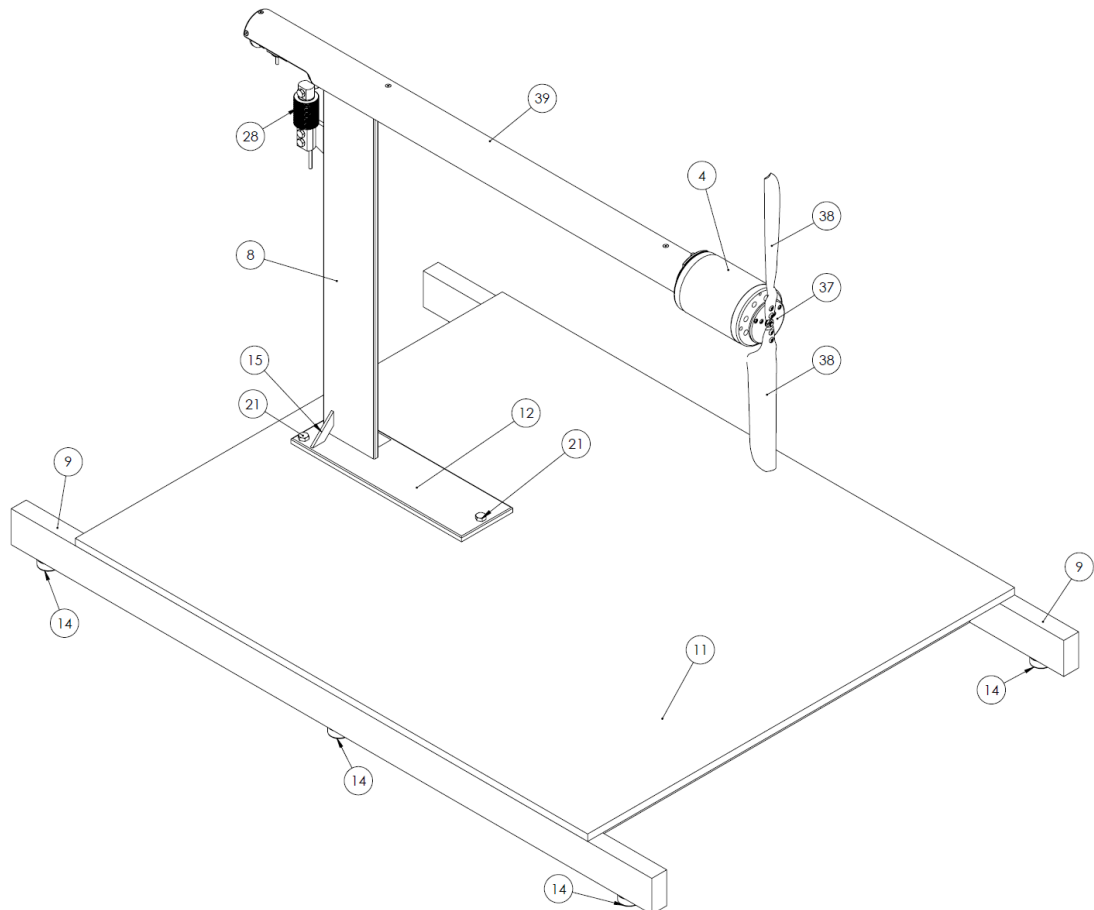
Figure 12.1.1. Overview of the assembly with the main components numbered.

Table 12.1.1. List of the main components with index referring to Figure 12.1.1 and Figure 12.1.2 below.

Index	Component	Index	Components	Index	Components
4	Motor	12	Base support plate	28	Torque load cell
8	Support plate	14	Rubber foot	37	Propeller hub
9	Base beam	15	Angle strut	38	Propeller blade
11	Base plate	21	Base screw	39	Circular beam

A rear view of the assemby is found on the next page.

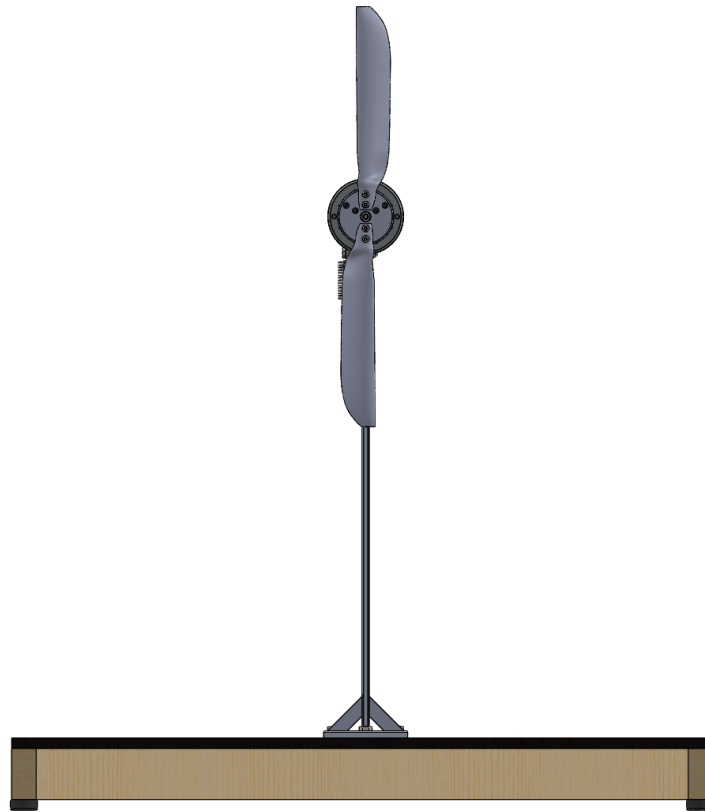*Figure 12.1.2. Overview of backside of the assembly with man components numbered.*
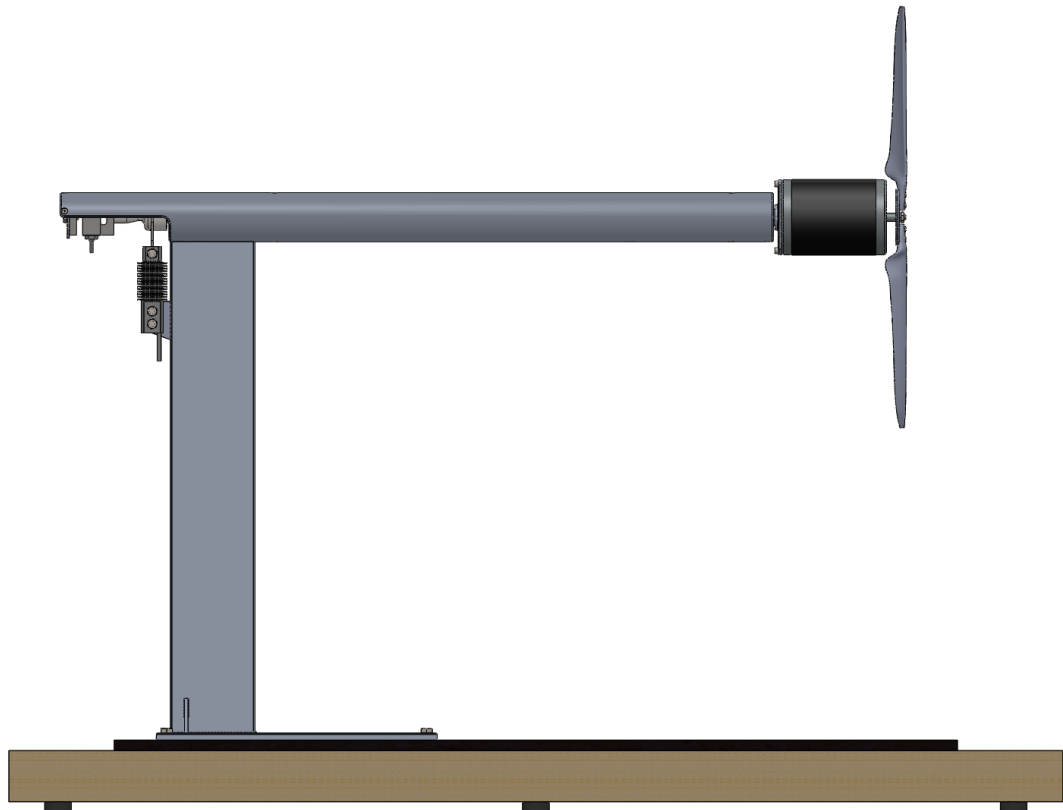
Figure 12.1.3. The experimental test rig in side view.

Figure 12.1.4. Front view of the experimental setup.

Figure 12.1.5. Rear view of the experimental setup.
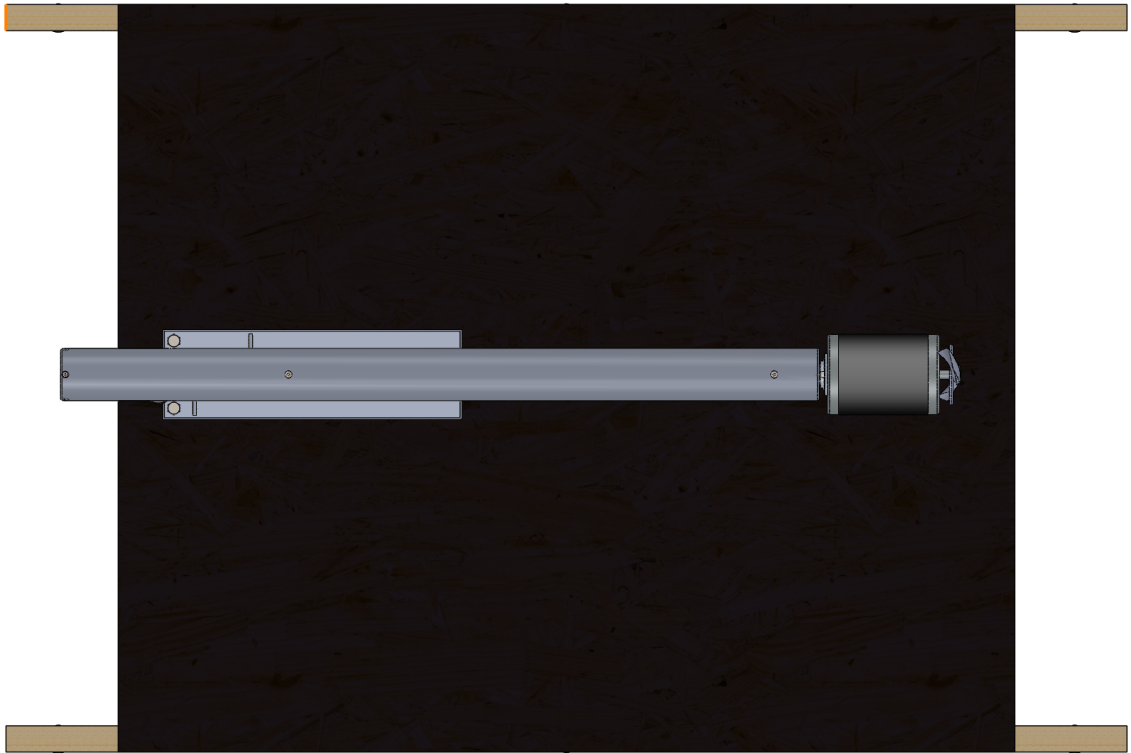
Figure 12.1.6. Top view of the experimental setup.

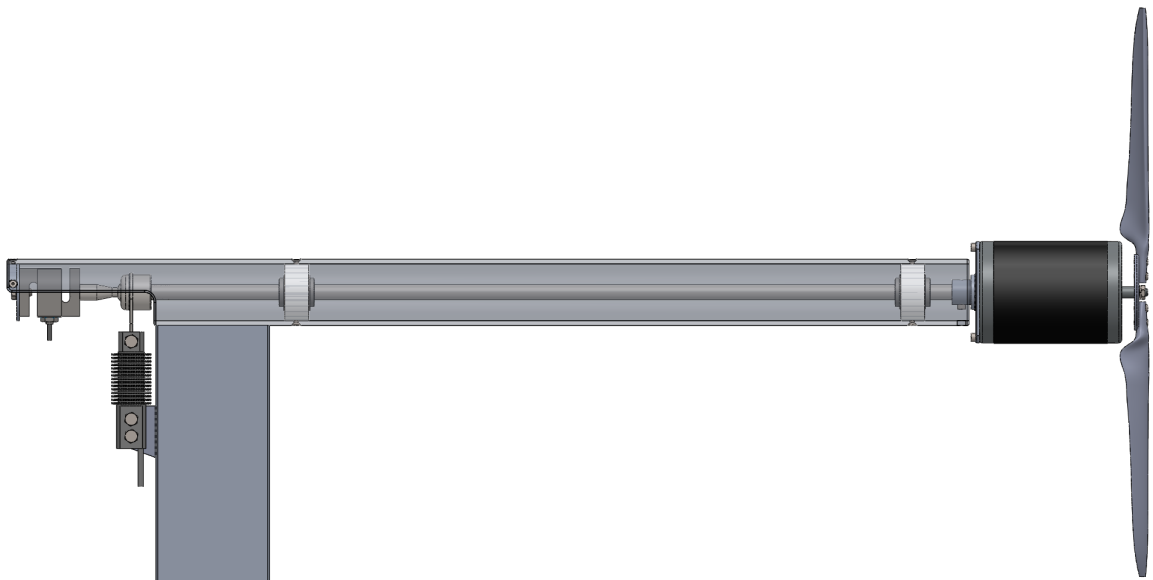*Figure 12.1.7. Perspective front view of the experimental setup.*

Figure 12.1.8. Perspective rear view of the experimental setup.

12.2 ASSEMBLY DETAILS

Figure 12.2.1. Side view of the top part of the setup. The circular beam is made transparent to make visible how the propeller motor assembly is connected to the load cells at the other end by a shaft supported by two linear ball bearings.
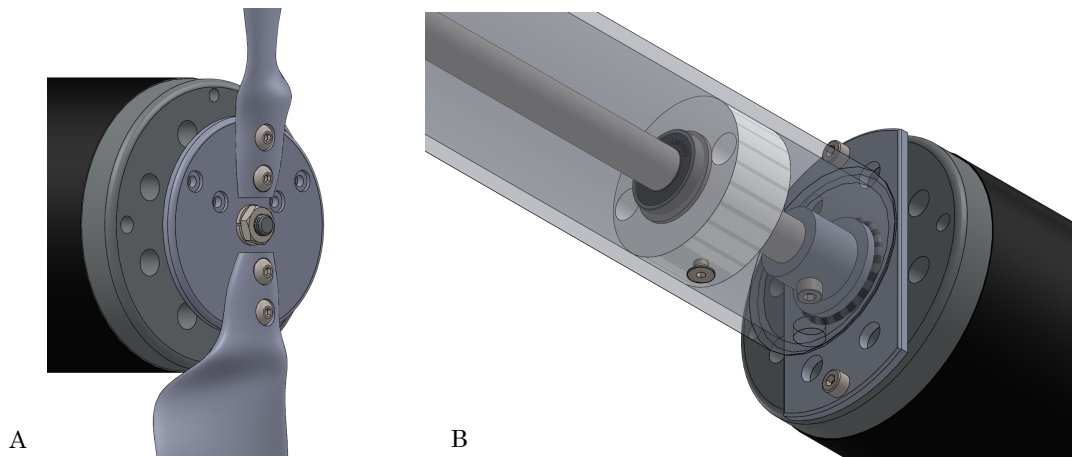
Figure 12.2.2. A: The propeller blades are connected to the hub with two M5 screws each. Dimensioning of the hub and propeller blades are outside the scope of this thesis. B: Connection of the motor to the shaft. An aluminum plate is bolted on the motor which is connected to the shaft through a M5 screw and a welded hub.
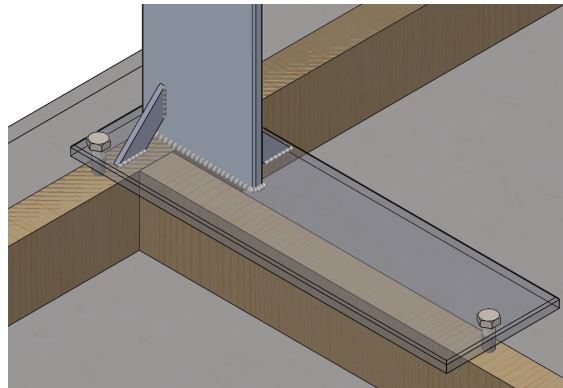
Figure 12.2.3. The vertical support plate is welded to the base support plate, which in turn is bolted in to the base beams through 10 mm wooden screws.

12.2.1 LOAD CELLS AND MECHANICAL SEPERATION
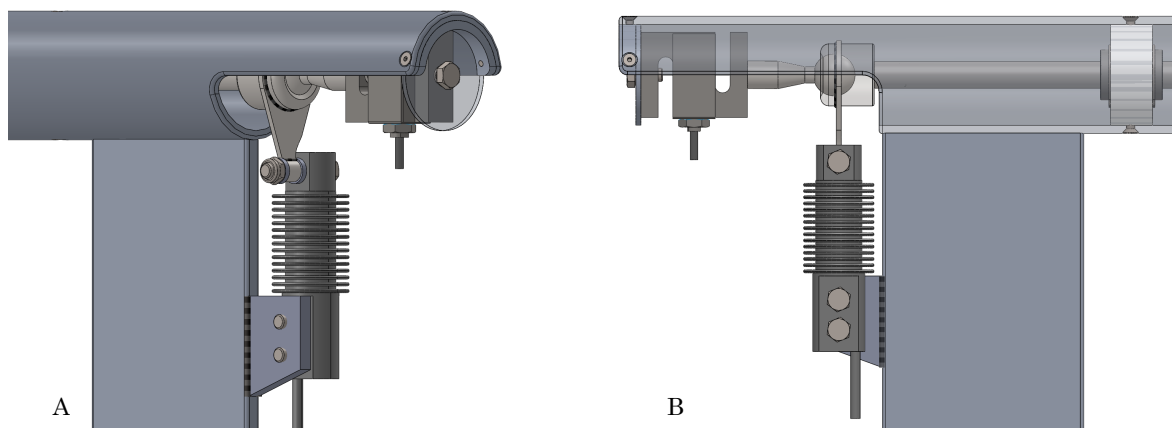
Figure 12.2.4. A: Connectivity of thrust/torque cell from the rear. B: Side view of the thrust/torque cell assembly with the circular beam and ball joint made transparent to visualize the mechanical separation between the thrust and torque cell.
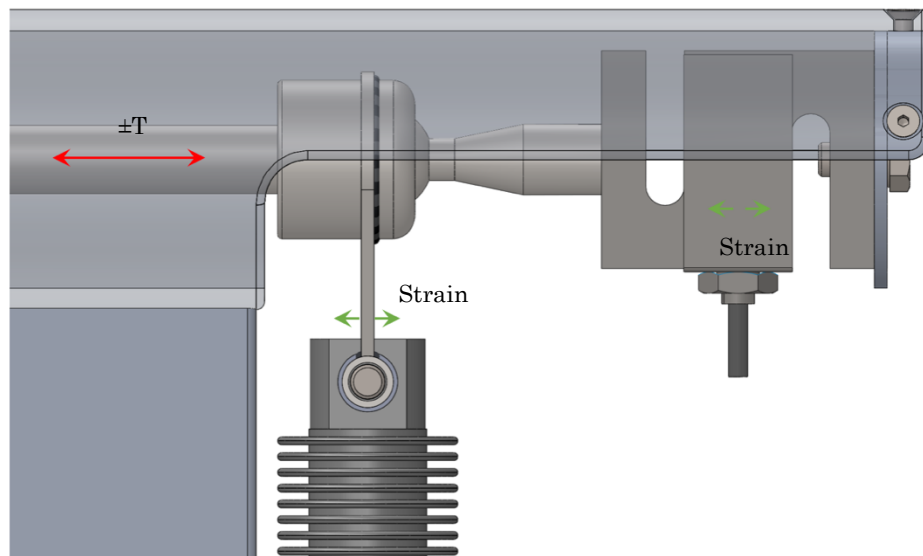
Figure 12.2.5. To avoid the torque cell from absorbing a component of thrust due to deflection of the thrust cell, the lever is not firmly connected to the torque cell and allowed some movement in axial direction. The torque cell and lever is separated by two nylon washers.

12.2.2 CABLING
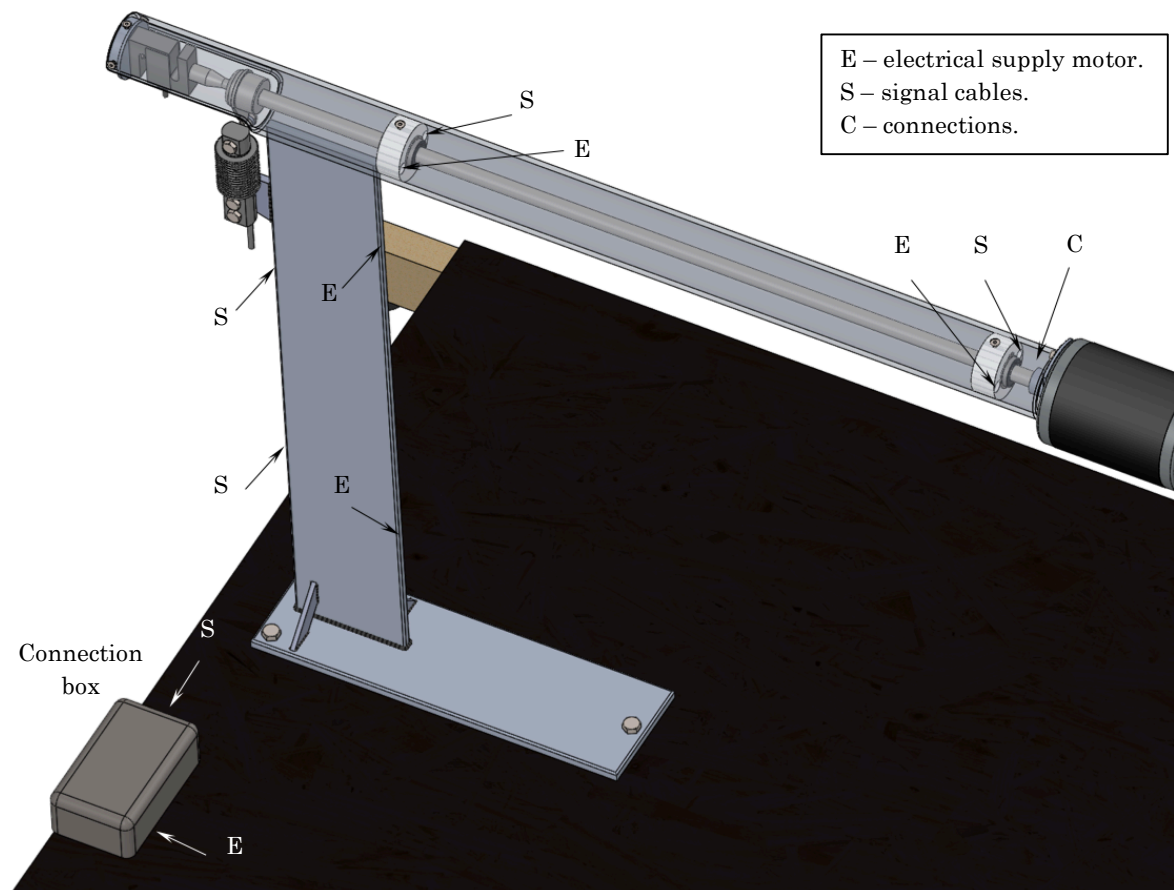
Figure 12.2.6. Overview of proposed layout of cabling. Making a connection point at C so that the motor can be easily disassembled. Laying both the supply cables for the motor and signal cable from the rpm sensor inside the circular beam at each side of the shaft through the holes in the bearing holders. The cables from the load cells and rpm sensor is laid down the backside of the support plate and in to the connection box. The supply cables are laid down the front side of the support plate an in to the other end of the connection box.

12.3 EXPANSIVE OPTIONS

This section illustrates the options for expanding the functionality of the test rig.

12.3.1 THREE BLADE EXPANSION.

Figure 12.3.1. Illustration of three blade expansion.

12.3.2 DUCT MOUNTING

A   B
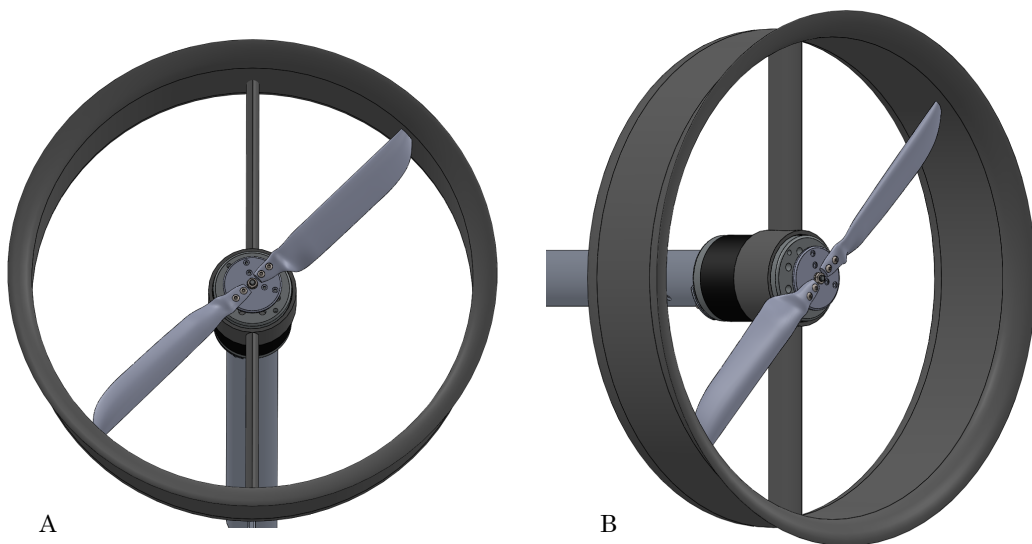
Figure 12.3.2. Illustration of proposed mounting of duct. The duct is for illustrative purposes only, when duct design is outside the scope of this thesis. A: Front view from underneath. B: Side view.

12.4 DESIGN OF MAIN COMPONENTS

To save cost and time the components were designed given available materials at the RealTek workshop.
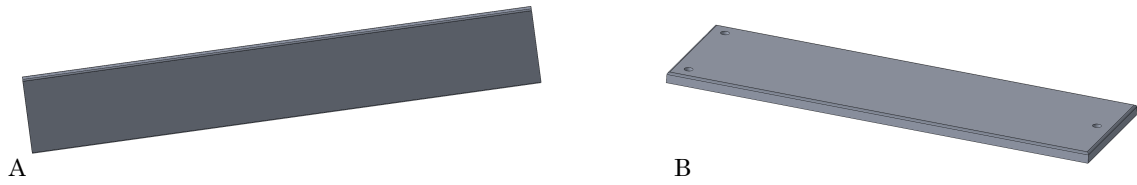
Figure 12.4.1. A: Support plate. B: Base support plate.
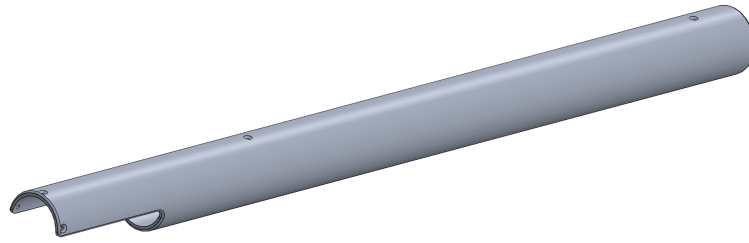
Figure 12.4.2. Circular beam with overhang at the end to protect thrust cell.
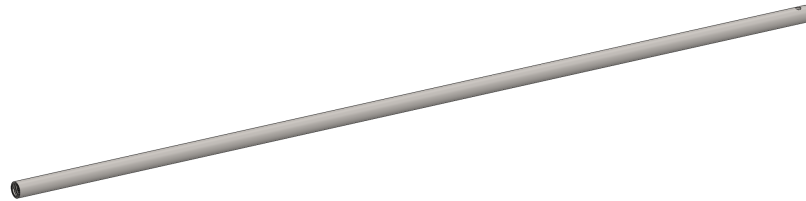
Figure 12.4.3. Shaft. M14 hole at the end for fastening ball joint.

Figure 12.4.4. Base plate from treated plywood.
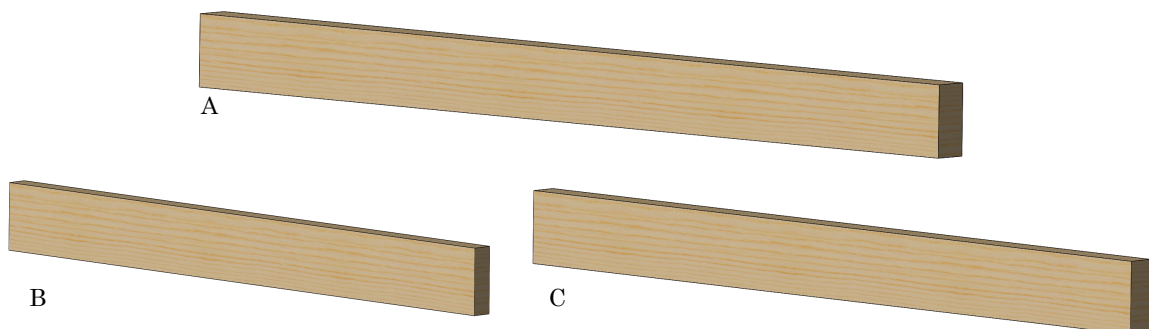
Figure 12.4.5. A: Base beam. B: Cross beam. C: Stiffener beam.

12.5 BRACKETS AND HOLDERS
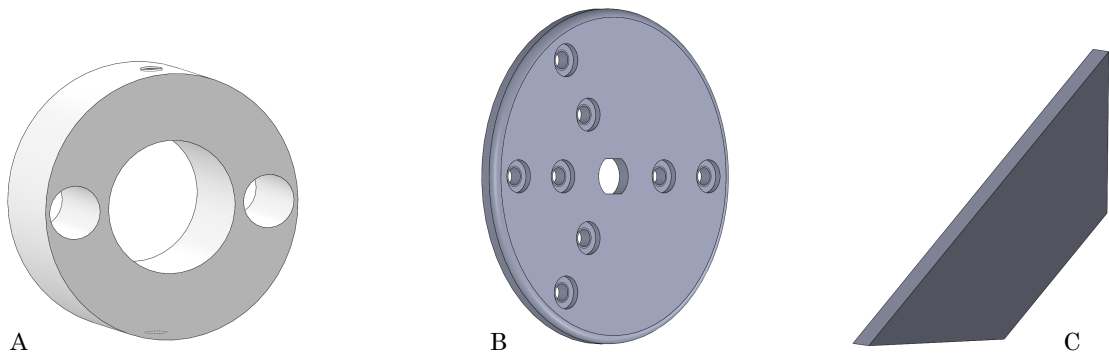
Figure 12.5.1. A: Bearing holder with holes for cabling. B: Propeller hub with 2 or 3 blade option. C: Support plate strut.
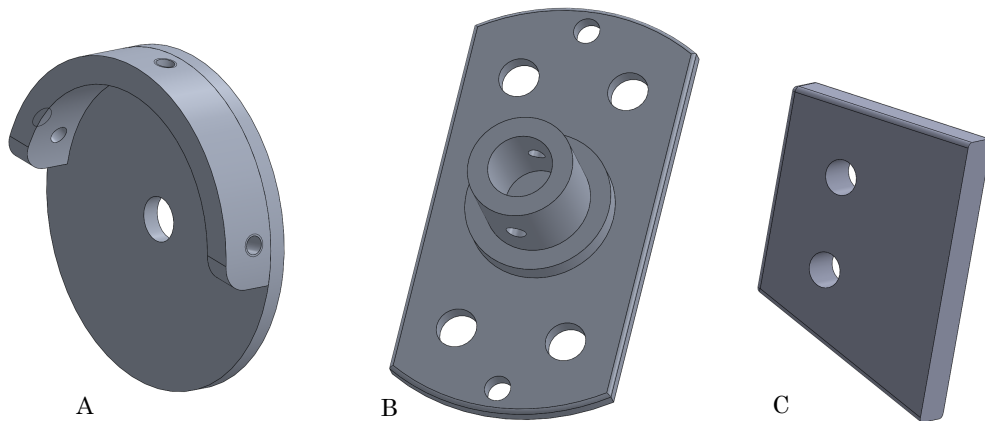
Figure 12.5.2. A: Thrust cell holder. B: Motor bracket with welded hub for shaft mounting. C: Torque cell bracket with two M8 tapped holes.
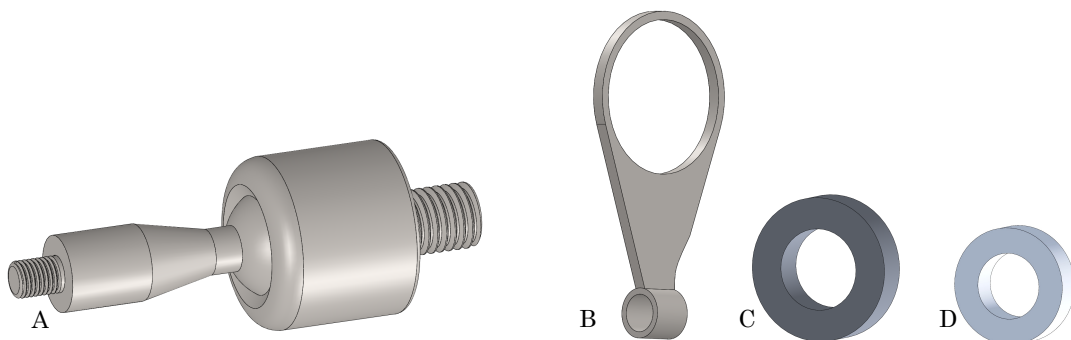
Figure 12.5.3. A: Modified automotive ball joint with M8 at the end to fit thrust cell. B: Torque cell lever. C: Spaced for torque cell. D: Nylon bushing.

12.6 STANDARD COMPONENTS

The standard components used can be seen in Figure 12.6.1 below.
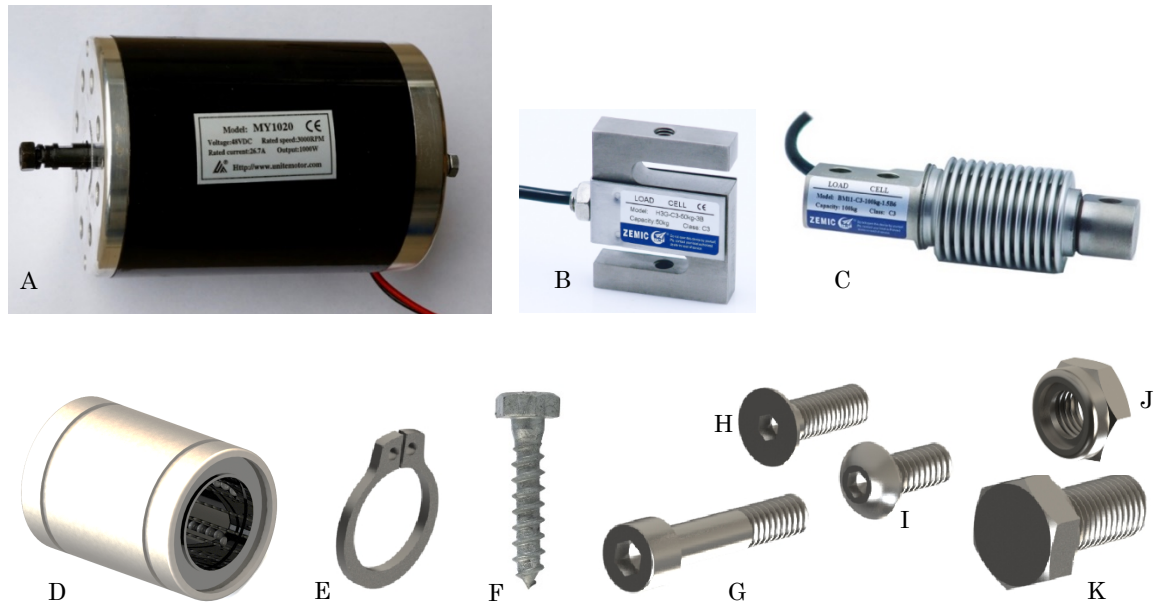
Figure 12.6.1. A: Electric motor. B: Zemic H3G[38]. C: Zemic BM11[38]. D: Linear ball bearing. E: Retaining ring. F: 10 mm wooden screw[40]. G: M5 hex socket screw. H: M5 countersunk hex screw. I: M5 hex screw. J: M8 locking nut. K: M8 bolt.

12.7 PRELIMINARY PROPELLER BLADE DESIGN

This section gives an overview of the details in the propeller blade designed. The design is based on values obtained from Texcel, yielding an ideal twist. The taper of the tip is arbitrarily chosen and a blunt end is left for compatibility with a duct. Airfoil choice and blade dimensions are listed in Table 12.7.1 below.

Table 12.7.1. Table showing airfoil characteristics and dimensions.

Dimension	Value	Unit
Airfoil	Eppler 423	-
R	300	mm
r_h	60	mm
α (max C_L/C_D)	6	degrees
$C_L(\alpha = 6)$	1.6	-
$C_D(\alpha = 6)$	0.015	-
c	50	mm
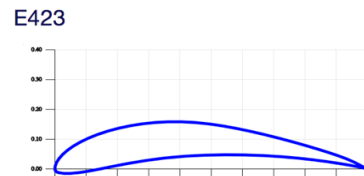
Figure 12.7.1. Airfoil cross-section used[1].

The airfoil cross section was generated in SW by coordinates [R]. The blade was designed in SW with ten divisions between tip and hub where each airfoil section was placed according to Table 12.7.2 and Figure 12.7.3 as seen in Figure 12.7.2.
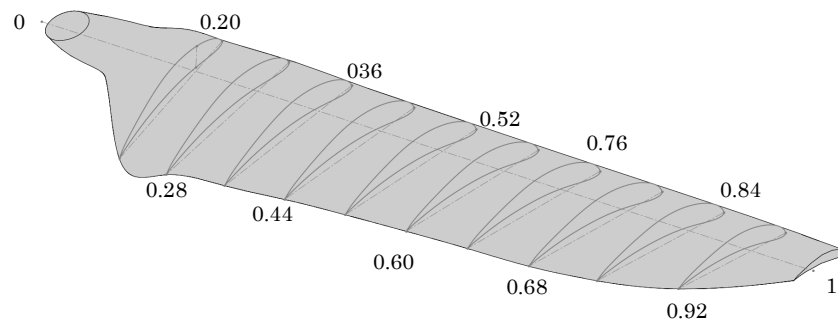
Figure 12.7.2. Sketch from SW showing design structure according to Table 12.7.2 and Figure 12.7.3.

Table 12.7.2. Showing scale of chord and angle of attack for each design plane.

r/R	0.20	0.28	0.36	0.44	0.52	0.60	0.68	0.76	0.84	0.92	1
Scale	0.9	1	1	1	1	1	1	1	0.95	0.8	0.4
α	6	6	6	6	6	6	6	6	6	6	6
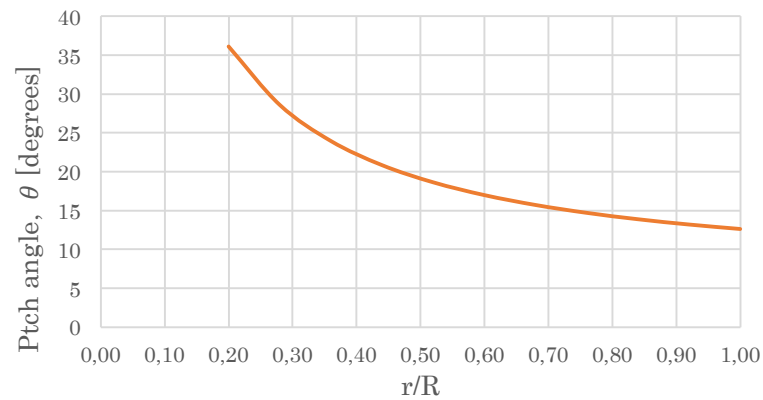
Figure 12.7.3. Graph of the twist distribution.

The finished blade is presented below.
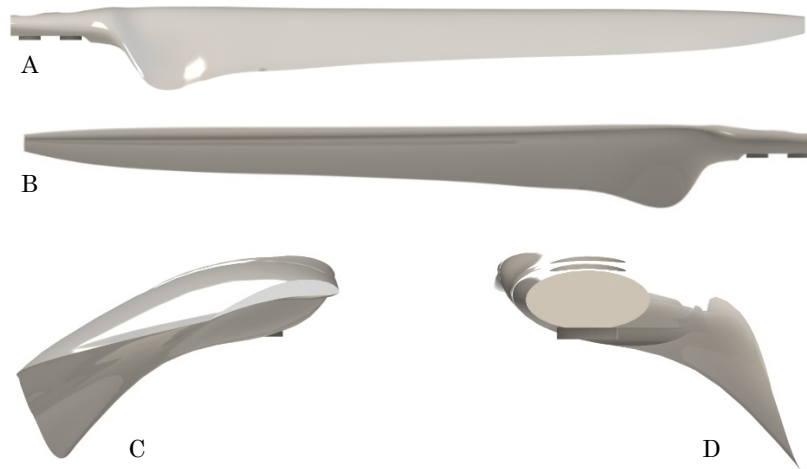
Figure 12.7.4. The propeller blade shown from four angles. A: Trailing edge. B: Leading edge. C: Tip. D: Root.

13 PRELIMINARY FLOW ANALYSIS

Flow analysis with numerical results and comparison with fundamental theory is found in this chapter.

13.1 SIMULATION GOALS

The main goal of this flow analysis is to test to what extent existing CFD-programs can be used to predict results.

The partial goal for the flow analysis are:
   o   To simulate thrust produced by the propeller.
   o   To simulate torque generated by the propeller.
   o   To simulate mechanical power needed to turn the propeller.
   o   To simulate slipstream power.
   o   To compare simulated results with predicted results from Texcel.

13.2 SIMULATION SETUP AND SETTINGS

The simulation was divided into two cases:
   o   Case 1: The motor and circular beam are downstream of the propeller, Figure 13.2.1 A.
   o   Case 2: The motor and circular beam are upstream of the propeller, Figure 13.2.1 B.
Simulation of slipstream power were only done in case 2.
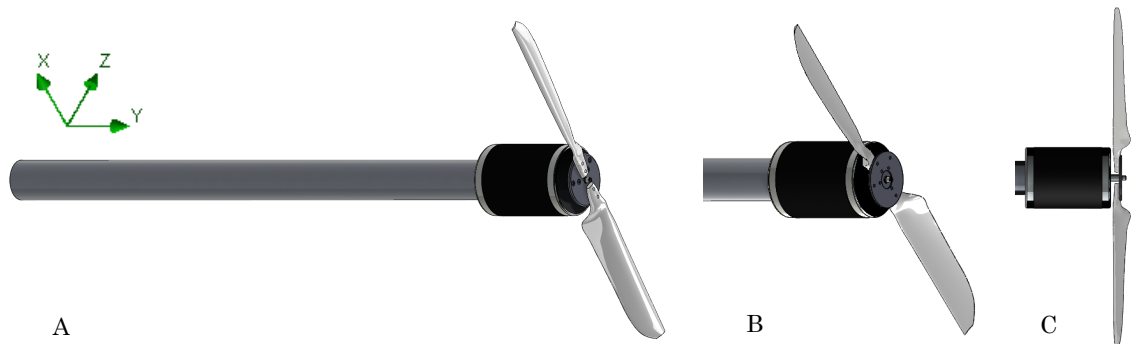
Figure 13.2.1. A: complete view of the simulation case 1 with motor and circular beam downstream. B: Case 2, blades and rotation reversed with motor and circular beam upstream. C: A circular surface were inserted 50 mm downstream in case 2, to obtain induced velocity.

Table 13.2.1 shows the settings used in FS for an averaging solution with 500 iterations.

Table 13.2.1. Settings for external simulation of case 1 and 2 in FS.

Setting	Value/setting	Unit
Temperature	20	C
Density	1.205	kg/m^3
Computational Domain	x = ±3.5R, z = ±3,5R, y= 3R and -6,5R	mm
Surface goal on propeller blades	Force in y-direction	N
	Torque in y-direction	Nm
Surface goal slipstream. Case 2 only	Average velocity y-direction	m/s
Equation goal Power	Torque in y-direction · rotational speed	W
Mesh	2.7 million cells	-
Rotational speed	2000, 2500, 3000, 3500	rpm

13.3 SIMULATION RESULTS

The two cases were simulated with four rotational speeds ranging from 2000 – 3500 rpm. Table 13.3.1 lists the thrust, torque and power figures produces by FS for a given rotational speed.

Case 1:

Table 13.3.1. Table of numerical values produced by FS for four relevant rotational speeds.

n [rpm]	2000	2500	3000	3500	Unit
T	26	41	54	81	N
Q	1.3	1.9	2.9	4.2	Nm
P	409	597	908	1301	W

Case 2:

Table 13.3.2. Table of numerical values produced by FS for four relevant rotational speeds.

n [rpm]	2000	2500	3000	3500	Unit
T	28	43	59	82	N
Q	1.4	2.2	3.1	4.1	Nm
P	437	678	973	1297	W
$\bar{V}_i$	7.3	9.2	10.5	12.4	m/s
η_p	0.46	0.59	0.64	0.79	-

The thrust and power results from Table 13.3.1 and are plotted in Figure 13.3.1 and compared with predicted results from both MT, both ideal and adjusted for figure of merit of 0.75.
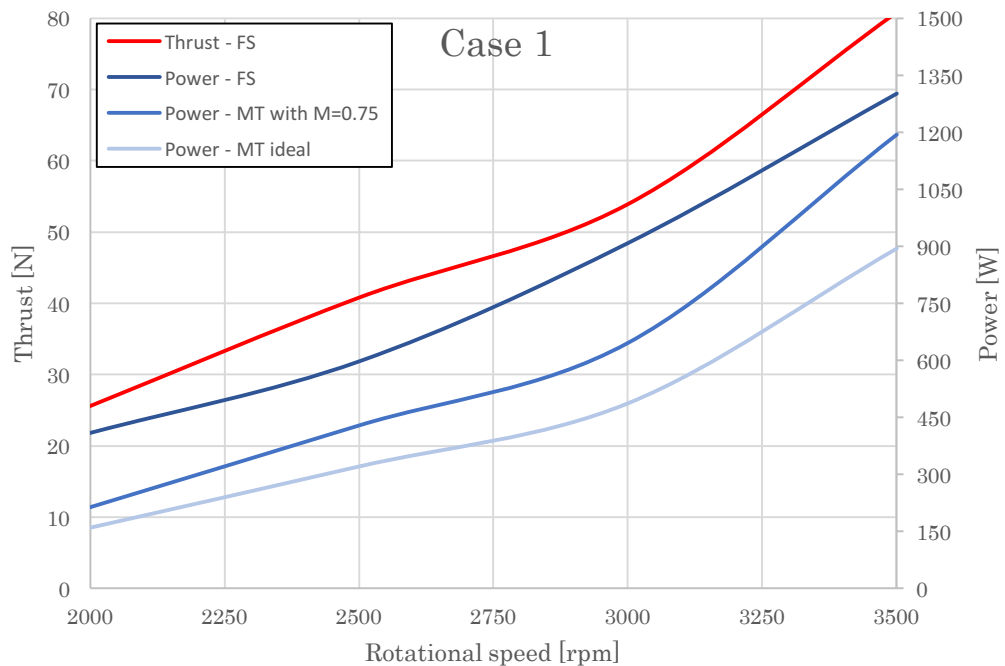
Figure 13.3.1. Plotted results of thrust and power vs. rpm from Case 1. Also, power predicted to produce the same amount of thrust in Table 13.3.1 by momentum theory with figure of merit 0.75 and an ideal case, are included for comparison.
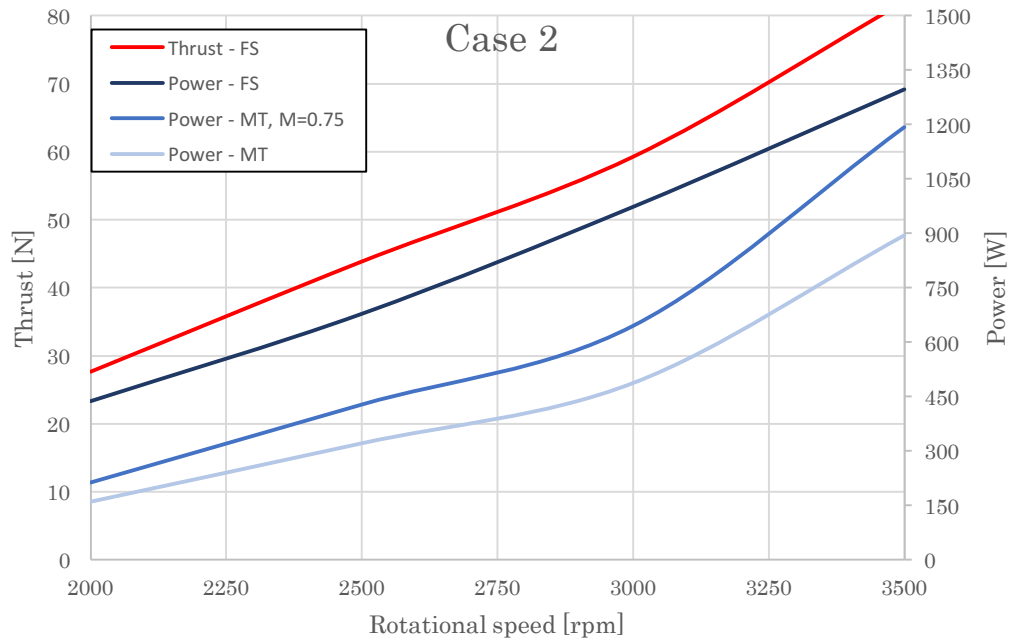
Figure 13.3.2. Plotted results of thrust and power vs. rpm from Case 2. Also, power predicted to produce the same amount of thrust in Table 13.3.1 by momentum theory with figure of merit 0.75 and an ideal case, are included for comparison.

In Figure 13.3.3 the figure of merit is plotted for both cases and the propeller efficiency in Case 2 are also included.
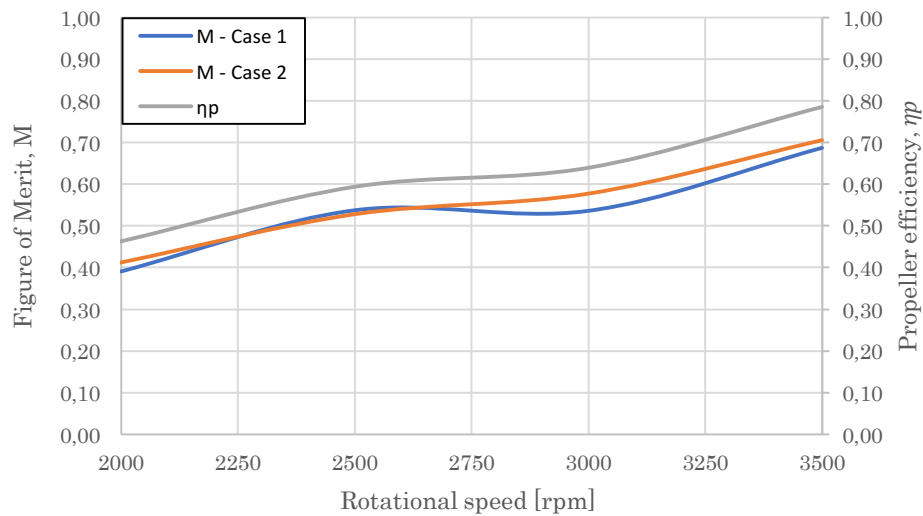
Figure 13.3.3. Plot of figure of merit for both cases and propeller efficiency in Case 2 against rpm.

Below, the velocity plots from Case 1 and 2 are presented. The results are discussed in section 16.3
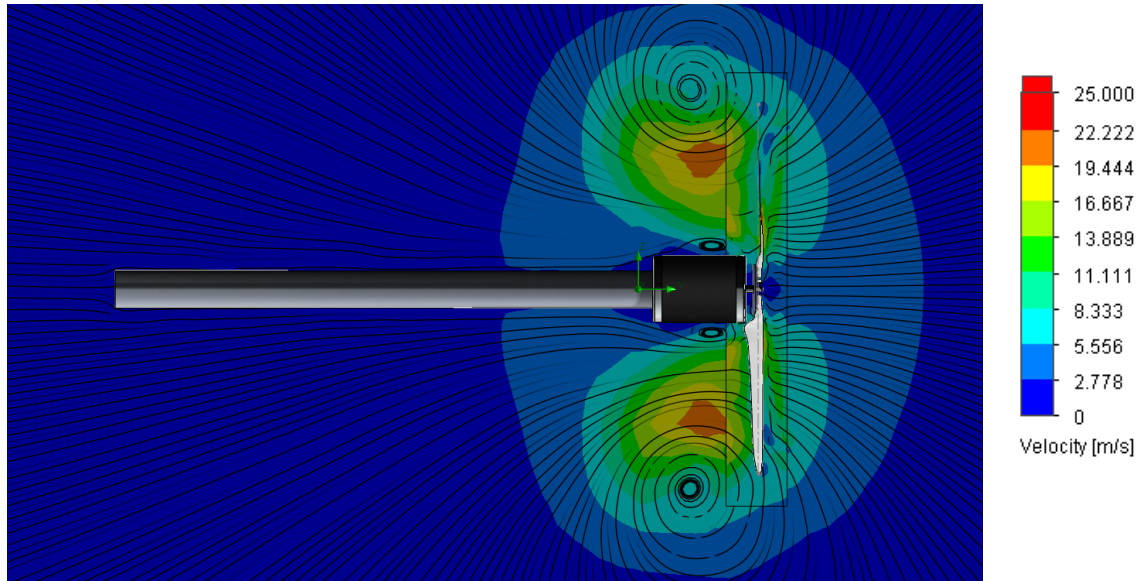
Figure 13.3.4. Velocity plot Case 1 with 3000 rpm.
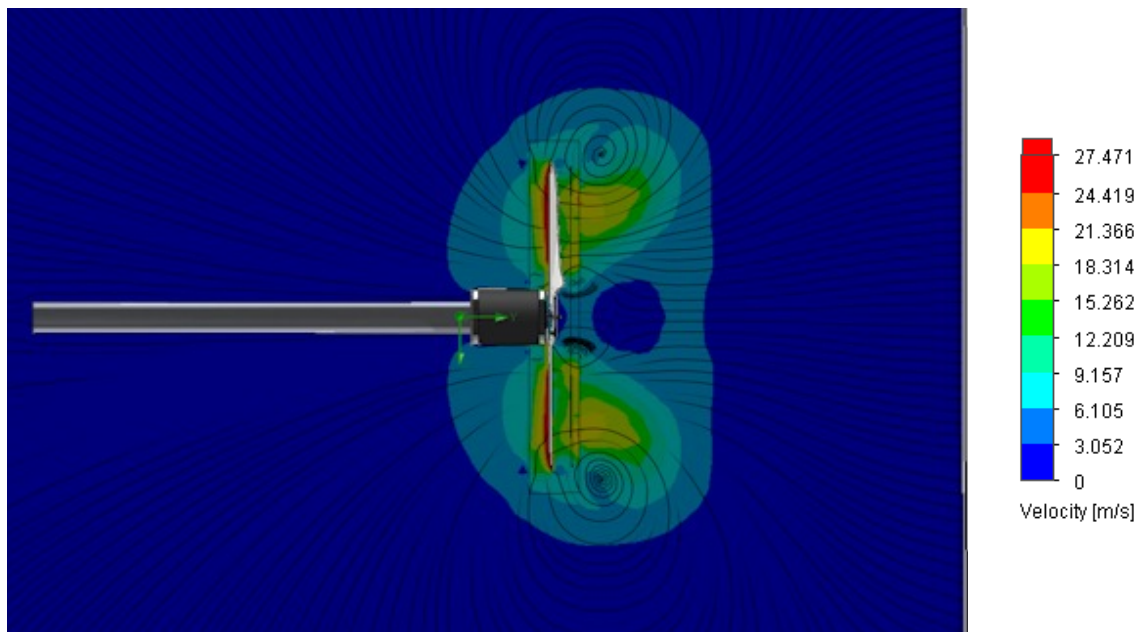
Figure 13.3.5. Velocity plot for Case 2 with 3000 rpm.

14 ROBUSTNESS AND MAINTENANCE

A brief discussion of structure optimization, material choices and weight follows.

14.1 STRUCTURE OPTIMIZATION

FEM-analysis and optimization of propeller blades and hub are left for future work.

14.2 MATERIAL CHOICE AND WEIGHT

An overview of the materials for each component follows.

Table 14.2.1. Table of material for each component with key mechanical properties.

Component	Material	Mass	Yield strength	E-modulus
Circular beam	Al 6082-T6	2.7 kg	250 MPa	70 GPa
Support plate	Al 6082-T6	2.7 kg	250 MPa	70 GPa
Base support plate	Al 6082-T6	2.3 kg	250 MPa	70 GPa
Angle strut	Al 6082-T6	0.005 kg	250 MPa	70 GPa
Base plate	Plywood	10 kg	25 MPa	8.2 GPa
Base beam	Spruce	1.3 kg	-	-
Base beam cross	Spruce	0.8 kg	-	-
Base beam cross	Spruce	0.8 kg	-	-
Baring holder	PVC	0.01 kg	15 MPa	2
Bracket thrust cell	Al 6082-T6	0.014 kg	250 MPa	70 GPa
Ball joint	Low alloy steel	0.35 kg	235 MPa	210 GPa
Motor bracket	Al 6082-T6	0.06 kg	250 MPa	70 GPa
Thrust cell plate	Al 6082-T6	0.05 kg	250 MPa	70 GPa
Plastic bushing	Nylon 46	0.001 kg	45 MPa	1 GPa
Propeller hub	Al 6082-T6	0.02 kg	250 MPa	70 GPa
Shaft	AISI 440B	1.3 kg	1280 MPa	200 GPa
Torque lever	Low alloy steel	0.02 kg	235 MPa	210 GPa
Propeller blade	Onyx nylon [Q]	0.64 kg	36 MPa	2.9 GPa
		23.9 kg		

Total weight of the whole rig including motor:

29 kg

14.3 SURFACE TREATMENT

All welded steel components must be surface treated to avoid corrosion even though the rig is intended for indoor use.

15 MANUFACTURE AND PRODUCTION COST

A brief description of production method for each part and a short economic analysis follows.

15.1 MANUFACTURE

Table 15.1.1. An overview of the production method for the main components.
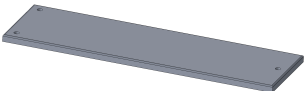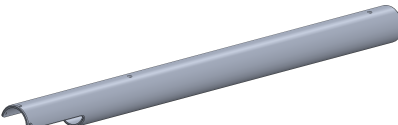
Main Component	Production method	
	o Cutting o Welding	
	o Cutting o Drilling	o Welding
	o Cutting o Drilling	o Welding
	o Drilling o Threads	
	o Cutting	
	o Cutting	

Table 15.1.2. An overview of the production method for brackets and holders.
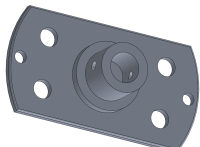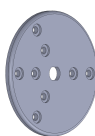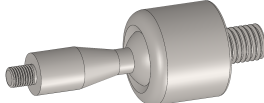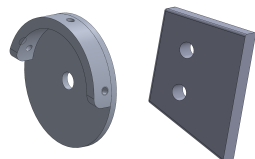
Component	Production method	Component	Production method
	o Turning o Drilling		o Cutting o Turning o Welding o Drilling
	o CNC milling o CNC turning		o Turning
	o Cutting o Welding		o Cutting o Turning o Welding
	o Cutting o Drillig o Welding		o Turning

Table 15.1.3. Table of proposed production method for the propeller blades.

Component	Proposed production method
	3D-printing using carbonfiber reinforced nylon

15.2 COST CALCULATION PROTOTYPE

The following cost calculation does only account for production of one rig.

Table 15.2.1. Table of timed activities and associated costs at the top and component pricing with a total prototype cost at the bottom.

Activity	Amount	Price NOK	Sum NOK
Investigation	220	650 /h	143 000
Theoretical work	150	650 /h	97 500
Development	180	650 /h	117 000
CAD-design	50	650 /h	32 500
Report work	250	650 /h	162 500
Sum concept development	**850**		**552 500**
Parts manufacturing	30 h	500 /h	15 000
Welding	5 h	500 /h	2 500
Assembly and adjustment	20 h	500 /h	10 000
Miscellaneous	5 h	500 /h	2 500
Sum manufacturing	**60 h**		**30 000**

Components	Amount	Price NOK	Sum NOK
Unite MY1020 motor	2	2100	2100
Zemic H3G	1	2200	2200
Zemic BM11	1	2200	2200
LM16UU linear bearing	3	128	385
Bosch 1000x16 steel shaft	1		472
Onyx 3D-print material*	2 x 543 cm³	2 /cm³	2172
Base 35x73 wood	5.5 m	17 /m	94
Base plate plywood	1	350	350
Rubber foot	6	8 /piece	40
Alu plate 120x10*	2,7 kg	50 /kg	135
Alu tube*	2,5 kg	50 /kg	125
Various alu parts*	1 kg	50 /kg	50
PVC*	0,2 kg	85 /kg	20
Screws and fasteners*	-	-	100
Wooden screws	1 pack		80
Various material expenses	-	-	1200
Sum materials			**11 722**
Total sum prototype			**594 222**

*Materials in-house at RealTek.

PRODUCT PRESENTATION

Rendered illustrations for the experimental setup is presented.
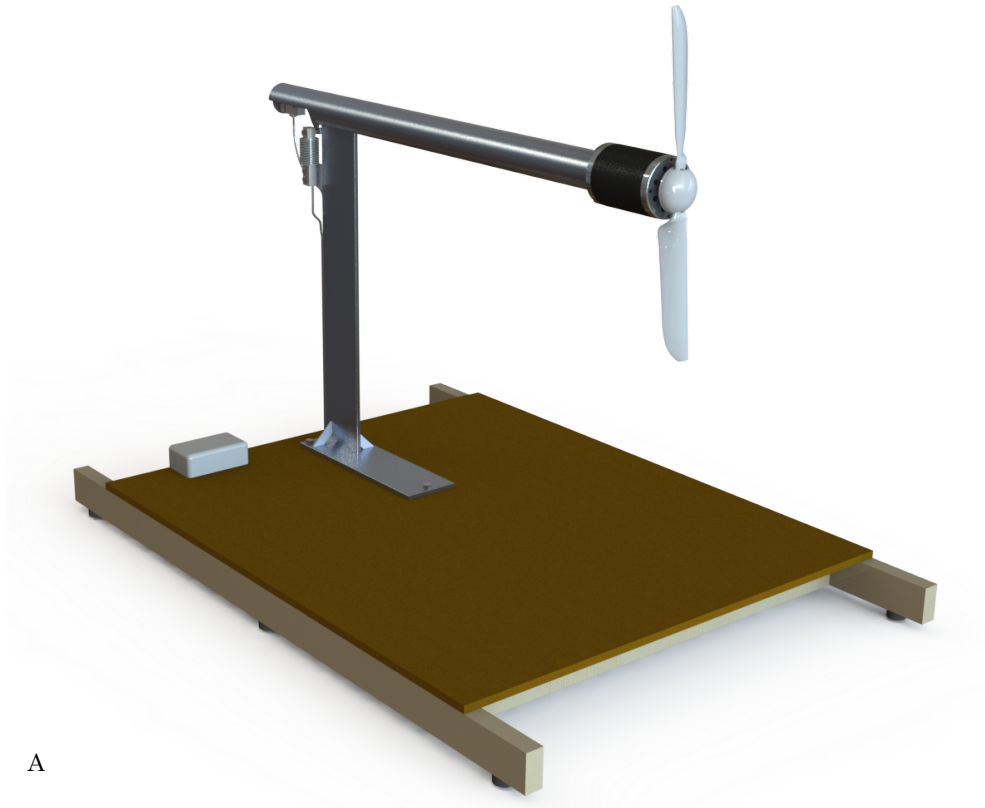
A
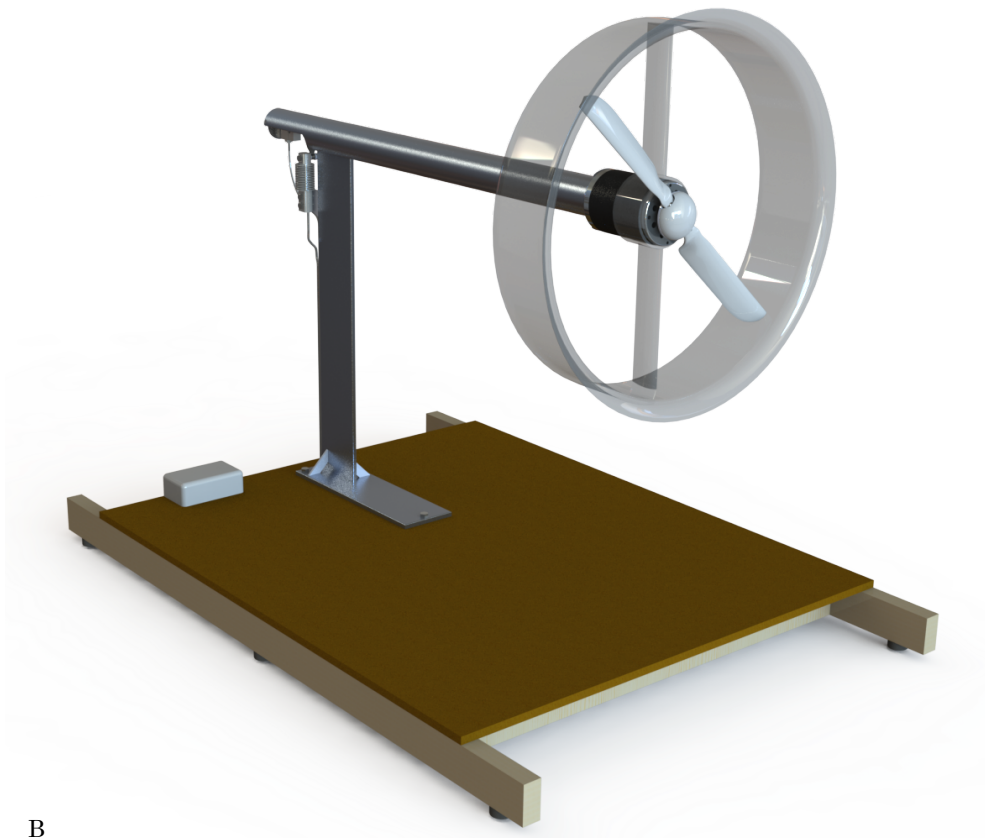
B

Figure 15.2.1. A: Setup with open propeller. B: Setup with ducted propeller. Duct is illustrative only.

16 PROCESS EVALUATION AND DISCUSSION

In this chapter the development process, revisions in design and results are discussed.

16.1 CONCEPT DEVELOPMENT WORK, IMPROVEMENTS

Initially, the main objective for this thesis were to both design a whole thruster unit and conduct tests. As work in reviewing theory and developing theoretical tools progressed, the level of ambition had to be significantly reduced and the objectives had to be revised. The fundamental theory was established and gave estimates for power consumption for given thrust. With the extension of the Texcel sheet with BET, important design parameters such as number of blades, chord length, and radius could be inputted to see how the power was distributed and give estimates on torque and rotational speed. Developing detailed theoretical tools requires time and high level of aerodynamic understanding and mathematical problem-solving skills. Therefore, theory developed and used in this thesis are a basis only and have high uncertainty. Focus was then turned to planning an experimental setup that will lay the foundation for future learning and validation of theoretical tools.

Development Process

- o The cyclic concept generation described in section 3.2.3 by Pughs method were used in Section 11.1 and 11.2. The initial concept generation for the experimental setup gave an initial best concept, but after discussion with fellow students, a new concept emerged as a combination of previous concepts. This concept also turned out to be the concept selected. For the selection of load cell configuration, only concept A and B were first generated. Although not described in the report, the use of a s-type load cell for measuring thrust in concept C, were inspired by the concept A, and how the 2-axis load cell were fitted. Hence, the concept selected for load cell configuration were generated from two other concepts.

Improvements

- o Should have attempted a parallel simulation in ANSYS Fluent at an earlier stage to generate comparable results with FS.
- o Could have involved available expertise for the search for suitable electric motors. Motors for large radio controlled planes and helicopters were not thoroughly investigated.
- o A search for bearing alternatives for the mechanical separation of the thrust and torque cell should have been given more priority.

16.2 REVISIONS IN DESIGN AND PRODUCTION

This section handles revisions for the results in Part Two only, since the results from Part One are initial.
- o Supports struts at the end of the circular beam may be required if duct is mounted on the motor.
- o Consider torsional dampening on shaft to avoid any shocks and noises when starting the motor.
- o Redesigning bracket for torque cell and lever so the torque cell is positioned directly behind the support plate.

- A safety wire or small chain between the motor and the circular beam should be fitted in case the shaft becomes loose during operation or the motor is started by mishap without the load cells connected. This can prevent serious damage if the propeller/motor/shaft assembly flies off the rig.
- Mounting foldable wheels at the base, allows for easy movement of the rig.
- Ball bearing separation of thrust and torque cell for reduction in friction.
- The base made from wooden beams might be replaced by an aluminum construction to improve robustness and wear. The base plate could also be made from aluminum with pre-drilled holes for attaching addition equipment.
- The support plate can possibly be made of two interlocking parts that facilitates adjustment to the height of the circular beam to adjust for possible undesirable aerodynamic effects, which may be caused by the base.
- The calculated weight based on the proposed Onyx 3D-print material for the propeller blades are high when considering centrifugal forces. Alternatives materials should be investigated.
- Mounting tapered covers to ease the transition between motor and circular beam to avoid separation. Also, covering the load cell assembly at the back with covers may help with possible disturbances in the airflow.

16.3 DISCUSSION OF RESULTS

Part One

- Implementing the BET as defined in section 4.5 on ducted fans the same way it was applied on open propellers, proved unsuccessful. The higher induced velocity by MT produced torque and power figures far from the MT-prediction in section 4.3.2. If the requirements for propeller protection, and the noise reduction that ducted fans offer - warrants further investigated in the future - specific BET that takes in to account the presence of a duct or shroud needs to be developed [11]. Se [42] as a starting point. However, as shown in section 4.6, ducted fans have considerable challenges in transversal flight and should be approached with skepticism.
- The thruster layout of coaxial propellers is beneficial for tip speed considerations when in normal operations. However, the objectives of a protection from the rotating blades might be challenging to achieve since a coaxial configuration increases the height of the thruster itself, the efficiency of coaxial rotors increases with increasing separation, see [13]. Any duct fitted around separated coaxial rotors will have a large cross section normal to the air flow in transversal flight which increases drag, giving a challenging starting point.

Part Two

- Considering the flow plots from the flow analysis that did not show a contracting slipstream, might be explained in the following way: The strength of the tip vortices is too high compared to the propeller radius and the slipstream cannot form. Several settings for turbulence strength were tested in FS, but with no significant change. This can imply that the propeller blades have poorly designed tips. However, the results for induced velocity in Case 2 showed a maximum of mean value of 12.4 m/s in axial direction and 0 m/s, a distance 0.5 meters downstream, this condition is hardly realistic. FS has clearly met its limitations for generating detailed flow patterns that makes sense. This means that a dedicated program needs to be developed, implementing existing vortex models such as Goldstein's hypothesis and the Betz condition (see [21] and [13]), combining incremental MT and detailed analysis of airfoil

dimensions and aerodynamic characteristics at each incremental radial station. Such programs are available e.g. JavaProp [43]. However, using such a code, requires detailed understanding of BET, MT and vortex models in the first place – warranting the development of an in-house code to be developed that can be customized to suit the application in hand.

o   Increasing efficiency with rpm in the simulation (section 13.3) can be explained by the increase in Reynolds numbers – hence better airfoil characteristics.

o   If the simulated results in FS are overestimates, the current motor might be low on rpm and a higher revving motor may be required.

o   The relative deflection of the circular beam of 0.23 mm should not cause any problems for the alignment of the linear bearings, however it is hard to tell whether it will be a problem before the rig is built. Also, the relative deflection of the shaft on relation to the circular beam of 0.7 mm and its effects on pinching in the circular bearings are unknown and must be checked. Alternatively, the shaft diameter and bearings can be changed to 20 mm, although it will reduce the room for cabling inside the circular beam.

17 CONCLUSION

In this chapter, conclusions regarding objectives, results, recommendations and how the future work should proceed, are presented.

17.1 ACHIEVEMENT OF OBJECTIVES

Investigation and theoretical development led to initial specifications for a thruster unit and can be found in Part One of this report, including outer dimensions, layout, required thrust and power. Also, suggestions for type of electric motor and initial propeller dimensions can also be found.

Full specification and drawings for a scaled test rig can be found in Part Two of this report. Also, a simple experimental plan with experimental method and equipment is also defined.

17.2 RESULTS AND RECOMMENDATIONS

In this section, the physical results and important recommendations are presented.

Main Results

Part One:
Through investigation and theory development, initial specifications for a thruster unit are as follows:
- o Assuming a gross weight of 450 kg, a thruster unit with two coaxial contra-rotating propellers will require a power of 50 kW and a total swept area of 2.26 m². This gives a specific weight of 2.25 kg/kW.
- o Minimum hover power is 18 kW for each thruster.

Part Two:
- o An experimental test rig for measuring thrust and torque produced by a propeller is designed with full specifications and technical drawings for a total cost of 595 000 NOK. A simple experimental plan overviewing method and experimental equipment is also found in this report.
- o The rig is 1500 mm long, 1000 mm wide and 890 mm high without the propeller. Total weight is 29 kg.
- o The test rig is optimized for the specified engine of 1 kW and the designed propeller of 600 mm, but is also capable of handling up to 3 kW of power, and up to 800 mm diameter propellers.

Important Recommendations

Part One:
- o An implementation of a wing area for forward flight is recommended since relying on the thrusters to both keeping the aircraft in the air and horizontal motion yields a high energy consumption.
- o The theoretical results in part one are highly ideal and a dedicated code/program for predicting and designing propellers/fans/rotors are recommended to be developed.
- o In regards of noise, more investigation on tip speed as a noise driver is recommended.
- o For their contributions in efficiency and possible noise reducing effects, ducted fans should be investigated further, but with caution. Many challenges are associated with ducted fans.

Part Two:
- o The mechanical separation of thrust and torque should be developed further to reduce friction. Possibly some type of conical bearing that can handle compression/tension axially. This is a critical point of the test rig since predicted torques are low and friction must be handled with care.
- o When measurements are done, care must be taken so that the slipstream can escape freely and the air can circulate back upstream of the propeller. Open space in radial direction should at least be 5R. The rig must possibly be elevated somehow if disturbance from the floor is significant.
- o Alternative materials and production for propeller blades can be high strength nylon with CNC-machining.
- o Evaluate the possibility of tipping or movement of the rig. Consider weighting of the test rig to avoid movement and other problems that may be associated with the relative low weight of the whole test rig.
- o A replacement of wooden base in an aluminum structure to improve robustness and stability.
- o If the current electric motor turns out to be too heavy or inefficient, a search into electric motors is recommended. Only the motor bracket needs to be modifies to accommodate a new motor. However, review the engine characteristics carefully as they are designed for propellers, whose characteristics are unknown.

17.3 FUTURE WORK

Concept Development Process

- o If available, involving alternative simulation program in parallel with the main simulation program chosen to acquire more information about the validity of the results.
- o When searching for suitable electrical motors, the expertise available in electric equipment should be involved right a way to bring to light all alternatives.
- o When alternatives for a critical component is to be found - in this case the bearing or joint for the mechanical separation - allocating more time and resources for the search should be done. This can prevent critical details from disrupting the outcome of the design.

Design and Production

Part One:

- o Development of a program/code for prediction and design of propellers.
- o Investigate how a wing area can be implemented into the drone/aircraft design.

Part Two:

Please see section 16.2 and 17.2, however important points are:
- o Evaluate stability of the experimental rig - possible weighting.
- o Develop a design for a duct with attachment to either motor or base plate. Se [42] as a starting point.
- o Structure optimization, material choice, frequency analysis and production method for propeller blades and hub.
- o Evaluate friction characteristics for the ball joint and investigate ball bearing alternatives.
- o A detailed deflection calculation of the shaft to consider pinching in linear bearings.

18 REFERENCES

All references including written, personal interview and web sources are found in this chapter.

18.1 WRITTEN SOURCES

3. Finnøy, S.E., *Waste Heat Recovery System for The Dolphin Concept Car.* 2014, Norwegian University of Life Sciences, Ås.
4. Henriksen, V.G. and J.K. Bøe, *Utvikling, dimensjonering og konstruksjon av dampturbinløsning for Dolphin-konseptet ; Development, Dimensioning and Construction of a Steam Turbine Solution for the Dolphin Concept.* 2016, Norwegian University of Life Sciences, Ås.
5. Sundquist, P. and A.M. Thue, *Utvikling, dimensjonering og konstruksjon av multifuel gassturbinmotor (Multifuel turbinmotorkonsept) ; Development, dimensioning and construction of multi-fuel gas turbine engine (Multi-fuel turbine engine concept).* 2012, Norwegian University of Life Sciences, Ås.
8. Terjesen, G., *Sveiste forbindelser Eurokode 3.* 2015.
9. Samset, K., *Prosjekt i tidligfasen : valg av konsept.* 2008, Trondheim: Tapir akademisk forl.
10. Pugh, S., *Total Design: Integrated Methods for Successful Product Engineering.* 1991: Addison-Wesley Publishing Company.
12. Gieck, K. and R. Gieck, *Engineering Formulas. Vol.* 1997, McGraw-Hill.
13. Johnson, W., *Rotorcraft Aeromechanics.* Vol. 36. 2013: Cambridge University Press.
14. Finnemore, E.J. and J.B. Franzini, *Fluid Mechanics with Engineering Applications.* 2009: McGraw-Hill.
15. Abbott, I.H. and A.E. von Doenhoff, *Theory of Wing Sections: Including a Summary of Airfoil Data.* 2012: Dover Publications.
16. Tipler, P., *Tipler and G. Mosca, Physics For Scientists and Engineers With Modern Physics.* 2008, WH Freeman and Company, New York.
17. Lazareff, M., *Aerodynamics of Shrouded Propellers.* AGARDograph, 1968. **126**: p. 237-289.
18. Platt Jr, R.J., *Static tests of a shrouded and an unshrouded propeller.* 1948.
19. Black, D.M., H.S. Wainauski, and C. Rohrbach, *Shrouded propellers--a comprehensive performance study.* 1968: American Institute of Aeronautics and Astronautics.
20. Poisson-Quinton, P., *Introduction to V/STOL aircraft concepts and categories.* BLANK PAGES IN THIS DOCUMENT WERE NOT FILMED, 1968: p. 2.
21. Phillips, W.F., *Mechanics of flight.* 2nd ed. ed. 2010, Hoboken, N.J: Wiley.
23. Graf, W.E., *Effects of duct lip shaping and various control devices on the hover and forward flight performance of ducted fan UAVs.* 2005, Virginia Tech.
25. Weir, R.J., *Ducted propeller design and analysis.* Sandia National Laboratories, Albuquerque, 1987.
36. Taylor, J., *Introduction to error analysis, the study of uncertainties in physical measurements.* 1997.
42. McCormick, B.W., *Aerodynamics of V/STOL flight.* 1967: Courier Corporation.

18.2 PERSONAL INTERVIEW

11. Nygaard, T.A., *Professor.* 2017.

18.3 WEB SOURCES

1. Tools, A. 2017; Available from: http://airfoiltools.com/.
2. International, F. *Bell X-22A Analasys of a VTOL research vehicle.* 1967 01.09.2016]; Available from: https://www.flightglobal.com/pdfarchive/view/1967/1967 - 0453.html.
6. Flynn, D. *Boeing Sky Commuter 'flying car' prototype sells for over $70,000.* [Picture] 2015 20.08.2016]; Available from: http://www.ausbt.com.au/boeing-sky-commuter-flying-car-prototype-sells-for-over-70-000.
7. International, M. *Skycar 400.* 2016 30.08.2016]; Available from: http://www.moller.com/moller_skycar400.html.

22.   Database, A.I. 2017; Available from: http://airfoildb.com/.
24.   CNET. *Electric aircraft energize Paris Air Show.* 2017; Available from:
        https://www.cnet.com/.
26.   Ehang, I. *Specifications.* 2016 [cited 2016 29.08.2016]; Available from:
        http://www.ehang.com/ehang184/specs/.
27.   Terrafugia. *TF-X.* 2016 30.08.2016]; Available from: https://www.terrafugia.com/tf-x/.
28.   Expert, A. *AgustaWestland Project Zero VTOL Aircraft.* All Auto Experts 2016;
        Available from: http://www.allautoexperts.com/.
29.   Wang, J. *AW Project Zero.* 2017; Available from: http://www.youtube.com/.
30.   Company, X.A. *Trifan 600.* 2016 31.08.2016]; Available from:
        http://www.xtiaircraft.com/trifan-600/.
31.   SKELDAR, U. *Skeldar V-200.* 2017; Available from: http://umsskeldar.aero/.
32.   e-volo. *Volocopter VC200.* 2017; Available from: http://www.e-volo.com/.
33.   Argodesign. *Drone ambulance.* 2017; Available from: http://www.argodesign.com/
34.   Motor, L. 2017; Available from: http://lynchmotors.co.uk/.
35.   Motors, J. 2017; Available from: http://www.jobymotors.com/.
37.   Futek. *MBA500.* 2017; Available from: http://www.futek.com/.
38.   Zemic. *BM11/HG3.* 2017; Available from: http://www.zemiceurope.com/.
39.   Astrup. *Runde aluminiumsrør.* 2017; Available from: http://www.astrup.no/.
40.   Tingstad. *Treskruer sekskant.* 2017; Available from: http://www.tingstad.no/.
43.   Hepperle, M. *JavaProp - Design and Analysis of Propellers.* 2017; Available from:
        http://www.mh-aerotools.de/.
44.   Helicopter, B. *Bell 429.* 2017; Available from: http://www.bellhelicopter.com/.

19 APPENDIX

A: Exploded view of assembly

B: Assembly with dimensions

C - E: Momentum Theory for Open Propellers in Axial Flight

F: Physical properties of air

G - I: Solutions for Derived Expressions in Chapter 4.7, Inputted in Excel

J: Print of Texcel Full Scale

K: Print of Texcel for Experimental Prototype

L: Performance Factor of a Commercial Helicopter

M: Unite MY1020 motor

N: Lynch motors

O: Joby motor

P: Price Futek MBA500

Q: Onyx 3D-print material

R: Coordinates for Eppler 423

EXPLODED VIEW OF ASSEMBLY

A
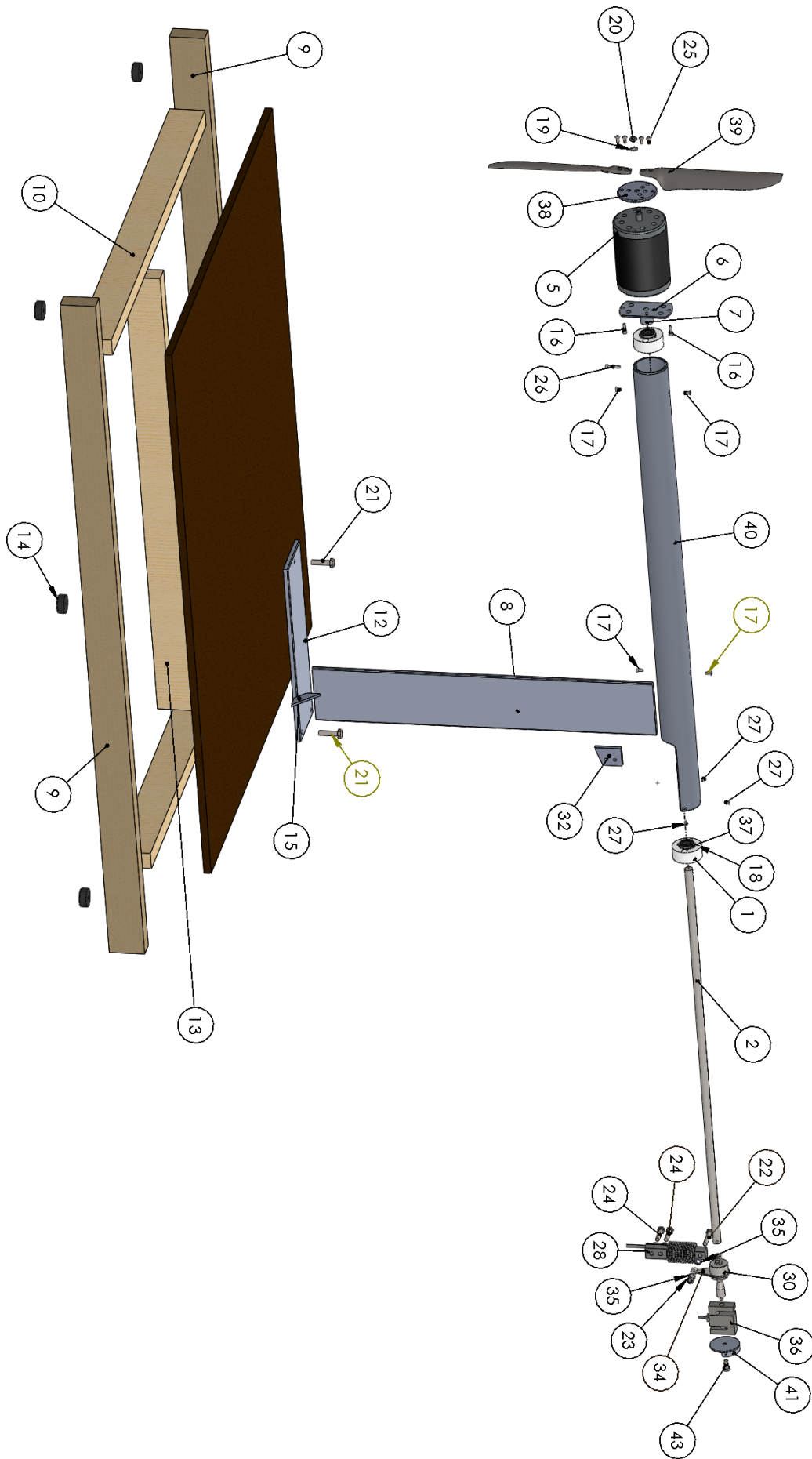
TECHNICAL DRAWING OF ASSEMBLY

Dimensions (top-left view): 1000, 1500, 1200, 400, 120, 35

Dimensions (right view): 745, 150, ⌀70, 1015, 700, 120, 52

Dimensions (lower view): 88, ⌀80, 10, 15, ⌀108
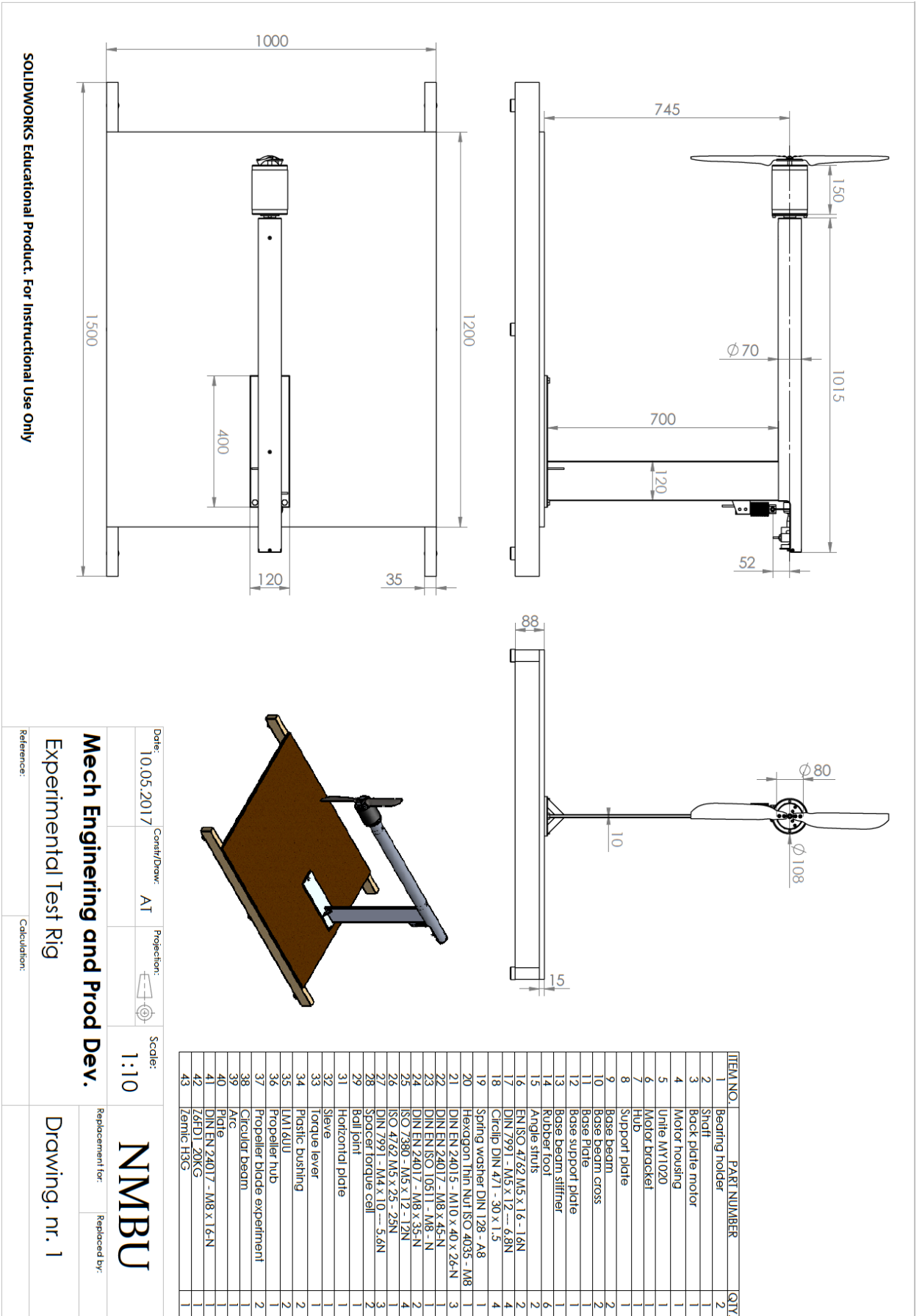
Date: 10.05.2017
Constr/Draw: AT
Projection:
Reference:
Calculation:

Mech Enginering and Prod Dev.
Experimental Test Rig

Scale: 1:10

NMBU

Drawing. nr. 1

Replacement for: Replaced by:

ITEM NO.	PART NUMBER	QTY.
1	Bearing holder	2
2	Shaft	1
3	Back plate motor	1
4	Motor housing	1
5	Unite MY1020	1
6	Motor bracket	1
7	Hub	1
8	Support plate	1
9	Base beam	2
10	Base beam cross	2
11	Base Plate	1
12	Base support plate	1
13	Base beam stiffner	1
14	Rubber foot	6
15	Angle struts	2
16	EN ISO 4762 M5 x 16 - 16N	2
17	DIN 7991 - M5 x 12 --- 6.8N	4
18	Circlip DIN 471 - 30 x 1.5	4
19	Spring washer DIN 128 - A8	4
20	Hexagon Thin Nut ISO 4035 - M8	1
21	DIN EN 24015 - M10 x 40 x 26-N	3
22	DIN EN 24017 - M8 x 45-N	3
23	DIN EN ISO 10511 - M8 - N	2
24	DIN EN 24017 - M8 x 35-N	2
25	ISO 7380 - M5 x 12 - 12N	4
26	ISO 4762 M5 x 25 - 25N	4
27	DIN 7991 - M4 x 10 --- 5.6N	3
28	Spacer torque cell	2
29	Ball joint	1
31	Horizontal plate	1
32	Sleve	1
33	Torque lever	1
34	Plastic bushing	2
35	LM16UU	2
36	LM16UU	2
37	Propeller hub	1
38	Propeller blade experiment	2
39	Circular beam	2
40	Arc	1
41	Plate	1
42	DIN EN 24017 - M8 x 16-N	1
43	Z6FD1_20KG	1
	Zemic H3G	1

B

MOMENTUM THEORY FOR OPEN PROPELLERS IN AXIAL FLIGHT

The model for momentum theory is illustrated in Figure 18.3.1. The ideal propeller disk consists of an infinite number of blades with area, A_p which is enclosed by a streamtube. Stations 1 and 4 are considered to have planes infinitely far upstream and downstream respectively. The induced velocity is evaluated by considering a streamline shown in Figure 18.3.1. The fluid far upstream has freestream velocity, V_∞ and freestream pressure, p_∞. The pressure reduces to p_u and the freestream velocity increases by the induced velocity V_i at station 2, just above the propeller disk. At station 3 downstream, the pressure jumps to p_d and the velocity is designated V_d. At the end of the streamtube at station 4 the pressure returns to freestream pressure and the slipstream velocity is designated V_s.
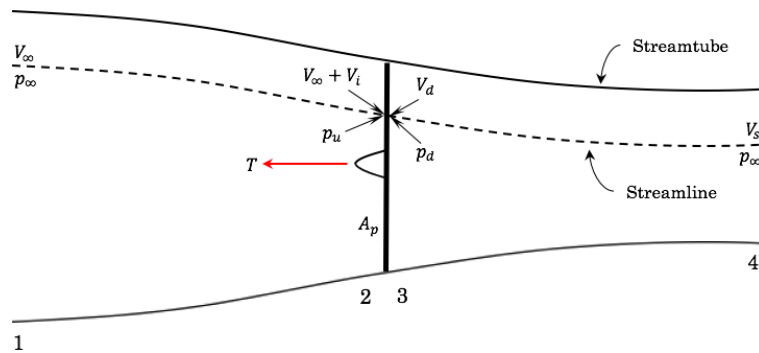
Figure 18.3.1. Momentum theory model for a rotating wing.
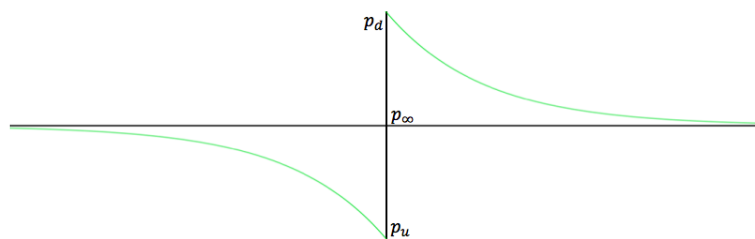
Figure 18.3.2. Pressure change across the propeller disk.
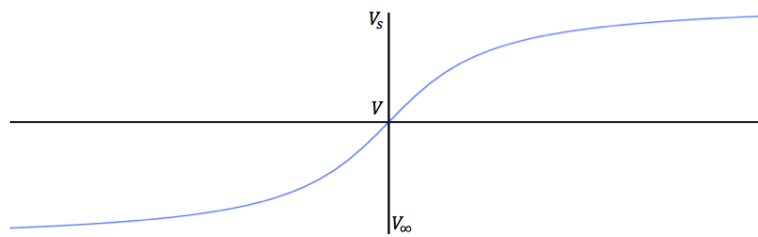
Figure 18.3.3. Velocity change across the propeller disk.

Applying conservation of mass on the propeller disk area, A_p

$$\rho A_p V_d = \rho A_p (V_\infty + V_i) \tag{18.3.1}$$

For the assumption of incompressible flow, this shows that the velocity is the same on both sides of the propeller disk (station 2 and 3) as illustrated in Figure 18.3.3.

$$V_d = (V_\infty + V_i) \tag{18.3.2}$$

C

The axial force acting on the propeller disk is given by the pressure difference upstream and downstream of the propeller disk. Hence the thrust can be expressed from the definition of pressure

$$T = A_p(p_d - p_u) \tag{18.3.3}$$

Since this force is applied directly to the fluid, there must be an increase in fluid momentum given by Newton's second law.

$$T = \dot{m}(V_s - V_\infty) \tag{18.3.4}$$

Where the mass flow through the propeller disk is: $\dot{m} = \rho A_p(V_\infty + V_i)$, inserted in Eq. (18.3.4)

$$T = \rho A_p(V_\infty + V_i)(V_s - V_\infty) \tag{18.3.5}$$

Putting Eq. (18.3.3) equal to (18.3.5) eliminates thrust

$$A_p(p_d - p_u) = \rho A_p(V_\infty + V_i)(V_s - V_\infty) \tag{18.3.6}$$

Applying Bernoulli's equation in - energy per unit mass - along the streamline shown in Figure 18.3.1 upstream from station $1 - 2$ and downstream from station $3 - 4$ respectively,

$$\frac{p_\infty}{\rho} + \frac{V_\infty{}^2}{2} = \frac{p_u}{\rho} + \frac{(V_\infty + V_i)^2}{2} \tag{18.3.7}$$

$$\frac{p_\infty}{\rho} + \frac{V_s{}^2}{2} = \frac{p_d}{\rho} + \frac{(V_\infty + V_i)^2}{2} \tag{18.3.8}$$

Subtracting Eq. (18.3.7) from (18.3.8) to evaluate the energy difference gives

$$\frac{V_s{}^2}{2} - \frac{V_\infty{}^2}{2} = \frac{p_d}{\rho} - \frac{p_u}{\rho} \tag{18.3.9}$$

Finally, using Eq. (18.3.6) to eliminate pressure from Eq. (18.3.9)

$$\frac{V_s{}^2}{2} - \frac{V_\infty{}^2}{2} = (V_\infty + V_i)(V_s - V_\infty)$$

$$\frac{(V_s + V_\infty)(V_s - V_\infty)}{2} = (V_\infty + V_i)(V_s - V_\infty) \tag{18.3.10}$$

Solving for V_s gives the result

$$V_s = V_\infty + 2V_i \tag{18.3.11}$$

Classical momentum theory predicts that the difference in slipstream velocity and freestream velocity is twice the induced velocity.

For static conditions with $V_\infty = 0$, the slipstream velocity is simply twice the induced velocity, which also implies that

$$A_s = \frac{1}{2}A_p \quad \text{,For static conditions} \tag{18.3.12}$$

D

Induced power and efficiency.

Power is given by force times velocity. Applying this principle to the system in Figure 18.3.1 the induced power that must be delivered by the propeller is defined as the following,

$$P = T(V_\infty + V_i) \qquad (18.3.13)$$

Using Eq. (18.3.5) and (18.3.11) the thrust can be written as

$$T = 2\rho A_p(V_\infty + V_i)V_i \qquad (18.3.14)$$

Inserting Eq. (18.3.14) in (18.3.13) gives

$$P = 2\rho A_p(V_\infty + V_i)^2 V_i \qquad (18.3.15)$$

The induced velocity can now be expressed in terms of thrust and freestream velocity. Solving Eq. (18.3.14) for V_i and inserting in the quadratic formula gives

$$V_i = \sqrt{\frac{V_\infty{}^2}{4} + \frac{T}{2\rho A_p}} - \frac{V_\infty}{2} \qquad (18.3.16)$$

Inserting Eq. (18.3.16) in (18.3.13) the brake power required can be expressed in terms of the thrust and freestream velocity

$$P = T\left[\frac{V_\infty}{2} + \sqrt{\frac{V_\infty{}^2}{4} + \frac{T}{2\rho A_p}}\right] \qquad (18.3.17)$$

The propulsive efficiency for the propeller is given by the propulsive power output, TV_∞ divided by the brake power, P (the power applied to the propeller). Since the flow is considered inviscid and incompressible, the propulsive efficiency becomes the upper theoretical limit and is called ideal efficiency. Inserting Eq. (18.3.5) combined with (18.3.11) for T and Eq. (18.3.15) for P, the ideal efficiency can be written as

$$\eta_i = \frac{TV_\infty}{P} = \frac{\rho A_p(V_\infty + V_i)(V_\infty + 2V_i - V_\infty)V_\infty}{2\rho A_p(V_\infty + V_i)^2 V_i} = \frac{V_\infty}{(V_\infty + V_i)} = \frac{1}{1 + \frac{V_i}{V_\infty}} \qquad (18.3.18)$$

Momentum theory for open propellers are relatively simple and appealing, but does not account for the rotation of the fluid in the slipstream. There must be torque added to the propeller to support this rotation in the slipstream. Therefore, the simple momentum theory overestimates thrust and propulsive efficiency. Momentum theory can be extended to include the effects of rotation in the slipstream. The overestimation of basic momentum theory compared with momentum theory which include rotational effects in the slipstream, is in the order of 5 percent regarding induced velocity and propulsive efficiency for the range of thrust coefficient and advance ratio normally encountered in airplane propellers [21].

PHYSICAL PROPERTIES OF AIR [14]

TABLE A.2 Physical properties of air at standard sea-level atmospheric pressure[a]

Temperature, T	Density, ρ	Specific weight, γ	Absolute viscosity,[b] μ	Kinematic viscosity,[b] ν
°F	slug/ft³	lb/ft³	10^{-6} lb·sec/ft²	10^{-3} ft²/sec
−40°F	0.002940	0.09460	0.312	0.106
−20°F	0.002807	0.09030	0.325	0.116
0°F	0.002684	0.08637	0.338	0.126
10°F	0.002627	0.08453	0.345	0.131
20°F	0.002572	0.08277	0.350	0.136
30°F	0.002520	0.08108	0.358	0.142
40°F	0.002470	0.07945	0.362	0.146
50°F	0.002421	0.07790	0.368	0.152
60°F	0.002374	0.07640	0.374	0.158
70°F	0.002330	0.07495	0.382	0.164
80°F	0.002286	0.07357	0.385	0.169
90°F	0.002245	0.07223	0.390	0.174
100°F	0.002205	0.07094	0.396	0.180
120°F	0.002129	0.06849	0.407	0.189
140°F	0.002058	0.06620	0.414	0.201
160°F	0.001991	0.06407	0.422	0.212
180°F	0.001929	0.06206	0.434	0.225
200°F	0.001871	0.06018	0.449	0.240
250°F	0.001739	0.05594	0.487	0.280
°C	kg/m³	N/m³	10^{-6} N·s/m²	10^{-6} m²/s
−40°C	1.515	14.86	14.9	9.8
−20°C	1.395	13.68	16.1	11.5
0°C	1.293	12.68	17.1	13.2
10°C	1.248	12.24	17.6	14.1
20°C	1.205	11.82	18.1	15.0
30°C	1.165	11.43	18.6	16.0
40°C	1.128	11.06	19.0	16.8
60°C	1.060	10.40	20.0	18.7
80°C	1.000	9.81	20.9	20.9
100°C	0.946	9.28	21.8	23.1
200°C	0.747	7.33	25.8	34.5

[a] In these tables, if (for example, at −40°F) μ is given as 0.312 and the units are 10^{-6} lb·sec/ft² then $\mu = 0.312 \times 10^{-6}$ lb·sec/ft².
[b] For viscosity, see also Figs. A.1 and A.2. Absolute viscosity μ is virtually independent of pressure, whereas kinematic viscosity ν varies with pressure (density) (Sec. 2.11).

F

SOLUTIONS FOR DERIVED EXPRESSIONS IN CHAPTER 4.7, INPUTTED IN EXCEL

Thrust

$$T = \frac{N\rho c}{2} \int_{r_h}^{R} [C_L \cos \varphi(r) - C_D \sin \varphi(r)][\omega^2 r^2 + (V_\infty + V_i)^2] \; dr \qquad (4.7.10)$$

where

$$\varphi(r) = \tan^{-1}\left(\frac{V_\infty + V_i}{\omega r}\right) \qquad (4.7.4)$$

multiplying parentheses in Eq. $(4.7.10)$:

$$T = \frac{N\rho c}{2} \int_{r_h}^{R} [C_L \cos \varphi(r)\omega^2 r^2 - C_D \sin \varphi(r)\; \omega^2 r^2 + C_L \cos \varphi(r)\,(V_\infty + V_i)^2 - C_D \sin \varphi(r)\,(V_\infty + V_i)^2]\; dr$$

$$K_1 = \frac{N\rho c}{2}$$

$$K_2 = C_L \cos \varphi(r)\omega^2 r^2$$

$$K_3 = C_D \sin \varphi(r)\; \omega^2 r^2$$

$$K_4 = C_L \cos \varphi(r)\,(V_\infty + V_i)^2$$

$$K_5 = C_D \sin \varphi(r)\,(V_\infty + V_i)^2$$

$$T = K_1 \left(\int_{r_h}^{R} K_2 - \int_{r_h}^{R} K_3 + \int_{r_h}^{R} K_4 - \int_{r_h}^{R} K_5 \; \right) dr$$

wolframalpha.com gave the following solutions assuming C_L, C_D, V_∞, V_i, and r are positive:

$$\int_{r_h}^{R} K_2 \; dr = \left[\frac{C_L(\omega^2 r^2 - 2(V_\infty + V_i)^2)\sqrt{\omega^2 r^2 + (V_\infty + V_i)^2}}{3\omega} \right]_{r_h}^{R}$$

$$\int_{r_h}^{R} K_3 \; dr =$$

$$\left[\frac{1}{2\omega^2 r \sqrt{\frac{(V_\infty + V_i)^2}{\omega^2 r^2} + 1}} C_D (V_\infty + V_i) \left(\omega r \left(\omega^2 r^2 + V_\infty{}^2 + 2V_\infty V_i + V_i{}^2 \right) - (V_\infty \right. \right.$$

$$\left. \left. + V_i)^2 \sqrt{\omega^2 r^2 + V_\infty{}^2 + 2V_\infty V_i + V_i{}^2} \; \ln \left(\omega \left(\sqrt{\omega^2 r^2 + V_\infty{}^2 + 2V_\infty V_i + V_i{}^2} + \omega r \right) \right) \right) \right]_{r_h}^{R}$$

$$\int_{r_h}^{R} K_4 \; dr = \left[\frac{C_L(V_\infty + V_i)^2 \sqrt{\omega^2 r^2 + (V_\infty + V_i)^2}}{\omega} \right]_{r_h}^{R}$$

$$\int_{r_h}^{R} K_5 \; dr = \left[\frac{C_D(V_\infty + V_i)^3 \; \log \left(\omega \left(\sqrt{\omega^2 r^2 + (V_\infty + V_i)^2} + \omega r \right) \right)}{\omega} \right]_{r_h}^{R}$$

G

Torque

$$Q = \frac{N\rho c}{2} \int_{r_h}^{R} [C_L \sin \varphi(r) + C_D \cos \varphi(r)][\omega^2 r^2 + (V_\infty + V_i)^2] r \; dr \tag{4.7.14}$$

where:

$$\varphi(r) = \tan^{-1}\left(\frac{V_\infty + V_i}{\omega r}\right) \tag{4.7.4}$$

multiplying parentheses in (4.7.14):

$$Q = \frac{N\rho c}{2} \int_{r_h}^{R} [C_L \sin \varphi(r)\omega^2 r^3 + C_D \cos \varphi(r)\, \omega^2 r^3 + C_L \sin \varphi(r)\,(V_\infty + V_i)^2 r + C_D \cos \varphi(r)\,(V_\infty + V_i)^2 r]\; dr$$

$$K_1 = \frac{N\rho c}{2}$$

$$K_2 = C_L \sin \varphi(r)\, \omega^2 r^3$$

$$K_3 = C_D \cos \varphi(r)\, \omega^2 r^3$$

$$K_4 = C_L \sin \varphi(r)\, (V_\infty + V_i)^2 r$$

$$K_5 = C_D \cos \varphi(r)\, (V_\infty + V_i)^2 r$$

$$Q = K_1 \left(\int_{r_h}^{R} K_2 + \int_{r_h}^{R} K_3 + \int_{r_h}^{R} K_4 + \int_{r_h}^{R} K_5 \right) dr$$

wolframalpha.com gave the following solutions assuming C_L, C_D, V_∞, V_i, and r are positive:

$$\int_{r_h}^{R} K_2 \; dr = \left[-\frac{C_L(V_\infty + V_i)(2(V_\infty + V_i)^2 - \omega^2 r^2)\sqrt{\omega^2 r^2 + (V_\infty + V_i)^2}}{3\omega^2} \right]_{r_h}^{R}$$

$$\int_{r_h}^{R} K_3 \; dr =$$

$$\left[\frac{1}{2\omega^3 r \sqrt{\frac{(V_\infty + V_i)^2}{\omega^2 r^2} + 1}} C_D \left(\omega r(\omega^2 r^2 + V_\infty{}^2 + 2V_\infty V_i + V_i{}^2)(2\omega^2 r^2 - 3(V_\infty + V_i)^2) + 3(V_\infty \right.\right.$$

$$\left.\left. + V_i)^4 \sqrt{\omega^2 r^2 + V_\infty{}^2 + 2V_\infty V_i + V_i{}^2}\; \ln\left(\omega\left(\sqrt{\omega^2 r^2 + V_\infty{}^2 + 2V_\infty V_i + V_i{}^2} + \omega r \right) \right) \right) \right]_{r_h}^{R}$$

$$\int_{r_h}^{R} K_4 \; dr = \left[\frac{C_L(V_\infty + V_i)^3 \sqrt{\omega^2 r^2 + (V_\infty + V_i)^2}}{\omega^2} \right]_{r_h}^{R}$$

H

$$\int_{r_h}^{R} K_5 \ dr = \left[\frac{1}{2\omega^3 r \sqrt{\frac{(V_\infty + V_i)^2}{\omega^2 r^2} + 1}} C_D (V_\infty \right.$$

$$+ V_i)^2 \left(\omega r (\omega^2 r^2 + V_\infty{}^2 + 2V_\infty V_i + V_i{}^2) - (V_\infty \right.$$

$$\left. + V_i)^2 \sqrt{\omega^2 r^2 + V_\infty{}^2 + 2V_\infty V_i + V_i{}^2} \ \ln \left(\omega \left(\sqrt{\omega^2 r^2 + V_\infty{}^2 + 2V_\infty V_i + V_i{}^2} + \omega r \right) \right) \right) \right]_{r_h}^{R}$$

I

TEXCEL FULL SCALE

Full scale

Index	Value	Unit	Comment
rho	1,205	kg/m3	Input
rev	3000,00	rev/min	Input
omega ω	314,16	rad/s	
Nblades	3,00	-	Input
V freestream V_∞	0,00	m/s	Input
Thrust T	1100,00	N	Desired thrust - Imput needed to calc Vi by momentum theory
Tip radius R	0,600	m	Input
Hub radius r_h	0,100	m	Input
Disk area	1,10	m2	Input
Chord length c	0,08	m	Input
Cl	1,6	-	Input
Cd	0,015	-	Input
Tip Re	1 005 310	-	
Hub Re	167 552	-	

Open

Vi open	20,37	m/s	From momentum theory

Blade Element Theory

Open Propeller	Tip Mach nr	0,56 (Tip Mach < 0,6 => OK)

Calc Thrust	K1(K2-K3+K4-K5	**1657 N**	Calc Torque	K1(K2-K3+K4-K	**115 Nm**	Calc Power	**36,01 kW**
K1	0,1446		K1	0,1446			
K2=k1-k2	11158,8295 WA=Ok		K2=k1-k2	723,6818 WA=Ok			
k1	11168,7937		k1	724,328			
k2	9,9642287		k2	0,646207			
K3=k3-k4	17,6771132 WA=Ok		K3=k3-k4	47,36427 WA=Ok			
k3	15,023329		k3	47,50818			
k4	-2,6537843		k4	0,143908			
K4=k5-k6	321,660546 WA=Ok		K4=k5-k6	20,8606 WA=ok			
k5	400,821668		k5	25,99442			
k6	79,1611222		k6	5,133823			
K5=k7-k8	0,68771124 WA=Ok		K5=k7-k8	0,770756 WA=ok			
k7	4,71854169		k7	0,914666			
k8	4,03083045		k8	0,14391			

Momentum Theory — Open Propeller

Thrust	**1657**	N
Calc Torque	**132**	Nm
Calc Power	**41,5**	kW
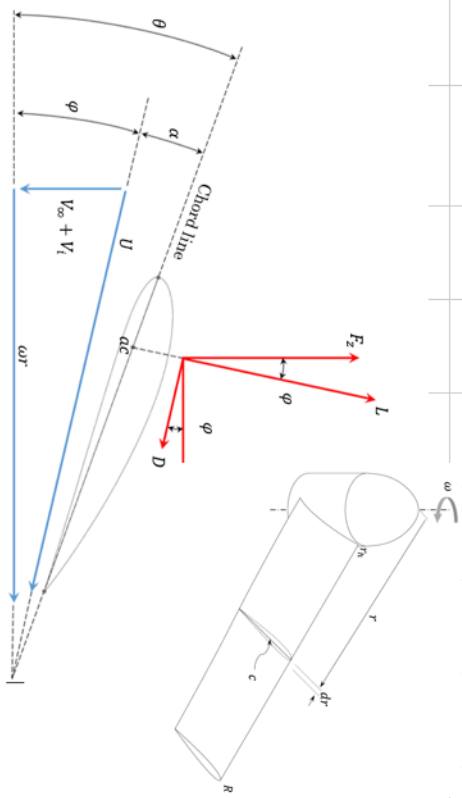
TEXCEL FOR EXPERIMENTAL PROTOTYPE

Experimental Prototype

Index	Value	Unit	Comment
rho	1,205	kg/m3	Input
rev	3000,00	rev/min	Input
omega ω	314,16	rad/s	Input
Nblades	2,00	-	Input
V freestream V_∞	0,00	m/s	Input
Thrust T	80,00	N	Desired thrust - Imput needed to calc Vi by momentum theory
Tip radius R	0,300	m	Input
Hub radius r_h	0,054	m	Input
Disk area	0,274	m2	Input
Chord length c	0,05	m	Input
Cl	1,6	-	Input
Cd	0,015	-	Input
Tip Re	314 159	-	
Hub Re	56 549	-	
Vi	11,02	m/s	From momentum theory
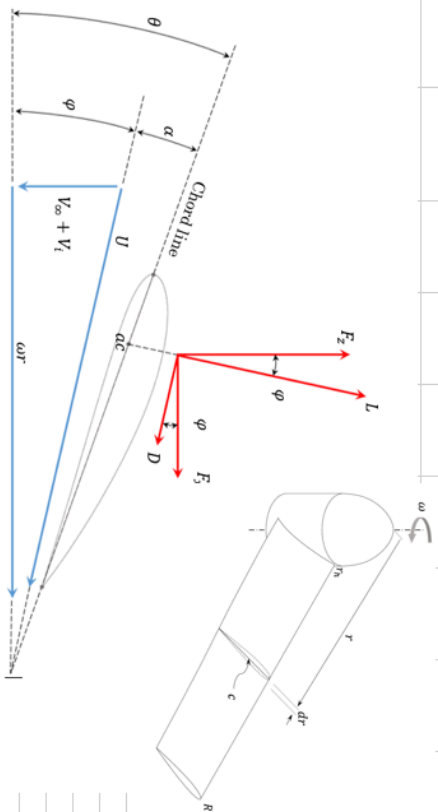
Blade Element Theory

Open Propeller	Tip Mach n	0,28	(Tip Mach < 0.6 => OK)

Calc Thrust	K1(K2-K3+K4-K5)	86 N	Calc Torque	K1(K2-K3+K4-K5)	3,22 Nm	Calc Power	1,011 kW
K1	0,06025		K1	0,06025		K1	
K2=k1-k2	1390,256 WA=Ok		K2=k1-k2	48,7458 WA=Ok			
k1	1391,806		k1	48,80014			
k2	1,549641		k2	0,054334			
K3=k3-k4	2,272183 WA=Ok		K3=k3-k4	2,956201 WA=Ok			
k3	2,199433		k3	2,961868			
k4	-,07275		k4	0,005666			
K4=K5-K6	46,13771 WA=Ok		K4=k5-k6	1,617702 WA=ok			
K5	58,63704		k5	2,055959			
k6	12,49933		k6	0,438257			
K5=k7-k8	0,045074 WA=Ok		K5=k7-k8	0,069575 WA=ok			
k7	0,304645		k7	0,075241			
k8	0,259571		k8	0,005666			

PERFORMANCE FACTOR OF A COMMERCIAL HELICOPTER

Eq. (6.4.4) solved for k:

$$k = \frac{2M^2 \rho A_p}{\left(\frac{W_G}{P}\right)^2 W g}$$

Bell 429 Commercial Helicopter [44]

Specifications	
Engine type	Gassturbine
Power	2 x 820 kW
Cruise speed	520 km/h
Gross weight	3175 kg
Specific weight	3.9 kg/kW
R	5.5 m
r_h	1.1 m
Disk area	90 m²

Has an estimated performance factor of:

$$k = \frac{2 \cdot 0.75^2 \cdot 1.205 \cdot 90}{(0.039)^2 \cdot 3175 \cdot 9.81} = \mathbf{1.37}$$

UNITE MY1020 motor

N(rpm)	Pout(W)	U(V)	I(A)	Pin(W)	η(%)
4500	2000	55.0	40.0	2000	100
4050	1800	49.5	36.0	1800	90
3600	1600	44.0	32.0	1600	80
3150	1400	38.5	28.0	1400	70
2700	1200	33.0	24.0	1200	60
2250	1000	27.5	20.0	1000	50
1800	800	22.0	16.0	800	40
1350	600	16.5	12.0	600	30
900	400	11.0	8.0	400	20
450	200	5.5	4.0	200	10

T(N.m): 0 1.00 2.00 3.00 4.00 5.00
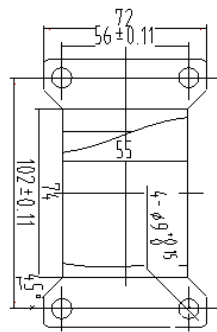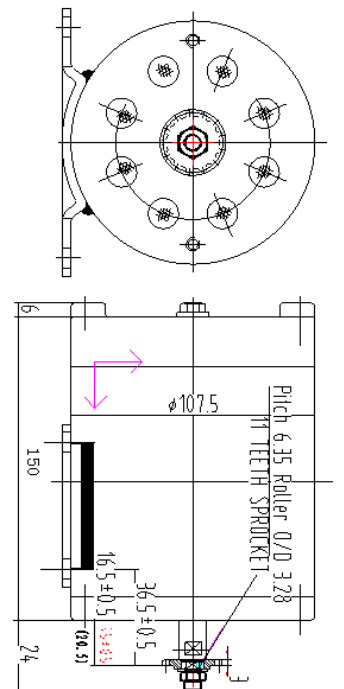
日期: **2012年 01月 19日**
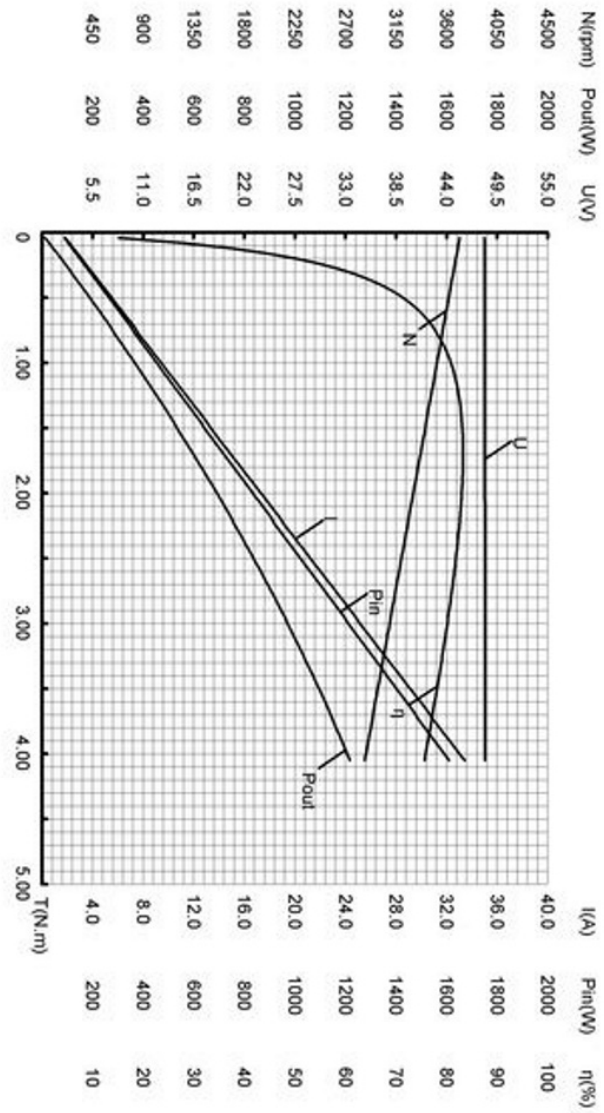
电压: 48.13 (V)

起始点: [0.04(N.m)]
转速: 3719 (rpm)
电流: 1.86 (A)

最大效率点: [83.26%]
转矩: 1.70 (N.m)
转速: 3369 (rpm)
电流: 14.94 (A)
输出功率: 598.94 (W)

最大转矩点: [4.05(N.m)]
转速: 2873 (rpm)
电流: 33.45 (A)
输出功率: 1218.81 (W)

最大输出功率点: [1218.81(W)]
转矩: 4.05 (N.m)
转速: 2873 (rpm)
电流: 33.45 (A)

Pitch 6.35 Roller O/D 3.28
11 TEETH SPROCKET

φ107.5

M

Technical Data

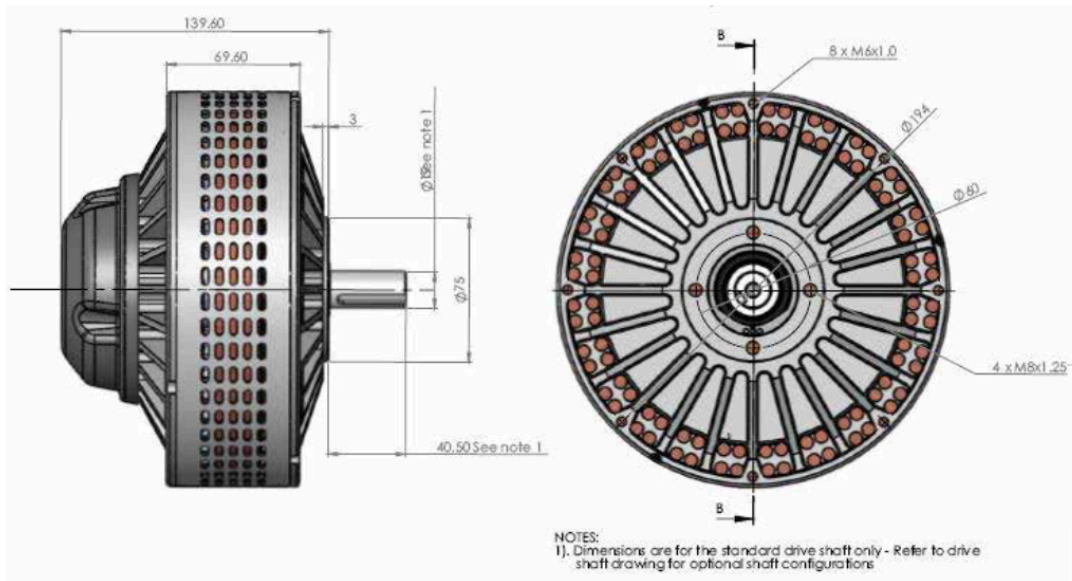| Motor	No Load Current	Torque Constant	Speed Constant	Armature Resistance DC	Armature Inductance @ 15kHz	Armature Inertia	Peak Power	Peak Efficiency	Peak Current	Rated Power	Rated Speed	Rated Voltage	Rated Current	Rated Torque
	A	Nm/A	Rpm/V	mΩ	µH	Kgm^2	kW	%	A	kW	Rpm	V	A	Nm
95	6	0.113	81	21.5	22	0.0238	18	92	400	10	3888	48	250	28
126	10	0.0737	105	175	6	0.0234	7.59	83	400	5.06	2520	24	270	19.2
127	5	0.15	54	22.5	23	0.0236	16.08	89	400	8.55	2592	48	215	31.5
D95B	6	0.14	76	20.5	11	0.0238	28.50	92	400	15.00	6000	72	210	30
D126	5	0.0748	100	138	5	0.0234	11.14	81	400	6.91	3600	36	250	18.3
D127	4	0.17	50	17.5	13	0.0236	25.38	92	400	12.56	3600	72	200	33.3
D135	3.5	0.185	45	16.75	16	0.0236	29.04	93	400	14.39	3780	84	200	36.4
D135 RAG	7.36	0.207	42	16.95	16	0.0238	34.32	93	400	16.84	4032	96	200	39.9
D135 RAGS	7.45	0.21	40	16.95	16	0.0238	36.00	93	400	18.00	4400	110	200	42.0

NOTES:
1). Dimensions are for the standard drive shaft only - Refer to drive shaft drawing for optional shaft configurations

JOBY
MOTORS

Motors

To ask questions or place an order please contact us.

Introducing the
JM1S motor
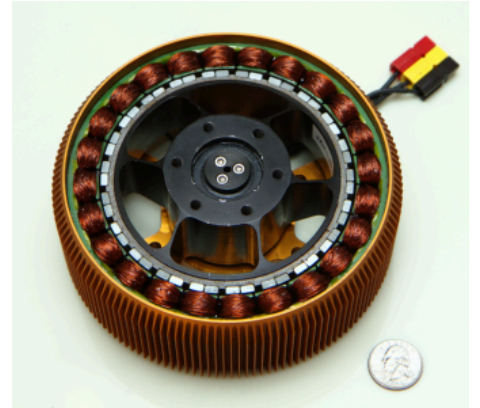
	JM1S	**JM1**	**JM2S**	**JM2**	
Construction	inrunner	inrunner	inrunner	inrunner	
Nominal Voltage	40–450	35–600	50 – 700	100 – 600	V
Poles	22	22	46	46	
Nominal RPM	6000	6000	2500	2500	
Maximum RPM	9000	9000	3500	3500	
Diameter	154	154	200	200	mm
Mass	1800	2750	3350	4000	g
Length	53.1	65	65	75	mm
Continuous Torque	13	21	40	53	N–m
Continuous Shaft Power at Nominal RPM	8.2	13.2	10.5	14	kW
Peak Torque	20	32	60	80	N–m
Peak Shaft Power at Nominal RPM (15s)	12.6	20.1	15.7	20.9	kW

o

PRICE FUTEK MBA500

Application Feedback [App 707] - Case# 201704240018

SM Stefan Mandorf <stefan@lisab.se>
I går, 17:12
Anders Christian Thømt

Ref.no: SM170425-006

Dear Mr Thømt ,

we are the representatives of FUTEK in Norway. See us on the web, www.lisab.no
Thank you for your inquiry.
Please find our quote below:

1pc	MBA500 Capacity: 222N and 5,65Nm	20855 SEK/each
	FSH00743 In stock: 0	
or		
1pc	MBA500 Capacity: 444N and 11,3Nm	20855 SEK/each
	FSH02709 In stock: 3	

If you need a traceable calibration, we offer:

SLB	NIST traceable load calibration w/ certificate,	
	tension and compression, 5 points	1885 SEK per cell
STB	NIST traceable load calibration w/ certificate,	
	clockwise and counter clockwise, 5 points	1885 SEK per cell

Delivery-time is normally 1-2weeks.
For the MBA500 not in stock, we will have to check with FUTEK about the delivery-time.
Please get back to us if you need a more specific delivery time
Shipping-cost to Norway is about 450 SEK

You will also need 2pcs of amplifiers for the multi-axel and
we recommend the LCV/USB2 amplifier for logging data to your PC via USB, read more

LCV/USB2 amplifier   4665* SEK/each
(*Price is based on free solder ends on sensor side)

We also construct and manufacture multi-axel sensors after your requirements.
Don't hesitate to contact us if you have any further questions.

Best regards
Stefan Mandorf

LISAB
LOAD INDICATOR SYSTEM AB

Växel | +46 31 722 79 00 | Switchboard
Direkt | +46 70 727 42 38 | Direct/Mobile

Askims Verkstadsväg 4
SE-436 34 Askim
Sweden

ONYX 3D-PRINT MATERIAL

Mechanical Properties of Nylon

Property	Test Standard	Tough Nylon	Onyx
Tensile Modulus (GPa)	ASTM D638	0.94	1.4
Tensile Stress at Yield (MPa)	ASTM D638	31	36
Tensile Strain at Yield (%)	ASTM D638	27	25
Tensile Stress at Break (MPa)	ASTM D638	54	30
Tensile Strain at Break (%)	ASTM D638	260	58
Flexural Strength (MPa)	ASTM D790*	32	81
Flexural Modulus (GPa)	ASTM D790*	0.84	2.9
Flexural Strain at Break (%)	ASTM D790*	n/a	n/a
Heat Deflection Temperature (°C)	ASTM D648 Method B	49 140†	145
Density (g/cm^3)	N/A	1.10	1.18
Izod Impact — notched (J/m)	ASTM D256-10 Method A	1015	334

*Measured by a method similar to ASTM D790
†Heat deflection temperature of a beam with less than 10% HSHT Glass added, see below for details

Dimensions and Construction of Plastic Test Specimens
- Tensile test specimens: ASTM D638 type IV beams
- Flexural test specimens: 3-pt. Bending, 4.5 in (L) x 0.4 in (W) x 0.12 in (H)
- Heat-deflection temperature at 0.45 MPa, 66 psi (ASTM D648-07 Method B)
- Flexural Strain at Break is not available because nylon does not break before the test ends

Design Principles for Bending

Markforged CFF™ technology **reinforces** 3D plastic parts with 10x stronger and 20x stiffer continuous fibers.

The above Material Properties therefore are **combined** in a part automatically by our Eiger software (although users may also customized the fiber distribution per layer).

In automatic mode, Markforged's Eiger software defaults to creating embedded Sandwich Panels — well-known reinforced structures widely used in aerospace and construction that provide excellent **bending** performance.

Overall part stiffness and strength, represented by tensile and compressive Material Properties above, depends very much upon fiber content, and is strongly related to the amount of fiber the user chooses for a part.

However, per engineering sandwich theory, **flexural** or bending performance tends to benefit **strongly** from **modest** reinforcement in a sandwich panel form (see images on the right).

For more information, please our more detailed "Thermomechanical Stability" white paper.
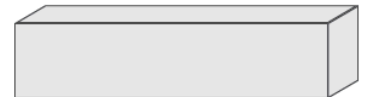
127 layer Nylon FFF Beam:
(not to scale)
Heat Deflection: 49 °C

127 layer HSHT Sandwich Beam:
(not to scale)
117 layers nylon,
10 layers HSHT Glass CFF (~10% by vol.)
Heat Deflection: 140 °C

127 layer HSHT Filled Beam:
(not to scale)
2 layers Nylon,
125 layers HSHT Glass CFF:
Heat Deflection: 150 °C

Q

COORDINATES FOR EPPLER 423 [1]

Index	x	y	z
1	1.000000	0.000000	0
2	0.996550	0.001590	0
3	0.987060	0.006500	0
4	0.973040	0.014340	0
5	0.955300	0.023810	0
6	0.933580	0.033760	0
7	0.907340	0.044000	0
8	0.876710	0.054810	0
9	0.842210	0.066200	0
10	0.804360	0.078030	0
11	0.763730	0.090100	0
12	0.720900	0.102150	0
13	0.676440	0.113910	0
14	0.630920	0.125060	0
15	0.584910	0.135240	0
16	0.538930	0.144100	0
17	0.493470	0.151160	0
18	0.448700	0.155930	0
19	0.404640	0.158280	0
20	0.361490	0.158240	0
21	0.319470	0.155900	0
22	0.278850	0.151380	0
23	0.239870	0.144850	0
24	0.202860	0.136570	0
25	0.168160	0.126760	0
26	0.136110	0.115620	0
27	0.107000	0.103370	0
28	0.081060	0.090230	0
29	0.058520	0.076460	0
30	0.039530	0.062320	0
31	0.024210	0.048120	0
32	0.012620	0.034190	0
33	0.004810	0.020930	0
34	0.000710	0.008790	0
35	0.000020	0.000880	0
36	0.000330	-0.001920	0
37	0.000710	-0.003620	0
38	0.001250	-0.005180	0
39	0.001570	-0.005900	0
40	0.001940	-0.006560	0
41	0.002370	-0.007170	0
42	0.002880	-0.007710	0
43	0.003480	-0.008230	0
44	0.004150	-0.008740	0
45	0.005710	-0.009690	0
46	0.007510	-0.010570	0
47	0.010650	-0.011770	0
48	0.013650	-0.012660	0
49	0.028920	-0.014850	0
50	0.049470	-0.014820	0
51	0.075330	-0.012360	0
52	0.106700	-0.007400	0
53	0.143850	-0.000020	0
54	0.187270	0.009220	0
55	0.236880	0.019130	0
56	0.291960	0.028650	0
57	0.351630	0.036870	0
58	0.414490	0.042830	0
59	0.478670	0.046260	0
60	0.542750	0.047600	0
61	0.605790	0.047150	0
62	0.666900	0.045010	0
63	0.725030	0.041260	0
64	0.779120	0.036250	0
65	0.828360	0.030500	0
66	0.872190	0.024440	0
67	0.910120	0.018440	0
68	0.941790	0.012860	0
69	0.966920	0.007940	0
70	0.985190	0.003900	0
71	0.996290	0.001060	0
72	1.000000	0.000000	0

R